INTERACTION OF YTTRIA AND MOLYBDENUM WITH UF_N (N=4,6) AT HIGH TEMPERATURES

BY

ZIYA ENGIN ERKMEN

A DISSERTATION PRESENTED TO THE GRADUATE SCHOOL
OF THE UNIVERSITY OF FLORIDA IN PARTIAL FULFILLMENT
OF THE REQUIREMENTS FOR THE DEGREE OF
DOCTOR OF PHILOSOPHY

UNIVERSITY OF FLORIDA

1992

ACKNOWLEDGEMENTS

I am grateful to my supervisor, Dr. S. Anghaie for his guidance throughout this dissertation and for his unlimited support in the continuous progress of my research. I was lucky working under his advise and to benefit from his flexibility which provided a peaceful working environment with freedom of decision and action. His positive and encouraging attitude at the most difficult moments made me work harder in order to reach the final goal. I am also thankful to Dr. Diaz for his steady support to INSPI where most of this work was accomplished. Special thanks for Dr. Dehoff for his contribution to the progress of this research. His help in any occasion and any time was very valuable for me. I also thank to my committee members Dr. Hanrahan and Dr. Hintenglang for their assistance in the preparation of this work. I also would like to extend my gratitude to Dr. Wang for his guidance in the experimental procedure and to Dr. Bozkurt for his contribution in the sample preparation and metallographic analysis. I also appreciate Dr. Sacks and Dr. Abbaschian's help for allowing me to use their lab. facilities. My final thanks would be for INSPI personnel, and my friends in general for their motivating support during this research.

This work has been mainly dedicated to my parents who spent their years in order to raise me in a harmonious and healthy environment. I also dedicate this work to all my instructors, both in USA and Turkey where my scientific background has its origins. Without the intimate relations among teachers and students of the University of Florida, and the immense scientific facilities, the USA offers for graduate students, I probably would not reach to the level as I am now. Finally, I praise God for making me come to the end of this work.

TABLE OF CONTENTS

LIST OF TABLES

LIST OF FIGURES

Abstract of Dissertation Presented to the Graduate School of the University of Florida in Partial Fulfillment of the Requirements for the Degree of Doctor of Philosophy

INTERACTION OF YTTRIA AND MOLYBDENUM WITH UF_n (n=4,6) AT HIGH TEMPERATURES

By

Ziya Engin Erkmen

August 1992

Chairman: Samim Anghaie
Major Department: Nuclear Engineering Sciences

The reaction of Yttria with UF_6 and UF_4, and the compatibility of molybdenum with the liquid and gaseous phases of UF_4 were investigated. High-density samples of yttria were processed using sintering and hot-pressing techniques. Yttria reacted extensively with UF_6 gas at 1173 K and formed two reaction layers. These layers were found to be composed of YF_3, UO_2, and U_3O_8. The reaction of yttria with gaseous UF_4 caused the formation of three consecutive reaction layers which were labeled as outer, center, and inner layer. The crystallization of dendrites and formation of a peritectic and a eutectic region occurred during cooling of the liquid outer layer. It was found that the outer layer included YU_xF_y (eutectic and peritectic regions) and UO_2 dendrites. The center layer was composed of

hypostoichiometric UO_2, while the inner layer contained a mixture of YF_3, Y_2O_3, and YOF. A reaction model was developed to explain the formation of these layers. The solid state diffusion analysis was performed based on the defect chemistry of the UO_2 layer, and the solidification scheme was drawn from the analysis of the microstructures. Fick's second law with the reacting boundary conditions was applied to the UO_2 layer and the analytical solution was derived using experimental data. The theoretical models for multicomponent, multiphase diffusion also was reviewed. A semi-quantitative model of diffusion in one dimension was developed and the flux-velocity relationship was derived for local equilibrium conditions at the interfaces for the existing components. According to the model, the calculated diffusion coefficients of the oxygen and uranium ions in UO_2 were compared with their experimental values.

Molybdenum metal also was tested at temperatures ranging from 1390 K to 1470 K and 1740 K to 2273 K in the liquid and gaseous phases of UF_4, respectively. Electron Microprobe analysis performed on the cross section and Energy Dispersive Spectroscopy on the surface of the samples showed no trace of uranium or fluorine diffusion. After the complete elimination of the oxygen from the reaction chamber, it was found that the molybdenum did not react with the media during the exposure testing.

CHAPTER 1
INTRODUCTION

In the beginning of the 21st century, space stations will be the new residence of men to provide them a scientific environment under microgravity. One alternative approach of the energy supply for propulsion and transportation is thought to be compact gas-core nuclear reactors in which uranium tetrafluoride (UF_4) gas will circulate as a working fluid. An ultrahigh temperature vapor core reactor (UTVR) powering a magnetohydrodynamic (MHD) generator is proposed for pulse mode operation. The use of UF_4 as the vapor fuel and added with metal fluoride as the working fluid in the UTVR/MHD generator allows for operation on a direct, closed-rankine type cycle (1). In this power cycle, the peak temperature of the fissioning gas can reach up to 4000 K, and the inner wall temperature of the reactor core can change between 1600 and 2000 K. Therefore, structural materials must necessarily possess high melting points and corrosion resistance for this severe environment.

The interaction of UF_4 with the candidate wall materials at temperatures above 1273 K is the main emphasis in this research. From this perspective, several materials have been tested in UF_4 environment at the Innovative Nuclear Space Power and Propulsion Institute (INSPI) laboratories.

Exposure testings have been performed at different temperatures and testing intervals. Uranium tetrafluoride (UF_4) is an intermediate product in the conversion of uranium ore to uranium hexafluorite (UF_6) and it is also used in the manufacture of UO_2 and uranium metal fuels (2,3,4). When mixed with various other metal fluorides (LiF, NaF, and KF), UF_4 proved to be the most suitable fuel for the molten salt reactor (3,5). Uranium tetrafluorite is a green color powder with monoclinic structure. At room temperature, it is non-volatile, insoluble in water, and relatively stable in air. It has a melting point of 1309 K and a boiling point 1715 K under one atmosphere. Its density is 6.7 g/cm^3 at solid phase and drops nearly to 6.36 g/cm^3 in liquid phase between 1340 and 1630 K (3).

Uranium (U) and fluorine (F) diffusion can determine the behavior of the candidate materials at high temperatures or under the influence of various external conditions. High temperature diffusional creep, coagulation of finely dispersed precipitates in heat-resistant alloys, appearance of different types of defects in diffusion, and migration of atoms in crystal lattices are only a few examples of the effects of diffusion on the properties of metals and alloys. Under these conditions, diffusion mobility of atoms is one of the decisive factors that determines the duration of the effectiveness of the materials.

Various methods are employed for determining the diffusion coefficients in solids. In the case of ceramic

oxides, diffusion takes place with the chemical reaction in which the speed of the reaction can be assumed equal to the diffusion rate of the species (6). From this standpoint, this research is intended to investigate the diffusion behavior of U and F atoms in molybdenum (Mo) and yttria (Y_2O_3). Uranium hexafluorite (UF_6) gas has been used to test yttria alone, and UF_4 for testing molybdenum and yttria in both liquid and gas phases. Due to its similarity with the problem of heat flow, the subject of atomic diffusion has been treated in many texts in conjunction with heat conduction, under the broad designation of transport phenomena. However, it should be emphasized that even in the simplest case of one-dimensional diffusion, in a three-component system, the system of equations could not be rigorously solved when the diffusion coefficients were independent of composition and the Kirkendall effect, which is the displacement of markers, initially located at the interface of two interdiffusing metals, was neglected. In the opening remarks of his work on the theory of heat, Fourier indicated a basic dilemma that although the primary causes are unknown, they are subject to simple and constant laws. These laws may be discovered by observation, and the study of them is the subject of natural philosophy.

In Chapter 2, sample processing techniques and, the experimental system are described and discussed in detail. In this research, some samples are prepared using sintering, hotpressing, and metallographic techniques, while some of

them are directly obtained from outside suppliers. Results of postexperiment analysis are discussed in Chapter 3. In this chapter, results of surface and bulk analyses such as scanning electron microscopy (SEM), x-ray diffraction (XRD) analysis and electron microprobe (EMP) analysis are provided. The EMP analysis is done for Mo samples exposed to UF_4 and yttria samples exposed to UF_6 and UF_4. In addition, the calculation of the reaction rate constant (k) is explained, referring to gravimetric and metallographic analysis.

In Chapter 4, evolution of the multilayer structure with the chemical reactions, solid state diffusion of ions through the UO_2 layer, and formation of different phases following the solidification are explained plausibly. In Chapter 5, Ficks diffusion law is applied with the reacting boundary conditions for the early stage of the experiment where a single phase is dominant. The analytical solution for a binary, single phase system is obtained and the results are compared with the experimental data. At the presence of the multiphases, the systems of equations for multicomponent diffusion is reviewed to reveal the complexity of the problem, and a semi-quantitative model is developed in order to estimate the fluxes and diffusion coefficients of the components. Three basic assumptions regarding the diffusion and reaction of UF_4 and UF_6 with yttria are made:

a. Chemical reactions occur only at the advancing interface but not in the bulk volume,

b. The diffusion coefficients are composition and time independent,

c. Diffusion and reaction occur only in x direction.

Diffusion problems and their solutions can be found in literature such as in Crank's The Mathematics of Diffusion (8) or Jost's Diffusion in Solids, Liquid, Gases (9). Crank also discusses diffusion with moving boundaries in his recently published book (10), while Hill explains the moving boundary problems in his introductory book of One-Dimensional Stefan Problems (11), which can be used in modelling of yttria reaction with UF_6 and UF_4 in future works. Barrer (12), Geiger and Poirier (13), Murch and Nowick (14), Romig and Dayananda (15), and Ozisik and Mikhailov (16) have also made valuable contributions in the analysis and solution of diffusion problems. The gas-solid reactions, which basically describe the phenomenology of our system, have been extensively described and modeled by Szekely, Evans, and Sohn in their book Gas-Solid Reactions (17). Wong in his master's thesis (18), provided a comprehensive summary of the models developed for the analysis of the gas-solid diffusion and reaction problems.

Additional information regarding the mass diffusion with and without chemical reactions in stationary medium can be found in Heat and Mass Transfer, written by Incropera and De Witt (19), in which Chapter 5 deals with cases relating to reaction boundaries. The problem of mass diffusion in

chemically reacting systems also were discussed systematically by Ozisik and Mikhailov (16).

A study about solid state diffusion, including diffusion of gases into and out of the solids, was published as an introductory book by Borg and Dienes (20). Information about derivation of diffusion coefficient by random walk theory and its measurement is given in this book, which also covers multicomponent scale formation and the formulation of the rate constant k_d. Multicomponent scale formation and solid state diffusion are major transport issues discussed in this thesis. A recent book by Wise and Oudar (21) provides similar discussion of layer formation of kinetics on the surface of oxide ceramics in Chapter 11. The subject of kinetics of chemical reaction is widely covered in Laidler's book Chemical Kinetics, first published in 1950 (22).

Kinetics of complex reactions (Chapter 7) are basically related to the work done with UF_6 and UF_4 reacting with Y_2O_3 (yttria) in this research. Kinetics and mechanisms of the gas phase reactions have been discussed in V.N. Kondratiev and E.E. Nikitin's book (23). The first chapter of their book is dedicated to the classification of different types of chemical reactions and the calculation of their rate constants. In this matter, Ovchinnikov, Timashev, and Belyy also studied the kinetics of diffusion-controlled chemical processes (24). A detailed work concerning the Diffusion in Reactor Materials, providing many data from a broad area of materials, was done by Federov and Smirnov in their book

published in 1984 (6). In this book, the problem of self-diffusion of Mo isotope is described in Chapter 1. Diffusion of impurity elements in metals and alloys including uranium diffusion in molybdenum were explained in Chapter 2. Diffusion in multicomponent systems was reviewed in Chapter 3.

Diffusion effect of UF_4 in Mo is studied in this work. Also, the composition of the multilayer scale formed on yttria surface is presented in Chapter 5. A discussion of diffusion of a multicomponent system can be found in Assuancao's work (7). In his thesis, Assuanco reviews the theory of ternary diffusion and using the EMP analysis, he provides the composition paths of ternary and quarternary alloys.

Few studies have been done about the diffusion of uranium into metals. Kuznietz, Livne, Cotler, and Erez (25,26,27) studied the diffusion of uranium into tantalum, molybdenum, and tungsten foils at temperatures 1433-1623 K for immersion times up to 20 hours. Uranium penetrated the tungsten and tantalum intergranularly. In the immersed tungsten foil, the intergranular uranium caused the detachment of the tungsten grains while it formed a multilayer structure in tantalum metal. In the case of molybdenum, progressive dissolution of the grains occurred in liquid uranium at 1433 K. Another diffusion study was done by Lundberg who reduced UO_2 by lithium in the molybdenum capsules (28). In his study, uranium made a solid solution

with molybdenum and also formed an intermediate U_2Mo phase at temperatures between 1400 to 1525 K.

The study of ceramic oxides and metals in UF_6 and UF_4 gases began in the 1960s. The preliminary study of the reaction of UF_6 with metals was done by Hale, Barber, and Berhardt (29). In their experiments, samples of nickel were exposed to static UF_6 at 1255 K for 24 hours. The results proved that intergranular corrosion occurs above 1000 K. In 1978, Florin (30) studied a variety of materials exposed to UF_6 at temperatures between 373 K-973 K. Materials tested were precious metals, common metals, ceramics, and polymers. Among them, aluminium oxide was the most resistant material up to 973 K. In 1985 Whitney, Kim, and Tucker (31) tested alumina, yttria, magnesia, and pyrophyllite $[Al_2(Si_2O_5)_2(OH)_2]$ which were exposed to UF_6 at 973 K at 87 Torr for one hour. In that experiment, the fluoride compounds showed high film failure temperatures at 1233 and 1323 K for alumina and magnesia, respectively. The highest film failure temperature of fluoride was 1423 K in the yttria sample. Another UF_6 corrosion study involving ZrO_2 with UF_6 gas was performed by Collins (32). In his study, Collins reported rates of reaction measured at 873, 973, and 1073 K using a discontinuous gravimetric technique. It was found that the reaction products were composed of ZrF_4, CaF_2, UO_3, U_3O_8, UO_2F_2, UF_4, and zirconium oxyfluorides. At 1073 K, ZrO_2 samples were completely reacted after one hour. A recent study on the UF_6 reaction with alumina (Al_2O_3) was reported by

Wang, Anghaie, Whitney, and Collins (33). In their work, sapphire and polycrystal alpha alumina were tested and it was found that the maximum service temperature of alumina in a UF_6 environment was 1273 K. Chapter 6 will contain a conclusion addressing yttria and molybdenum results separately.

An original example of a multiphase, multicomponent diffusion system was investigated in this research. The microstructure and morphology of the samples after the tests were throughly observed. The analytical and the phenomenological modelling of the problem was given with some assumptions.

CHAPTER 2
EXPERIMENTS

In this chapter, the experimental procedure for exposure testing of yttria and molybdenum samples to the UF_6 and UF_4 gases will be explained.

2.1 Exposure of Yttria to UF_6 and UF_4 Gas

2.1.1 Sample Preparation

2.1.1.1 Sintering

Yttria powder, approximately 1 micron in size and 98% purity,[†] was used as a raw material. The yttria powder was compressed manually by dry pressing to 170 MPa pressure for 10 to 15 minutes (min). The diameter and thickness of processed disks were approximately 2.54 cm and 0.20 cm, respectively. The green yttria disks were then mounted on a mullite plate. Some yttria powder was added between the plate and the disks to prevent contamination of the sample by the mullite substrate. The sample set was then placed in an electric furnace.[††] Samples were heated gradually up to 1973 Kelvin (K) at 473 K per hour (K/h) heating rate under atmospheric pressure in air. Then, they were kept for 1 hour

---

[†] Morton Thiokol, Inc., Alfa Products, 152 Andover Street, Danvers, MA.

[††] Deltec model 31-DTS-1, Deltec Inc., Denver, CO.

at 1973 K and subsequently cooled to room temperature in 25 hours (34,35,36). The Archimedes method was used to measure the density of the samples (37,38) according to ASTM C20-80a standards. Sample densities following sintering were approximately 85%, of the theoretical density. These samples were labeled Ytt85. For convenience, samples obtained through this process are called Ytt85.

2.1.1.2 Hot pressing

Yttria powder was pressed to 170 MPa in order to form green compact disks. A high-strength graphite die having a compression strength of 117 MPa was used to prepare yttria disks samples in the hot press†. The inner wall of the graphite die was spray coated with boron nitride in order to reduce carbon diffusion through the samples.

After the graphite die containing the green disk was placed in the hot press, the temperature was increased slowly by induction heating to about 773 K at a rate of 5-6°C/min under argon atmosphere. The samples were held at this temperature for about 1 hour. Then the temperature was raised to 1873 K, and a pressure ranging from 30 to 45 MPa was applied to a series of samples. They were kept at this pressure and temperature for up to 1.5 hours. Finally, the furnace was turned off to allow a cooling period of 8 hours,

---

† Centorr Associates, Inc., Suncook, NH, Model: 60-4x5 IND6-25

and the samples were left to cool down slowly. At the end of the hot-pressing process, it was observed that the color of all yttria samples had changed from white to black. In order to eliminate this problem, yttria disks were placed in an electric furnace and heated to 1473 K in air for 3 hours. After heat treatment, sample color changed from black to white. Three samples listed in Table 3.2 of Chapter 3 were hot pressed: the sample with 88.2% of theoretical density was prepared applying lower pressure and shorter time, while the high-density samples (98% and 99.5% of theoretical density) were processed at 40 MPa about 40 minutes. Hot-pressed and sintered samples are presented in Figure 2.1.

For convenience, samples with densities higher than 99% were labeled Ytt99. Next, a diamond saw was used to cut both high-density and low-density samples.

2.1.1.3 Density measurements

The densities of Ytt99 and Ytt85 were measured following the Archimedes method recommended by ASTM standards (37,38). Essentially, three measurements are necessary to obtain the density. These include

1. Saturated weight (Sat w): the weight measured after boiling the sample for two hours.
2. Suspended weight (Sus w): the weight measured in the water.
3. Dry weight (Dry w).

Volume = [(Sat w)-(Sus w)]x[ρ_{H_2O} (T)] (39) [2-1]

Bulk density = [Dry w/Volume] [2-2]

ρ_{H_2O} = Density of water at T(°C)

The results of density measurements for sintered and hot-pressed samples are given in Chapter 3.

2.1.2 UF_6 and UF_4 Characteristics

Uranium hexafluoride (UF_6) is the only uranium compound that is stable and gaseous at relatively low temperatures (4). It is the intermediate stage in the separation of uranium isotopes. Uranium hexafluoride is prepared exclusively by the action of elemental fluorine on uranium tetrafluoride:

$$UF_4 + F_2 \text{ ---------->} UF_6 \qquad [2\text{-}3]$$

$$\Delta H_{298} = -59 \text{ kcal/mol}$$

A scheme explaining the use of uranium fluorides in the nuclear fuel cycle is presented in Figure 2.2 (4).

The UF_6 is a colorless, crystalline (monoclinic), and deliquescent solid at room temperature (25°C). Its density is 4.68 g/cm^3, and its melting and sublimation points are 64.6 and 56.2 °C, respectively (39). As mentioned earlier, UF_4 is an intermediate product in the conversion of uranium ore to UF_6. It also is used in the manufacture of UO_2 and uranium metal fuels (2,3,4).

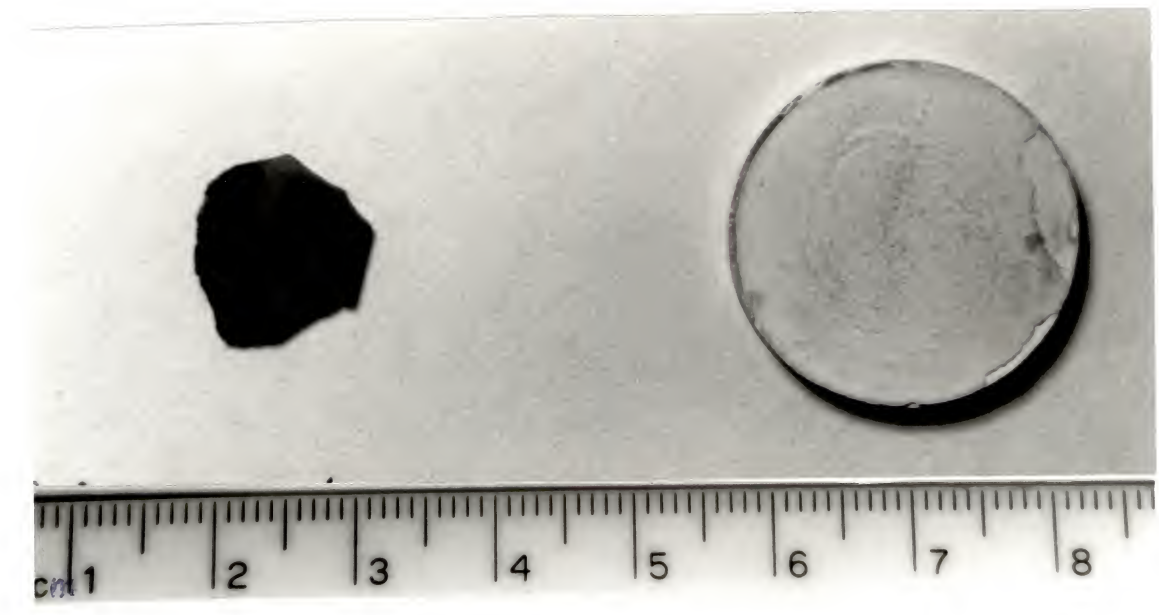

Figure 2.1 Hot-Pressed (99%) and Sintered (85%) Samples

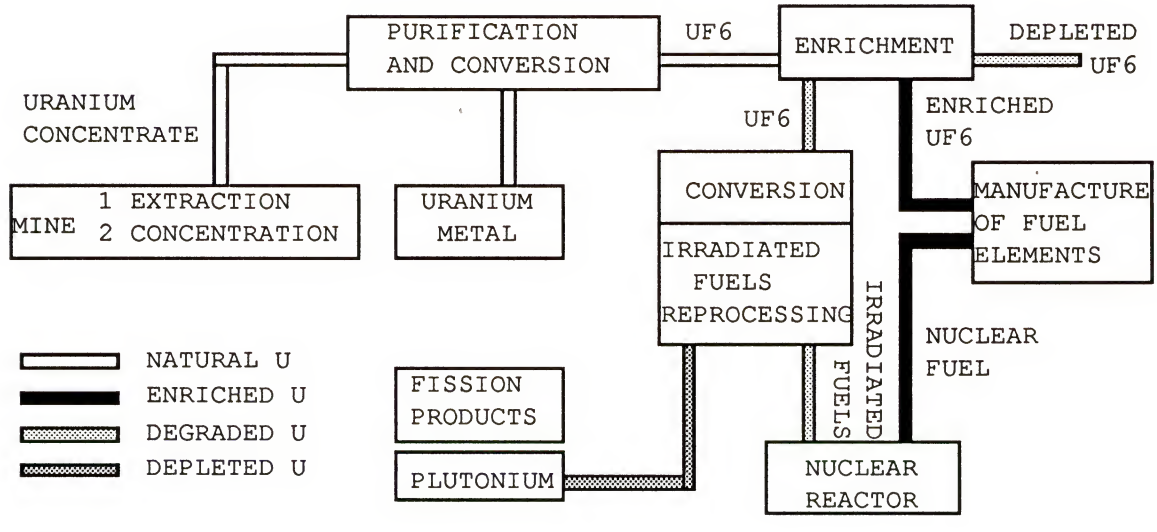

Figure 2.2 Nuclear Fuel Cycle and Fluorine Derivatives

When mixed with various other metal fluorides such as LiF, NaF, and KF, UF_4 was proved to be the most suitable fuel for the molten salt reactor (3,5). Uranium tetrafluorite (UF_4) is a green powder with a monoclinic structure. It is nonvolatile, insoluble in water, and relatively stable in air at room temperature. It has a melting point of 1309 K and a boiling point of 1715 K under one atmosphere. Its density is 6.7 g/cm^3 in the solid phase and drops to nearly 6.36 g/cm^3 in the liquid phase. This occurs between 1340 and 1630 K (3). The choice of this fluoride over chloride is necessary for its superior physical properties: stability, volatility, and purity. The industrial production of UF_4 is carried out almost everywhere in the world, following dry processing techniques. With the use of uranium dioxide treated at 500 °C to 700 °C by both gaseous and anhydrous hydrofluoric acid, UF_4 was obtained according to the following reaction:

$$UO_2 + 4HF \text{ <-----> } UF_4 + 2H_2O \qquad [2\text{-}4]$$

The quality of the UF_4 is very important. The eventual presence of untransformed UO_2 or of uranyl fluoride (UO_2F_2), resulting from an incomplete reduction of U^{6+} to U^{4+}, interferes in later stages of the reaction (fluorination to UF_6 or reduction to metal). Generally, the products are of

excellent quality and contain more than 97-98% UF_4 (4). In this research, 98% purity UF_4[†] was used.

2.1.3 Exposure of Yttria to UF_6 Gas

The corrosion test of yttria by UF_6 gas was carried out in a flowing test unit. A schematic diagram of the unit is shown in Figure 2.3. After measurement of the weight and the surface area, samples were put in an alumina boat and inserted into an alumina reaction tube for exposure testing. The alumina tube was placed at the center of a 1500 K horizontal furnace. Two Monel cylinders, one for UF_6 supply and one used as a cold trap, were installed in the system. The test system was evacuated to vacuum of 10^{-5} Torr with the aid of a diffusion pump. Connection tubes and joints were wrapped with heating tapes and heated to about 420 K to keep UF_6 in gas phase. The furnace temperature was increased to 1173 K at a rate of 423 K/h prior to UF_6 flow.

During the experiment, two pressure transducers were used to monitor the gas flow. Typical pressures being measured were 3.76×10^4 Pa at the inlet and 3.65×10^4 Pa at the outlet of the reaction tube. At the end of the test, UF_6 flow was stopped by turning off the valve of the supply tank, and the furnace was shut down to make the system cool down naturally. A decontaminant recovery pump was connected to

---

[†] U.S. Dept. of Energy, 55 Jefferson Circle, Oak Ridge, TN 37830

remove the residual gas which could exist in the monel tubes. After cooling was achieved, the alumina reaction vessel was removed and the samples were taken out. Residual weights of the exposed samples were measured using an electronic balance† upon removal from the reaction tube.

Preliminary exposure of yttria was performed at 1073 K for 90 min. No apparent reaction was observed on the surface of the sample after exposure at this temperature. However, a test conducted for 90 min at 1173 K resulted in complete decomposition to the point that no solid piece from the samples was left in the reaction vessel. Hence, it was necessary to reduce the exposure time to a maximum of 25 min in order to observe the corrosion of yttria at 1173 K.

2.1.4 Exposure of Yttria to UF_4

2.1.4.1 Experimental system

The experimental system was composed basically of four components:

1. a stainless steel reaction chamber,
2. two optical pyrometers attached to a DCU (digital controller unit),
3. a 20 kw 450 kHz induction power supply, and
4. a diffusion pump connected to a mechanical pump (Figure 2.4).

---

† Sartorius Electronic Balance, Model: R-180-D

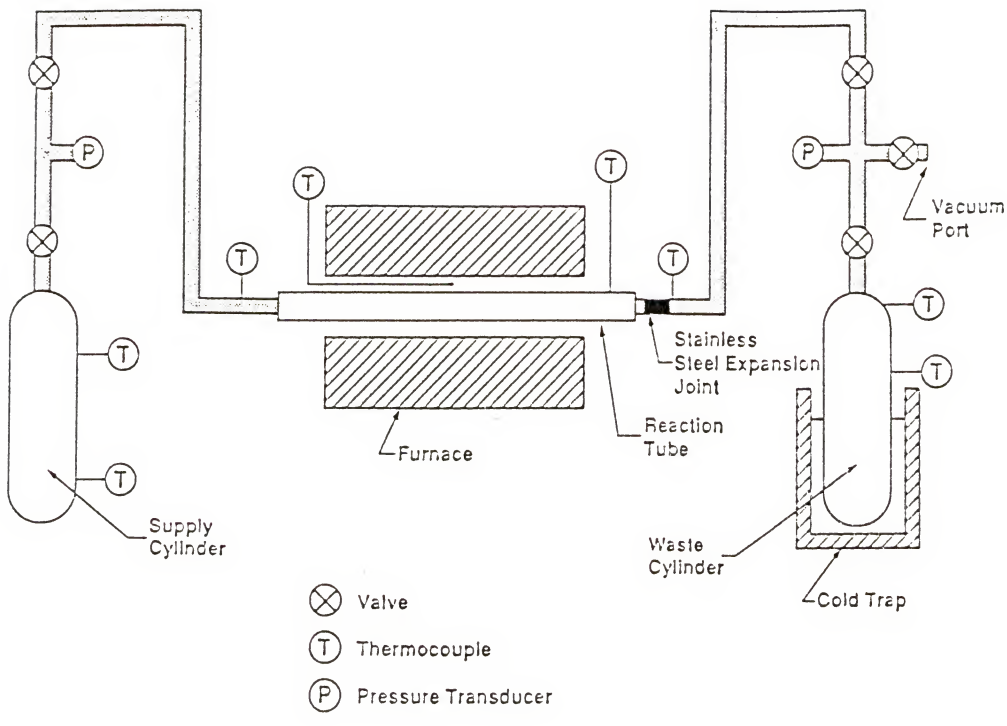

Figure 2.3 UF_6 Test Unit

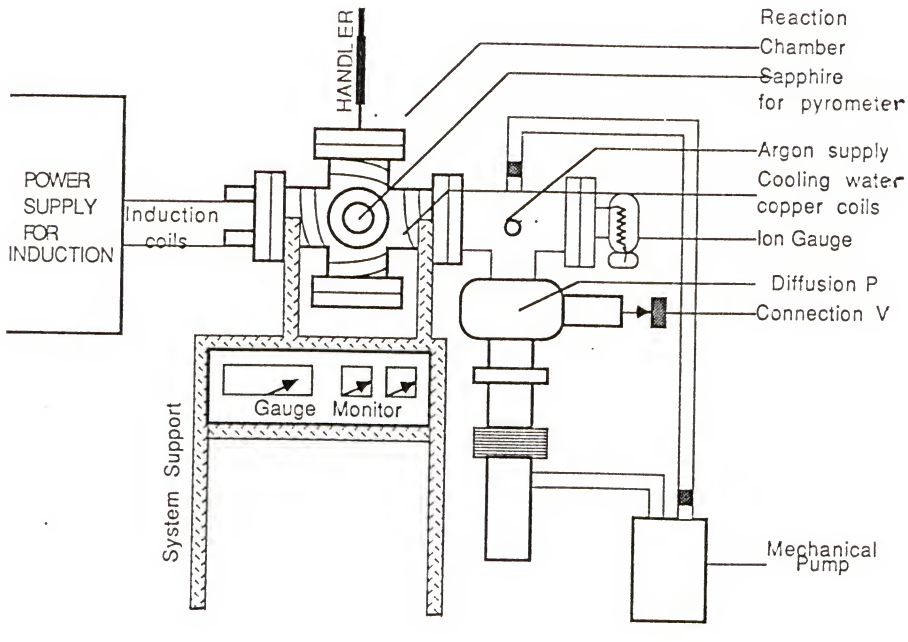

Figure 2.4 UF_4 Test Unit

The reaction chamber has two sapphire (Al_2O_3) windows, one for visual inspection, and the other for temperature measurement and control with optical pyrometers during the experiment. As seen in Figure 2.5, this system consists of a sensor and an indicator/DCU linked by a signal cable. The pyrometers measure the infrared radiance generated from the Mo tube. The intensity or brightness of this radiance varies with the temperature, which stimulates the detector to produce an electrical signal proportional to the radiant intensity and therefore analogous to the temperature being observed. Then, the pyrometer sends this signal to the indicator, which provides a digital display of the temperature on the front panel. The MR04 indicator has two channel operations which require the use of two different pyrometers. The measured temperature range for channel one lies between 1000 and 1755 K, and for channel 2, between 1640 and 3866 K. The temperature signals are digitized to provide data inputs for DCU. They also are linearized and scaled to the range of the instrument. The DCU monitors accuracy and periodically initiates a series of sensor tests and calibration checks in background mode without interrupting the ongoing measurements.

An ideal infrared radiator, called a blackbody, emits the maximum amount of infrared energy possible at each given temperature. It also has an emissivity (ε) of 1.0. As can be seen from Figure 2.6, the targets, in practice, are nonblackbodies.

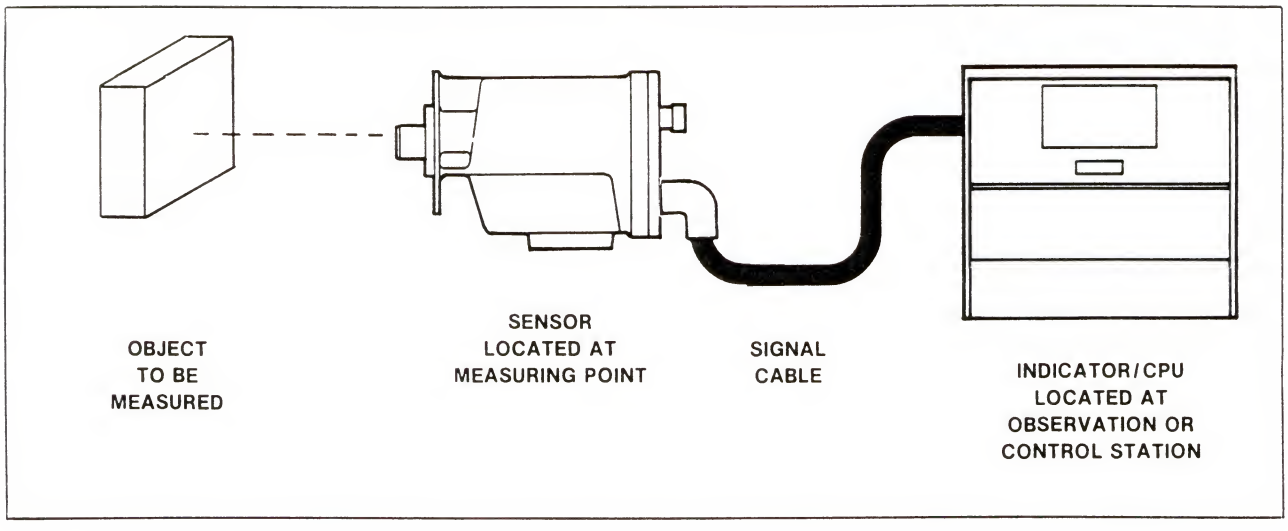

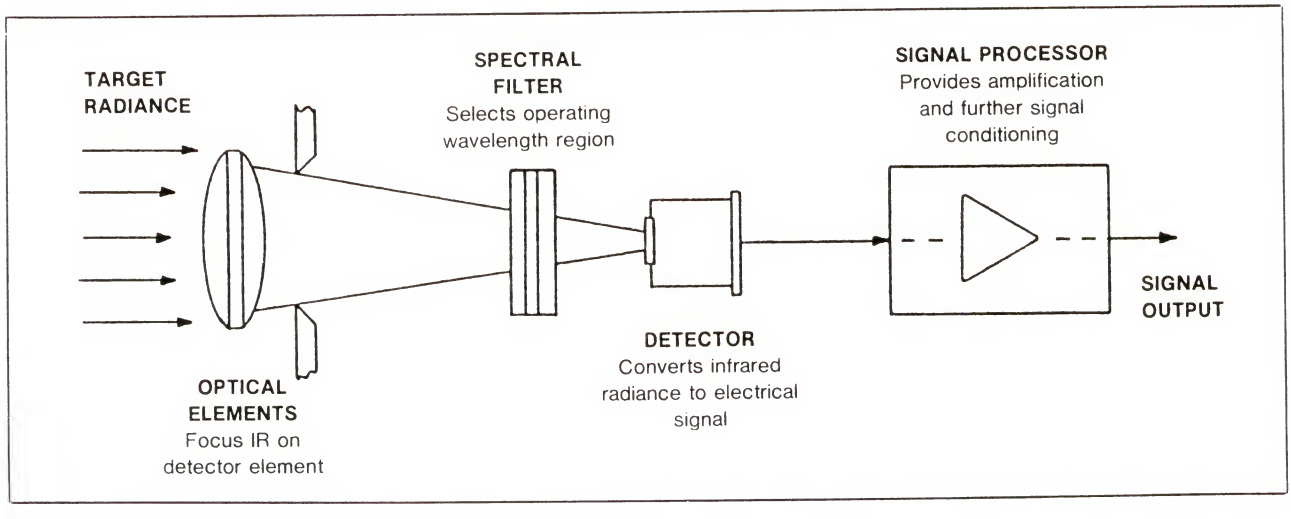

Figure 2.5 Optical Pyrometer and Its Functional Mechanism

The formula describing the physical situation can be given as follows: $E + T + R = 1$ in which E is the emissivity, R reflectivity, and T transmission factors. The difference in emissivities between the actual and the blackbody radiation was compensated by adjusting the E factor on the indicator, since the amount of radiance at a given temperature depends on the type and also on the surface characteristics of the material. In order to obtain a true measurement of temperature, E factor must be settled to match the E factor of the material under measurement. In the present system, the emissivity slope of polished molybdenum (Mo) tube is given as 1.06; hence, the indicator was adjusted before starting the experiment. As seen in Figure 2.6, the more times reflected radiation bounces on a surface, the less reflective the target. This is due to the fact that the surface absorbs more of the radiation at each bounce, leaving less and less radiation to be reflected away from the surface. Since targets that are less reflective have higher emissivities, the rough surface and the cavity represent increasingly high emissivity values even though they are made from the same material as the polished sample. During the experiment, the constant operating temperature was achieved by switching to auto-control mode, which starts a feedback system to stabilize the temperature. The reaction chamber was surrounded by copper tubes in which water circulated in order to cool the chamber walls during the test.

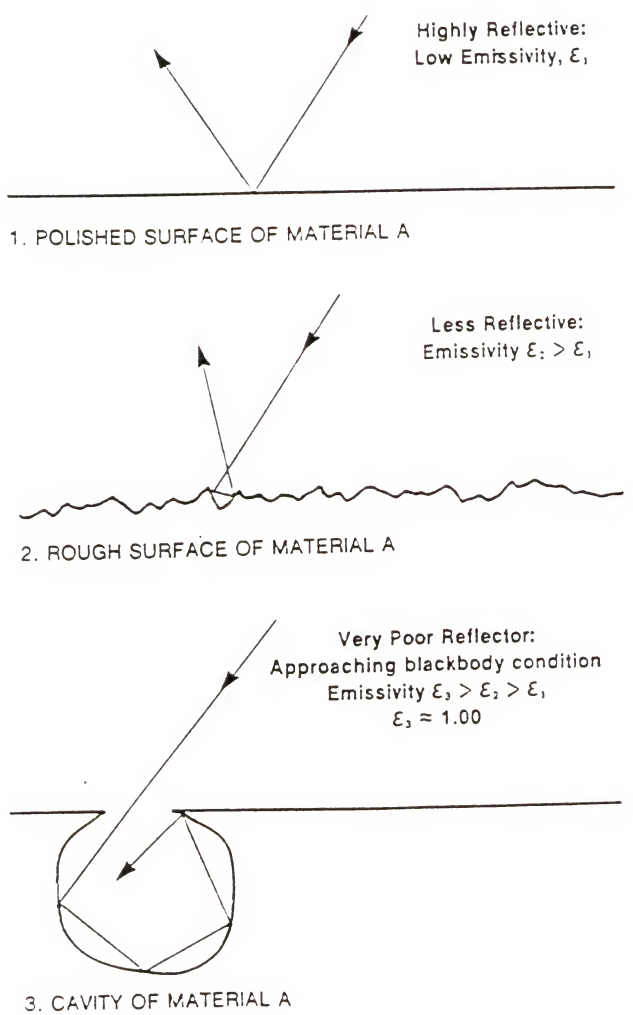

Figure 2.6 Emissivity Change Due to the Surface Conditions

Circular rings of copper-nickel alloy were used to prevent leakage along the junctions during the vacuuming period. Fittings provided necessary insulation of the power supply coils at the entrance of the chamber. The pressure of the chamber was recorded with two different gauges. The ion gauge was used to measure very low pressures under high vacuum, and the regular gauge was used to measure the argon pressure during the test. The induction power supply was a thermonic 20 KW power capacity generator which could produce a maximum potential of 460 volts, a current of 61 amperes, and a frequency of 450 KHZ. The induction furnace was used to provide the necessary thermal energy in order to melt, boil and superheat UF_4. As shown in Figure 2.7, the high alternating current of the helical copper coils created an alternating magnetic field on the crucible which in turn was heated by the resistance against the eddy currents formed on its surface. Finally, the pumping system was used sequentially in order to obtain high vacuum of the order of 10^{-6} Torr.

2.1.4.2 Temperature measurement of the molybdenum crucible and the wall

To measure the temperature differences between the inner and the outer wall of the Mo tube, a series of experiments under vacuum and under argon atmosphere were performed. The test scheme is described in Figure 2.7. For this reason the molybdenum tube was cut longitudinally and a rectangular

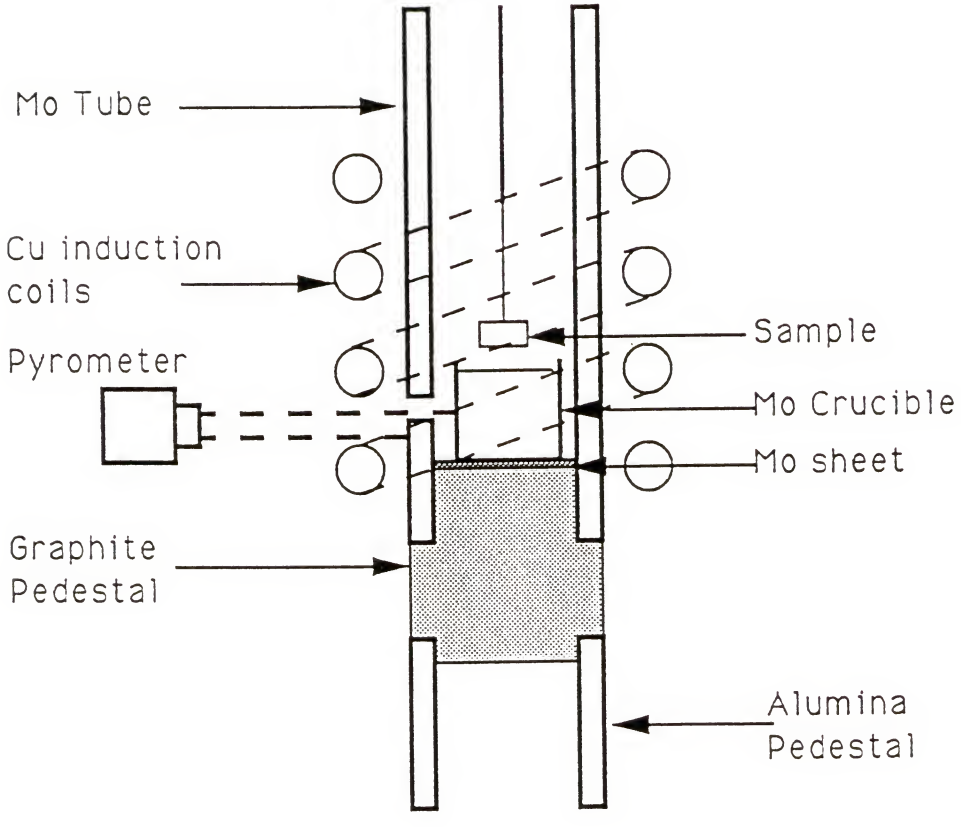

Figure 2.7 Temperature Measurement of The Inner and Outer Wall

piece was taken out. It then became possible to observe the radiance of the crucible and the tube simultaneously during the experiment. Initially, the temperature was stabilized at the maximum power (100%) for about 15 minutes. After the first recording, power level was decreased gradually (in 5 percent steps), and the corresponding temperatures were read from the pyrometer. The results are presented in Figure 2.8.

The temperature difference was observed to be 87°C in average under vacuum and 188.4°C under argon atmosphere. Although the crucible temperature did not change significantly, the outer tube temperature increased when argon gas was used close to the atmospheric pressure. These results showed that there was a significant amount of heat loss due to the radiative heat transfer under vacuum. It was found that there was a linear relationship between the crucible and tube temperature, as shown in Figure 2.9. Therefore, the test temperatures were corrected using the equation derived from the results.

2.1.4.3 Experimental procedure

The procedure can be explained as follows: Samples of yttria (Figure 2.10), in nearly equal dimensions (about 2 cm^2 total surface area), were prepared using a diamond saw and a diamond drill. Then, 10 g UF_4 was put delicately into a Mo crucible maintained on top of a graphite pedestal as seen in Figure 2.11. In between the pedestal and crucible, a thin sheet of Mo was placed in order to prevent carbon from contaminating the crucible.

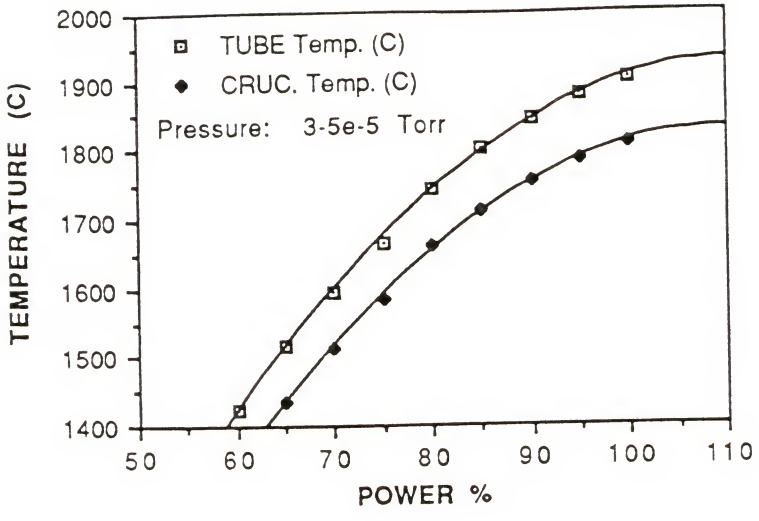

a

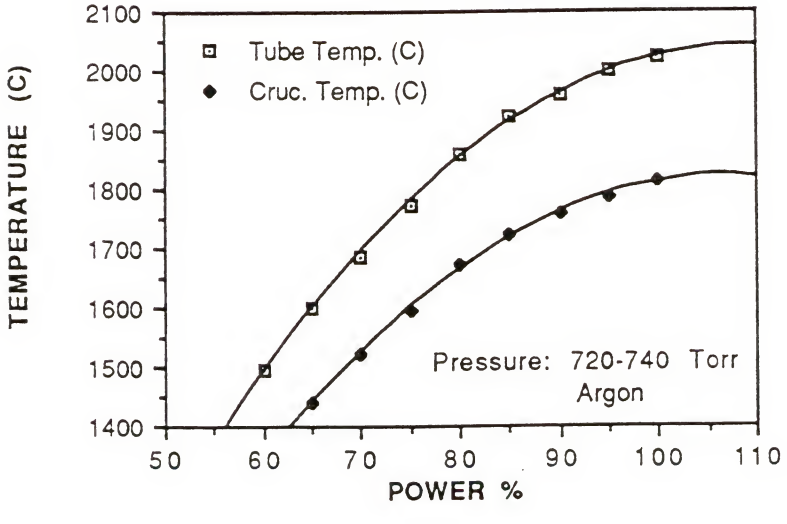

b

Figure 2.8 Temperature Corrections of Tube Crucible System a. Under Vacuum, and b. Under Argon

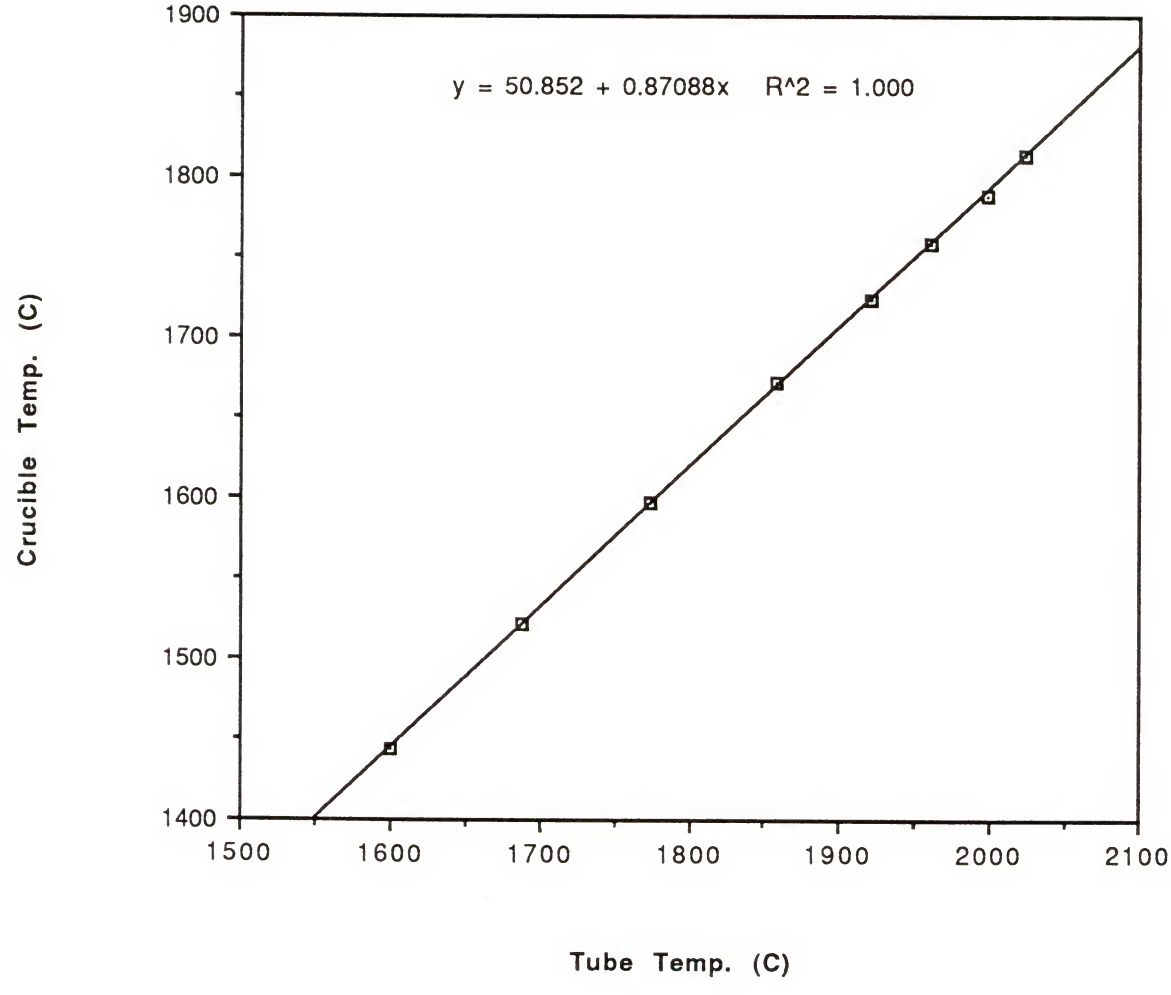

Figure 2.9 Tube and Crucible Temperature Relationship

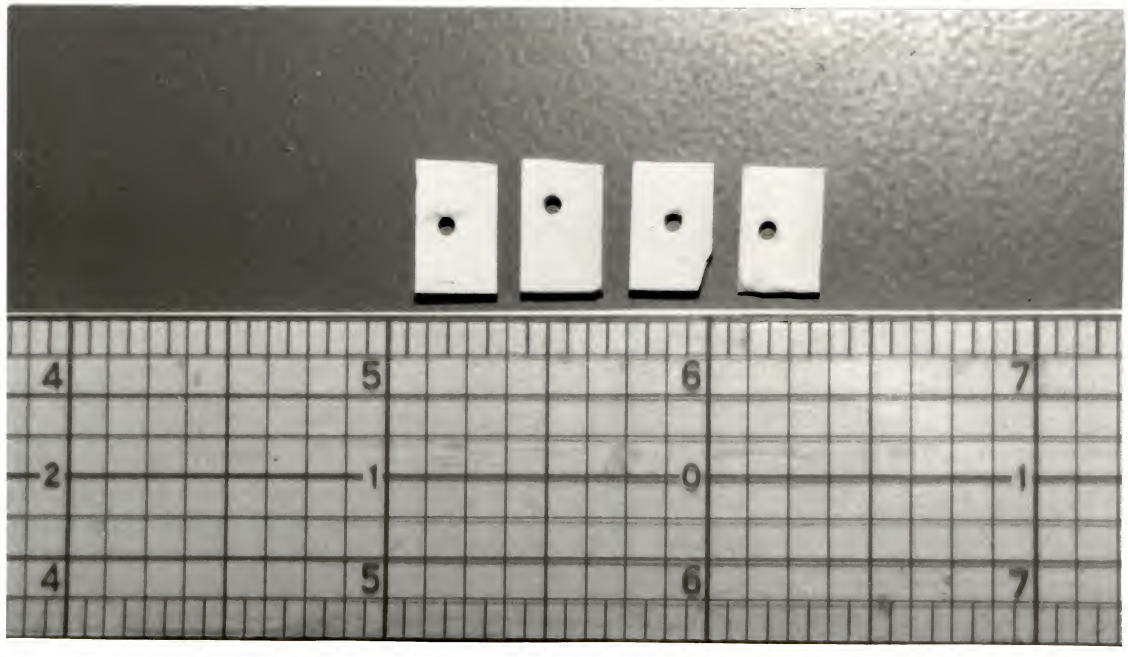

Figure 2.10 Yttria Samples Before the Exposure

Figure 2.11 Mo Tube, Crucible, Handler and Graphite Pedestal

A Mo tube of 2.6 cm diameter was placed then on the top of the pedestal. A thin Mo pin crossing the tube and the pedestal at the bottom provided fixture. This system of tube, crucible, and pedestal then was placed in the reaction chamber at the center of the copper-nickel helical coils. A vacuum range of 10^{-3} Torr first was reached by using a mechanical pump which was connected to a diffusion pump. Subsequently, 10^{-5} Torr was achieved using the diffusion pump. The induction furnace was used to provide the heat necessary to melt UF_4. The copper helical coils and the reaction chamber were cooled by water circulation. In the beginning, a relatively low power rate (20-25%) was used to heat the system to a level such that undesirable residues such as humidity, grease, and oils could be eliminated by evaporation. Then the diffusion pump was disconnected from the system, the reaction chamber was filled with argon until about 600 Torr pressure was reached, and the power was raised to reach the operation temperature. Argon was used for three reasons: (a) to suppress early vaporization of UF_4 due to the drop of its boiling point under high vacuum, (b) to prevent electrons sparking between poles, and (c) to produce a back pressure against outside pressure, hence preventing possible air leakage. In this case, since the boiling point of UF_4 was 1715 K at one atmosphere (atm), the testing temperature was held at 1650 K and 1740 K at about 0.8 atm pressure for two different sets of experiments.

As a first step, the argon pressure was measured with equal time intervals at the operating temperature without the presence of UF_4 and the sample. As a second step, UF_4 was placed in the reaction chamber, and the pressure of argon and vaporizing pressure of UF_4 was recorded. This pressure was established as the reference pressure. The third step was to record the inner pressure, which consisted basically of the partial pressures of argon, UF_4, and gases during the reaction. The difference between reference and reaction pressures provided the partial pressure of the reaction gases. The test sample was squeezed between two parallel thin sheets of Mo that were attached to a moveable handlebar. The sheets were doubly wrapped at the side of the sample in order to keep the sample firmly in place without damage (Figure 2.12) This method of adjustment pictured in Figure 2.12 facilitated the removal of the tested sample and the insertion of the new one for the following test. During the experiment, after the initial vacuum (10^{-5} Torr) was reached, temperature was increased in two steps. In the first step, a certain time was allowed (about 1/2 hour) for UF_4 to melt at about 300°C over its melting point. During this soak period, due to the gas expansion, the inner chamber pressure was increased. The second step was to raise the temperature above the boiling point of UF_4. After the testing temperature was reached, the inner pressure was adjusted to equal the initial reference pressure. Then the yttria sample, which was initially held

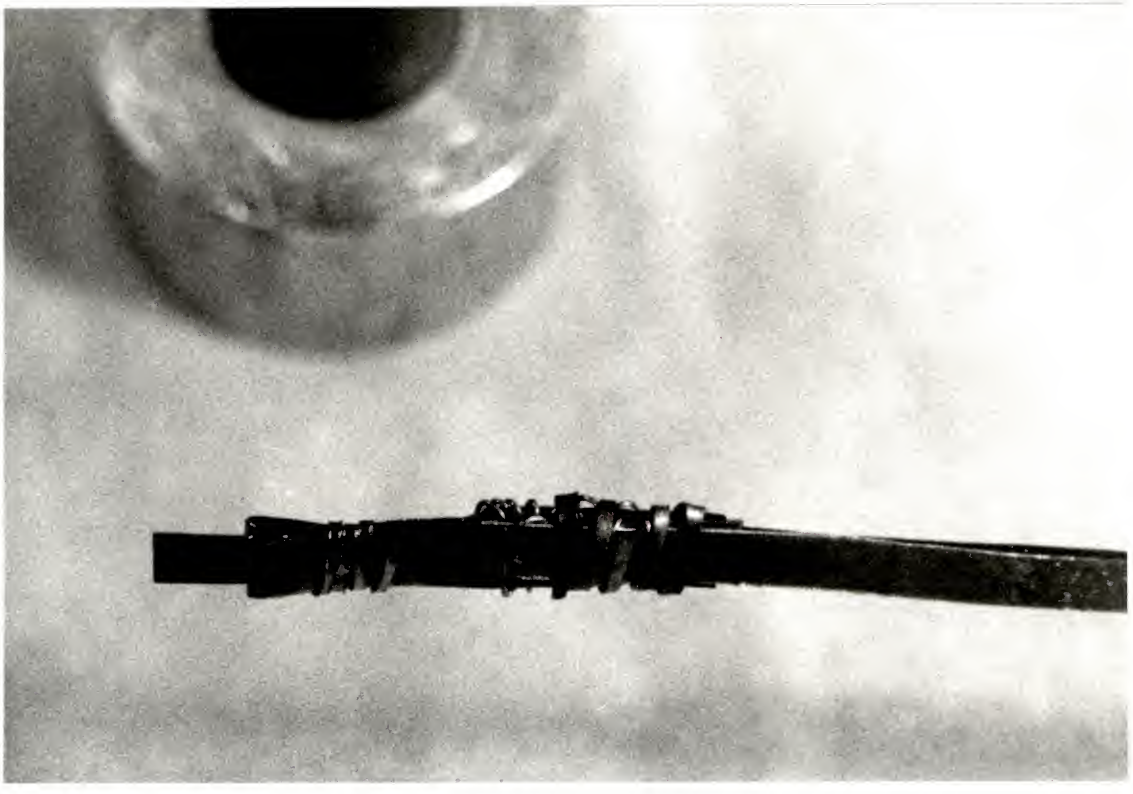

Figure 2.12 Doubly Wrapped Mo Sheets Holding the Mo Sample

far above the surface of the UF_4, was placed 0.312 inches above the boiling liquid where the vaporizing UF_4 was flaring its surface. At the end of the exposure, the sample was pulled back and the output power was turned off. In order for the sample to receive the same amount of gas flux, it was important that the same distance over the boiling liquid be maintained in each experiment. However, since UF_4 reacted with the sample or was condensed on the Mo wall, there were losses which increased the actual distance between the sample and the liquid after each experiment. At the end of the test, it was observed that the UF_4 level was below the

maximum heating zone. This zone was identified as the shiny white zone on the Mo tube located at the center of the helical heating coils (Figure 2.13). Reacting UF_4 with yttria showed more experimental accuracy and data control than UF_6 exposure. This was due to the compactness of the testing system and the easy manipulation of the sample before and after testing. At the end of the test, it was observed that the bottom portion of the sample was ellypsoidal in shape, while the upper portion more or less retained its original form (Figure 2.14). It was concluded that this was due primarily to the surface tension and gravitational forces acting on the sample. Another reason could have been that the bottom portion received more UF_4 vapor flux than the sides. In order to eliminate this situation, smaller samples were prepared. They were attached to a Mo wire hanging over the liquid during the experiment. At the end of a series of tests, it was again observed that the samples formed a product layer of ellypsoidal shape in the form of a droplet. This proved our initial assumption.

In order to expose the sample to liquid or gaseous UF_4, the handlebar of the chamber could move vertically along the tube without affecting the vacuum during the experiment. Both the chamber and its cover were made of stainless steel, and copper-nickel circular seals were used to join them.

During the experiment, UF_4 vapors were condensed on the walls of the molybdenum tube. Liquid droplets descended to

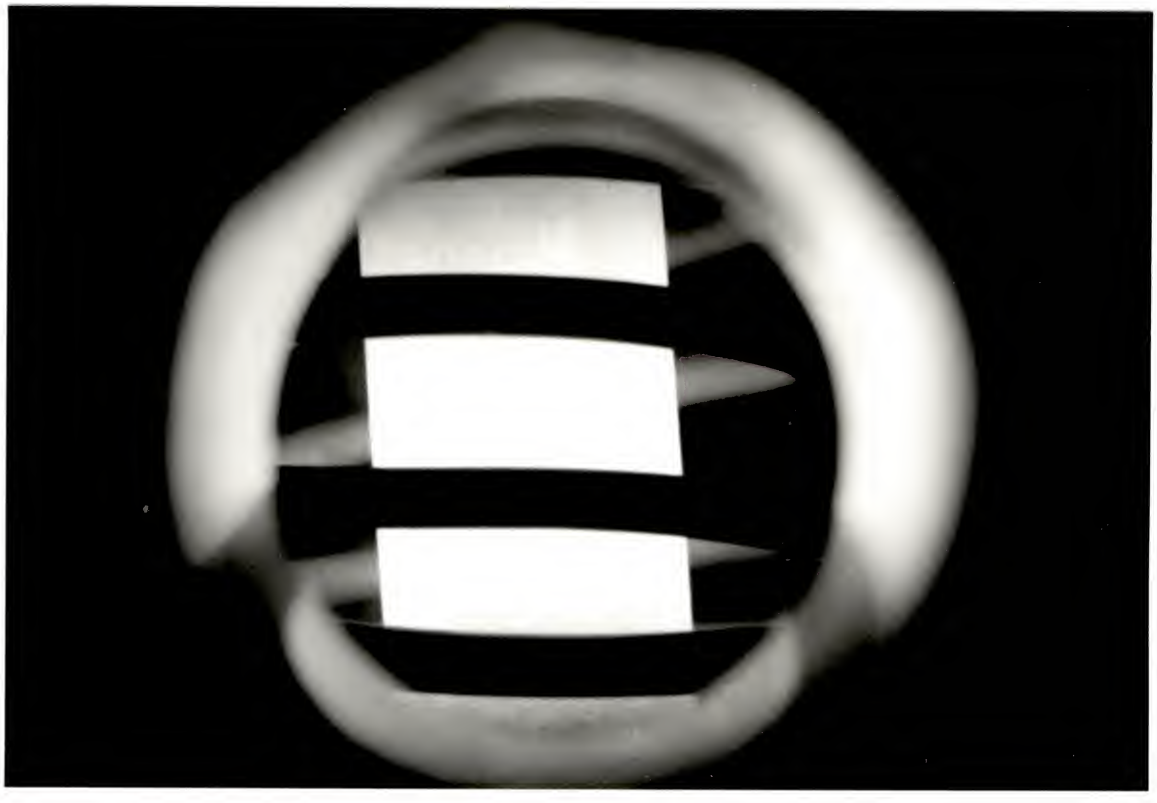

Figure 2.13 View of the Central Heating Zone

Figure 2.14 Yttria Samples Before and After the Reaction

the bottom due to gravity and vaporized again, providing a continuous circulation. Because of the immediate condensation on the walls, very small amounts of uranium tetrafluoride contaminated the chamber walls outside of the Mo tube. The sample weights were measured before and after both liquid and gas phase testing, using a digital microbalance.

2.2 Exposure of Molybdenum to UF_4

Thermodynamical data of the chemical reactions between UF_4 and different materials were obtained using a computer code for analysis of chemical thermodynamics, FACT (40). According to the computational analysis, Mo showed good compatibility under the operating conditions; in addition, due to its high melting point (2610 K) and low neutron absorbtion cross section (0.20 barn), Mo was thought to be one of the candidate materials for space power and propulsion applications.

During the first set of experiments, the operational temperatures in the crucible were held at 1390 and 1480 K over the melting point of UF_4 (1109 K). In the second set, it was held at 1740, 1825, and 1910 K over its boiling point (1715 K). The corresponding tube temperatures were 1500, 1600 K for liquid phase and 1900, 2000, 2100 K for gaseous phase, respectively. The melting of UF_4 was accomplished in about 1/2 hour at 1480 K. While UF_4 was melting, it shrank significantly; hence, reloading the crucible two or three times was necessary in order to completely fill it with UF_4.

The Mo sample was then attached similarly between the Mo sheets, which in turn was fixed to the end of the moveable handlebar. Following the initial pressure recording, the sample was slowly immersed into liquid UF_4. Sparking and short-circuit can happen if the sample comes in close contact with the wall of the Mo container or if there is not enough inert gas pressure in the chamber. During the exposure at this temperature, the increase in the chamber pressure was recorded with equal time intervals from the transducer. The test procedure was basically the same as the yttria case.

CHAPTER 3
POSTTEST ANALYSIS AND RESULTS

Characterization of the reaction layers was performed using analytical instrumentation techniques such as scanning electron microscopy (SEM), electron microprobe (EMP) analysis, and x-rays diffraction (XRD) analysis, and the results were evaluated phenomenologically.

3.1 Sample Preparation

3.1.1 For SEM and EMP Analysis

After the experiments, prior to the surface preparation, yttria and Mo samples were mounted in cylindrical shaped molds nearly 1 inch in diameter. Two different types of mounting material were used: for Mo samples, 2 parts of powder epoxy resin was mixed with 1 part of acrylic plastic liquid ingredient obtained from Fisher, Inc.† The mixture was mixed about 2 minutes until the solution became homogeneous and viscous enough to fill the edges of the sample. Exhotermic reactions occur at this stage, and heat evolution accompanies the solidification.

Yttria samples, due to their fragile reaction product layers, required more care than the Mo samples. Relatively

† Fisher Scientific, Inc., Fairlawn, NJ.

lower viscosity epoxy resin was used to mount the samples. From Fisher, Inc., low-viscosity 5cc methyl methacylate (CH_2:C(CH_3)$COOCH_3$) was mixed with 9 mg 2,2'- Azobis [2-methyl-propionitrile] ((CH_3)$_2$C(CN)N:NC(CN)(CH_3)$_2$). The sample was placed in a glass container and then the epoxy was poured into it. Next, containers were held in the electrical furnace at 65°C for about 7-8 hours.

In order to observe and analyze the microstructure, reacted samples must be sectioned, ground, and polished to make the surface flat and clean. Grinding was performed using 60, 120, 240, 320, 400, and 600 grades abrasive paper in sequence. Then, with vibrators, polishing was accomplished down to 1 micron using diamond powder. Prior to the SEM analysis, ceramic samples were carbon coated in order to make them conductive.

3.1.2 For XRD Analysis

X-rays diffraction analysis used a powder diffraction technique in which the samples were ground under 30 μ size. Characteristic X-rays generated from a copper target (Cu K) were collimated onto the powder, where they were diffracted at specific angles from the crystal planes of the samples. Computer analysis provided the diffraction angles, corresponding interplane spacings and relative intensities, and a list of possible compounds. For this reason, yttria samples were ground into powder after the exposure and then were stuck on a piece of slit with the aid of amyl acetate.

3.2 Characterization of the Reaction Layers After UF_6 Testing

3.2.1. Weight Change Analysis

Table 3.1 shows the results of weight change analysis of yttria samples after being exposed to UF_6 at 1173 K. Table 3.2 gives the hot press results for different temperature, pressure, and time conditions. The weight change of the samples was measured before and after the test using a digital micro-balance with an accuracy of 5 decimal points. In general, a weight increase was observed for both ytt85 and ytt99 samples for different testing times at 1173 K.

Table 3.1 UF_6 Reacting with Yttria at 1173 K

DENSITY %	TEST TIME (Min)	WEIGHT BEFORE (g)	WEIGHT AFTER (g)	W.CHANGE (g/cm^2)
85	5	0.3023	0.3794	0.0194
85	10	0.4694	0.5020	0.0181
85	15	0.2470	0.2700	0.0228
85	20	0.2184	0.2823	0.0600
85	25	0.2654	0.3494	0.0690
99	20	0.3487	0.5146	0.1120
99	25	0.5235	0.7709	0.1250

Table 3.2 Hot Press Results of Yttria Samples

TEMPERATURE C	PRESSURE MPa	TIME Min	THEO.DENSITY %
1700	30	10	88.30
1600	45	40	98.14
1600	40	90	99.45

The dissociation of UF_6 to F_2 and other lower compounds such as UF_4 over 1000 K and 760 Torr conditions (1) suggested that the extensive corrosion was due to the reaction of multitype gas molecules rather than a single specie UF_6. The

results of the weight change analysis (Figure 3.1) were used in the parabolic rate law formula derived for oxidation in order to obtain an approximate value of the rate constant of the yttria reaction with UF_6. Parabolic rate law formula is given as follows:

$$(\Delta W^*)^2 = Kt \qquad [3-1]$$

where $\Delta W^* = \Delta W/(W_i/A)$, ΔW^* = Dimensionless quantity

and ΔW = Weight change/A , Wi = Initial weight (g),

A = Surface area (cm^2), t = time (min)

From the slope of the line in Figure 3.1, rate constant K was found to be 0.00562 (min^{-1}). The sharp weight increase at 20 and 25 min and the complete decomposition of the sample for testing times greater than 1 hour showed that the film failure temperature of yttria was below 1423 K which is reported in a previous work (31). This might be due to the higher UF_6 pressures and to the flowing UF_6 rather than stagnant low pressure UF_6 (87 Torr) which was used in the past experiments (31). In addition, nearly 15% porosity might have some effect in the accelerated failure of the samples. For exposure less than 15 min, samples maintained their shape, and a relatively thin black product layer formed on the surface. After 20 and 25 min exposures, samples were almost decomposed following cracking and spallation (Figure 3.2). The sharp weight increase was probably due to the initiation of the cracks allowing the gas insert and react further with the sample.

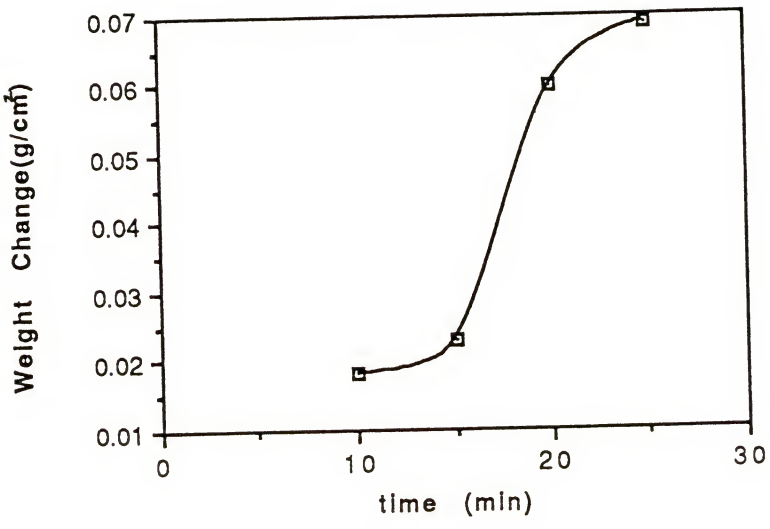

Figure 3.1 Weight Change Analysis of Yttria Samples of 85% Theoretical Density

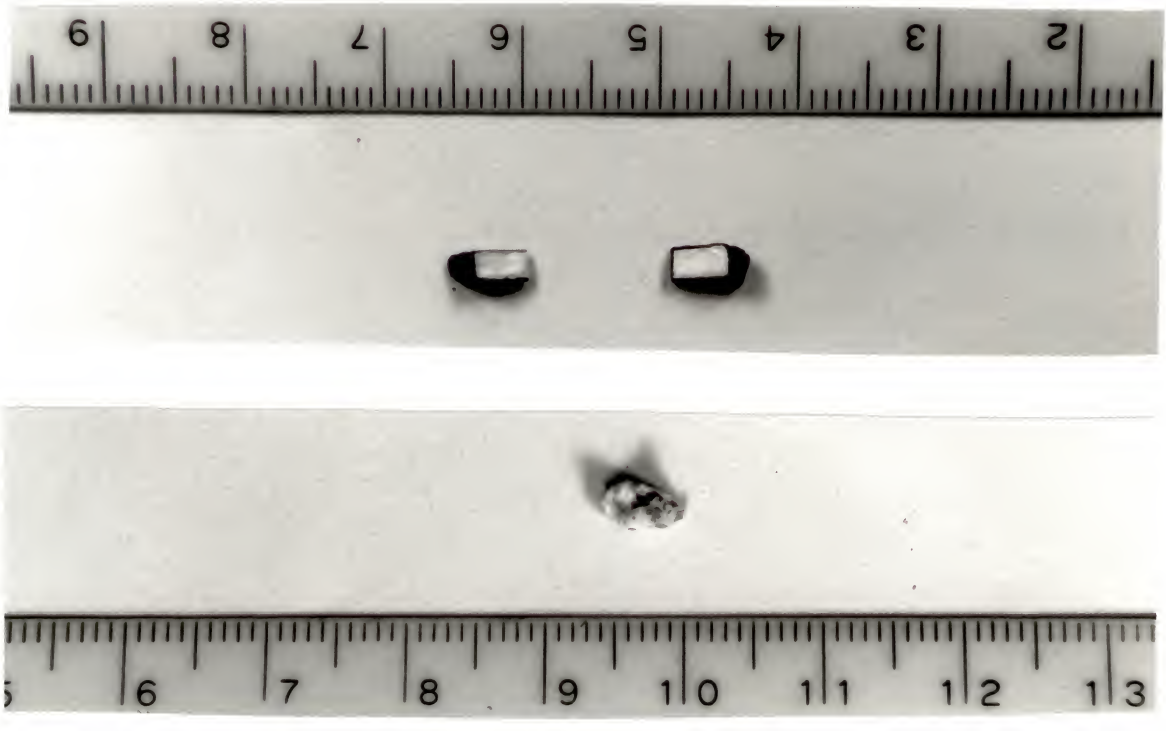

Figure 3.2 Yttria Sample After Being Tested in UF_6 at 1173 K a. 10 min. exposure b. 25 min. exposure [in cm]

3.2.2. SEM-EMP Analysis

At the end of the SEM analysis, it was observed that a soft, porous scale was formed followed by an inner layer (Figure 3.3). The EMP analysis was completed after scanning the sample for a total of 100 micrometers, with 20 equal steps. The measured elemental concentration profiles are plotted with reference to their micrographs as shown in Figures 3.4, 3.5, and 3.6.

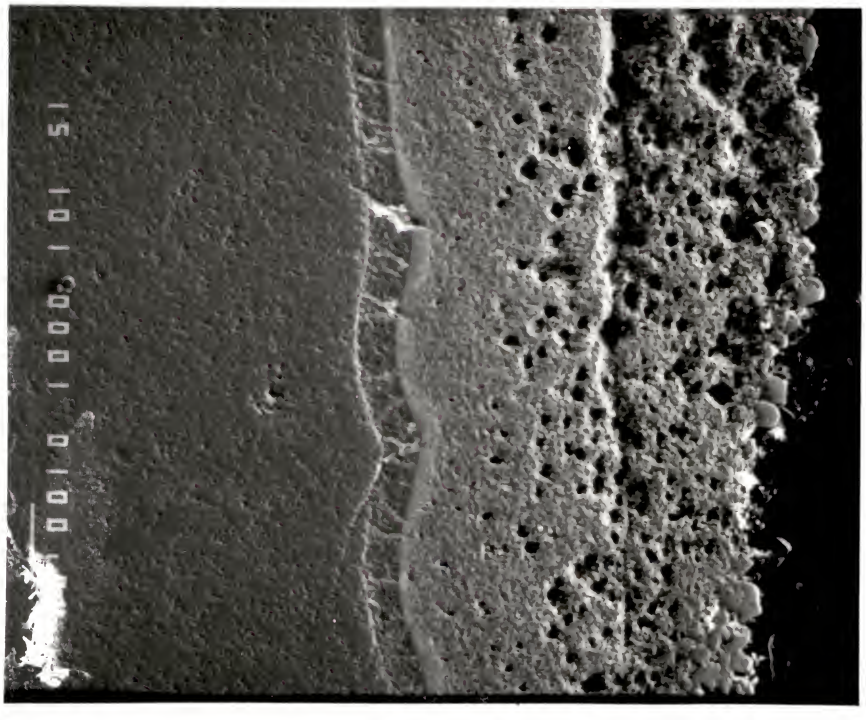

Figure 3.3 SEM Micrograph of Yttria Sample Exposed to UF_6 at 1173 K for 10 min; Outer Layer, Inner Layer, and Yttria Substrate

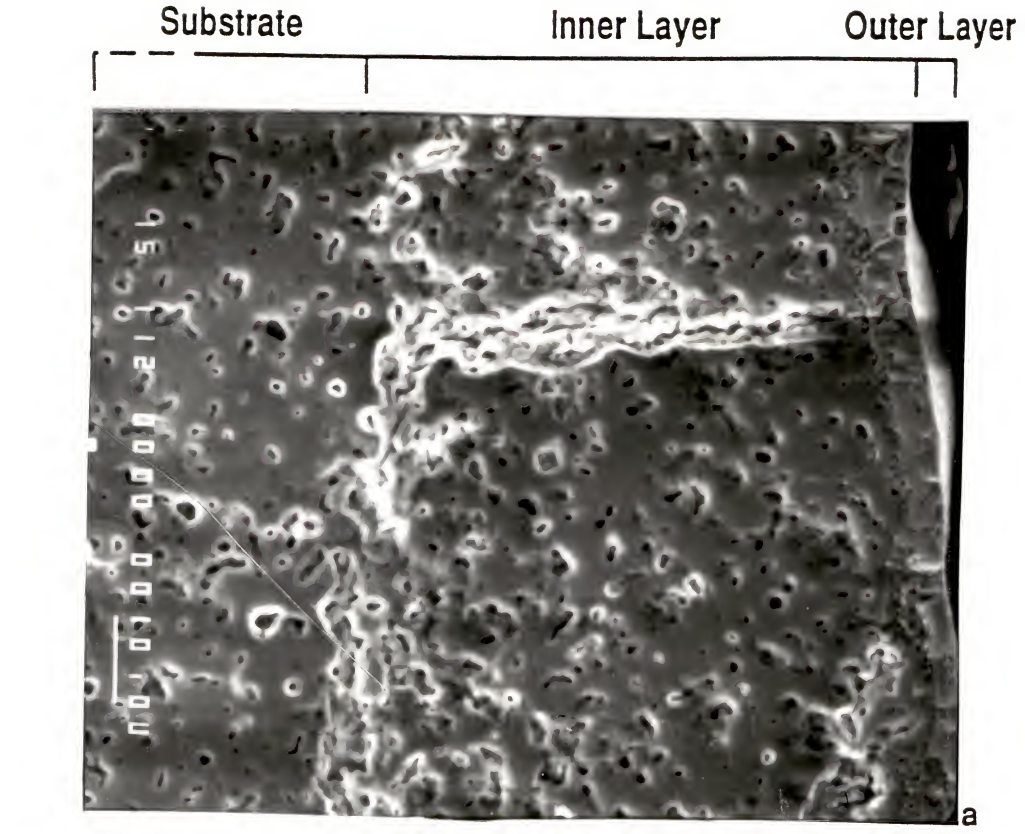

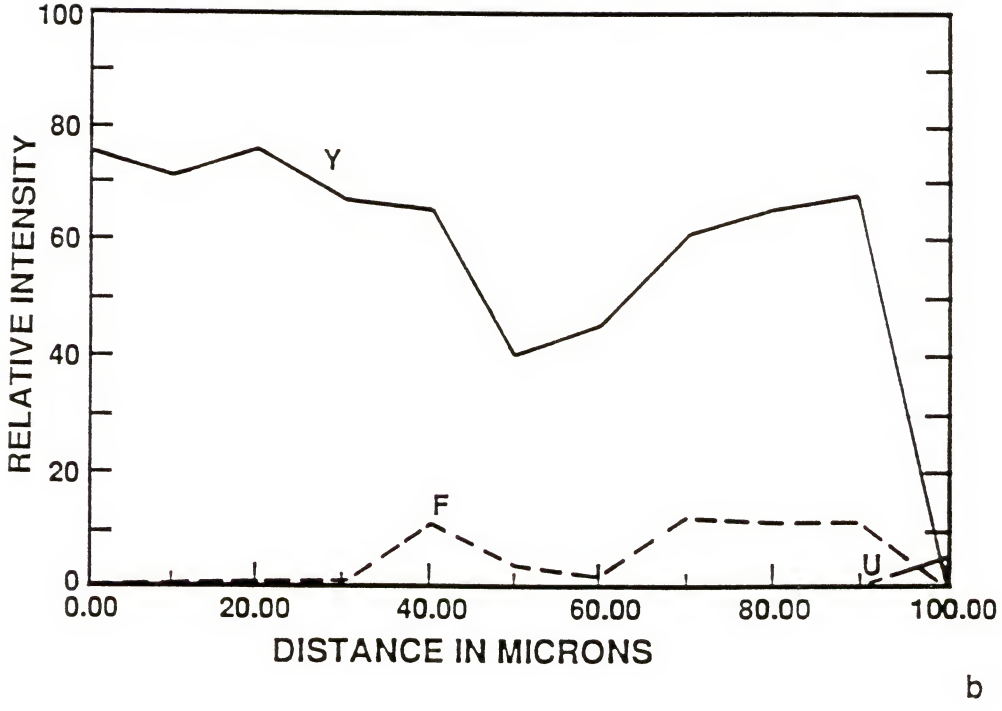

Figure 3.4 EMP Analysis of a Ytt85 Sample Exposed to UF_6
a. Cross Section of the Sample Tested for 5 min at 1173 K
b. Concentration Profiles

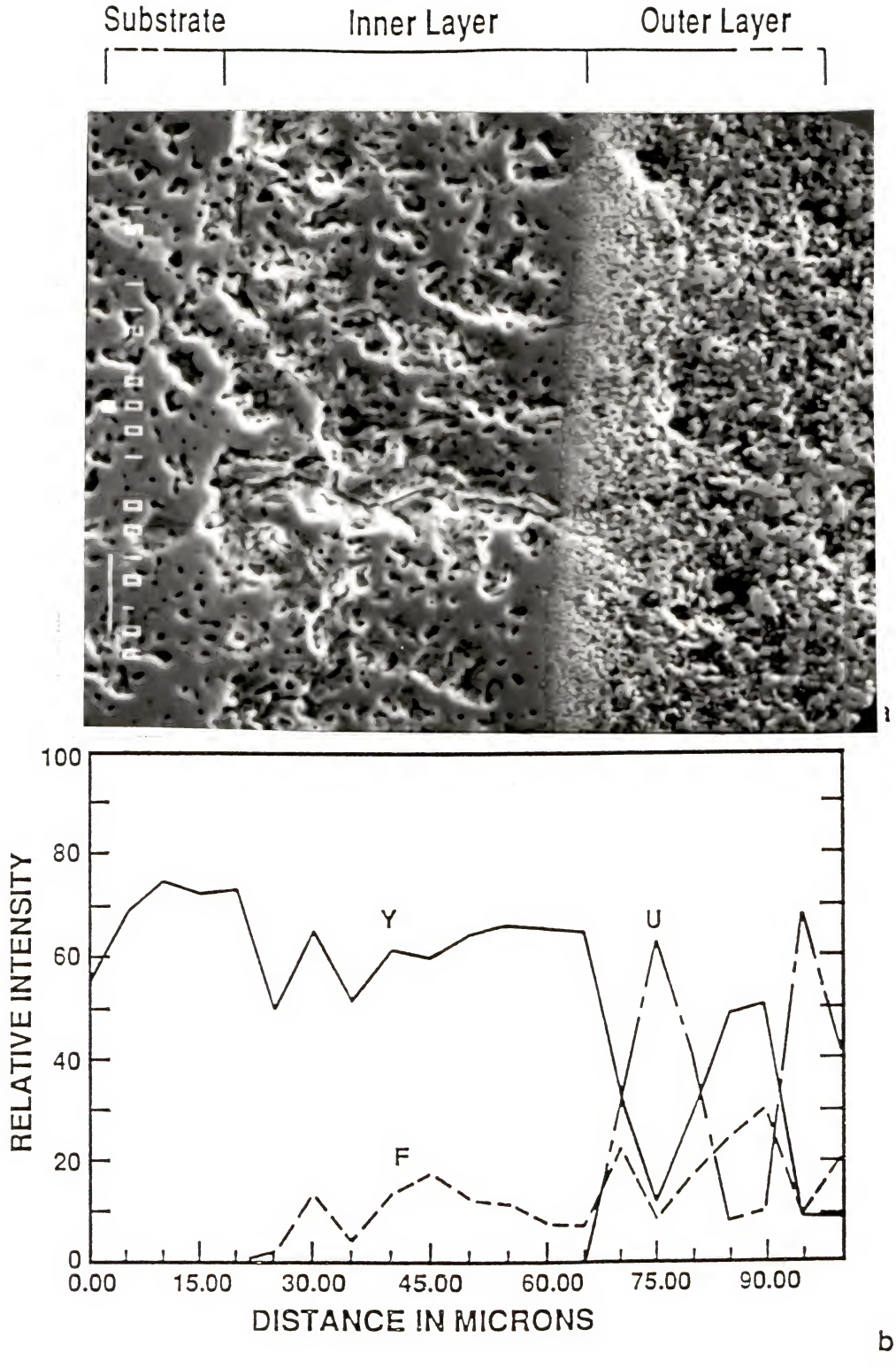

Figure 3.5 EMP Analysis of a Ytt85 Sample Exposed to UF_6
a. Cross Section of the Sample Tested for 10 min at 1173 K
b. Concentration Profiles

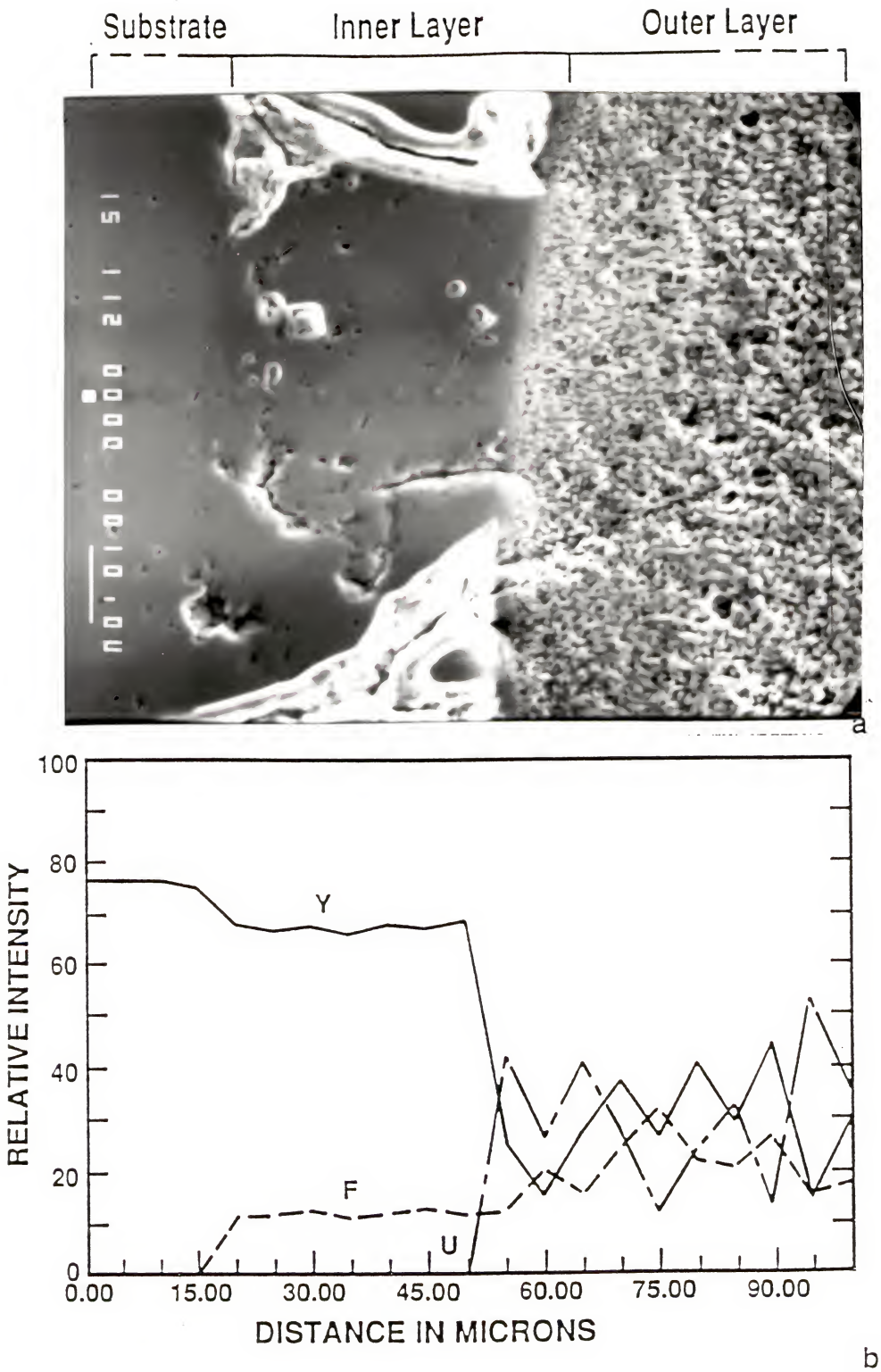

Figure 3.6 EMP Analysis of a Ytt85 Sample Exposed to UF_6
a. Cross Section of the Sample Tested for 20 min at 1173 K
b. Concentration Profiles

The elemental analysis by EMP established the formation of two layers of reaction products with different chemical constituents. As shown in Figures 3.4 to 3.6, the outer layer consisted of yttrium, fluorine, and uranium atoms, whereas the inner contained yttrium and fluorine atoms. The thickness of the inner layer was determined between the end points of uranium concentration at the outer interface (the interface of the inner and outer layers) and the fluorine concentration at the inner interface (the interface of substrate and the inner layer). It was found that the thickness of the inner layer decreased from about 90 to 55 micrometers as exposure time increased from 5 to 20 minutes (Figures 3.4 to 3.6).

3.2.3 XRD Analysis

X-ray analysis identified YF_3, UO_2, a small amount of U_3O_8, and Y_2O_3 as the reaction products. Similar XRD results were obtained for different exposure times. In Figure 3.7, and Table 3.3, the diffraction pattern for a 15 min exposure is given as an example. The standard patterns of the identified components (Y_2O_3, YF_3, UO_2, and U_3O_8) taken from JCPDS reference cards are also provided in Figure 3.7 and Table 3.3 for comparison with the sample pattern. The intensities between the experimental and the standard patterns were not exactly matched due to the overlapping of different compounds.

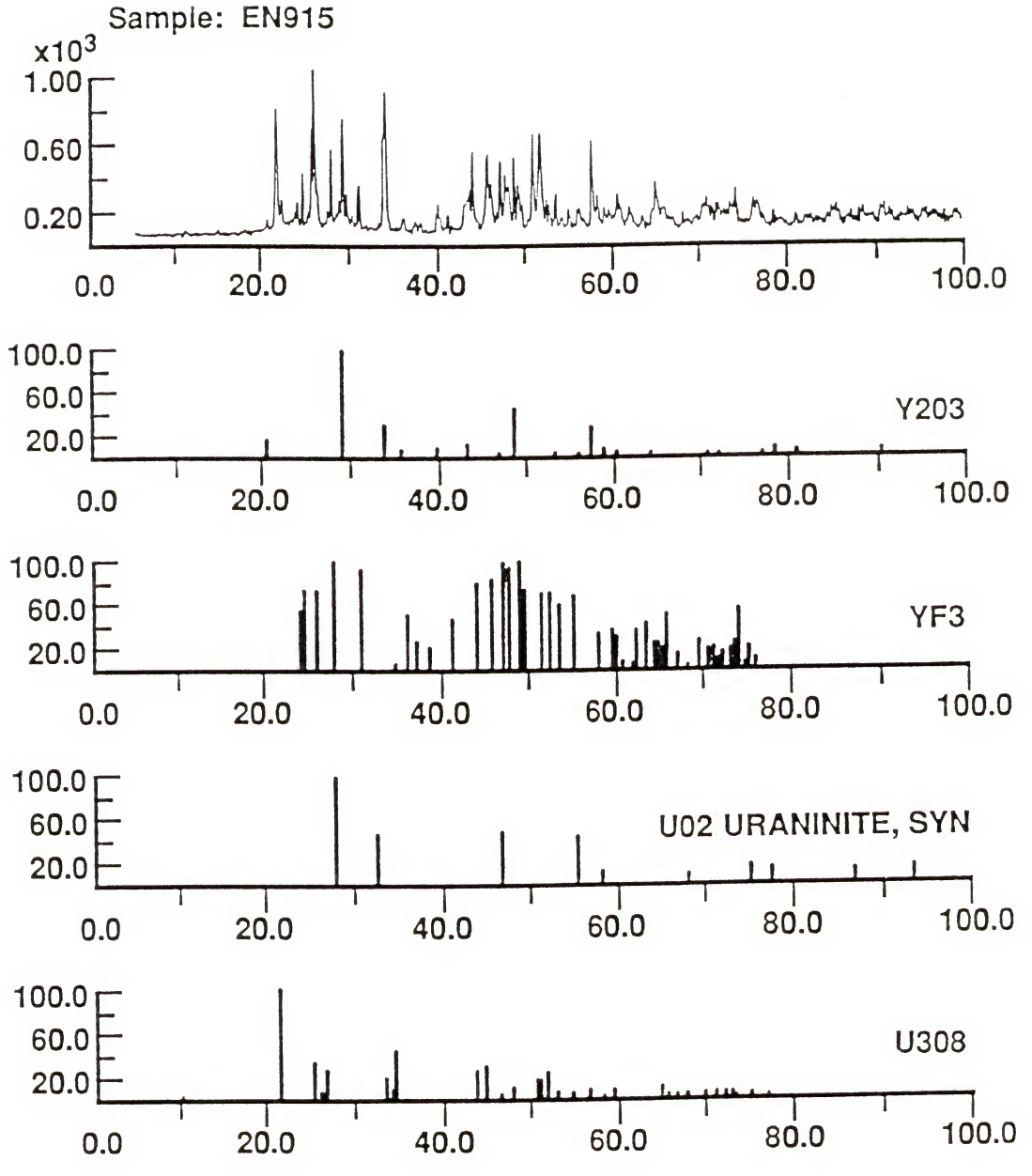

Figure 3.7 XRD Patterns of ytt85 Exposed to UF_6 at 1173 K for 15 min

Table 3.3 X-Ray Diffraction Powder Pattern of the Yttria Sample After UF_6 Reaction

EXPER. 2Ø	I/I_0 %	YF_3 2Ø	I/I_0	UO_2 2Ø	I/I_0	U_3O_7 2Ø	I/I_0
21.555	70.88	24.627	75	28.245	100	28.401	100
21.765	56.12	25.987	75	32.717	48	32.865	30
24.602	31.76	27.885	100	46.943	49	33.204	20
25.652	64.11	30.961	95	55.697	47	47.150	20
25.997	100.00	43.917	80	58.397	13	47.359	25
29.155	64.11	45.619	85	68.539	9	55.844	20
33.247	2.75	46.995	100	75.727	18	56.479	15
33.725	54.08	47.569	95	78.077	15	58.888	15
34.000	86.04	49.043	100	87.297	13	68.653	5
43.505	23.81	49.498	70	94.146	15	69.642	5
43.900	43.99	51.421	70	105.61	6	75.870	10
45.437	45.83	52.310	70	112.95	15	76.372	10
50.787	52.08	53.409	60	115.46	8	78.077	10
51.595	57.16	54.990	70	125.87	9	79.079	10
57.567	42.63	57.899	35	134.92	7		

3.2.4 Thermodynamic Analysis

The prediction of possible chemical reactions and end-products at certain combinations of temperature and pressure was performed by the Facility for the Analysis of Chemical Thermodynamics (FACT) (40) computer data base and code package. In particular, the equilibrium program (EQUILIBR) was used to analyze the reactions of UF_6, UF_4, and F_2 with yttria at 1173 K and 278 Torr (0.365 atm) average pressure. This program determines the molar concentrations of product species when specified elements or compounds react to reach chemical equilibrium. The calculation of the equilibrium concentra-tion is based on the minimization of the total free energy formation in the system. The EQUILIB program is designed to solve chemical equations for up to twenty reactants with a maximum of 12 elements. The reactants, reaction temperature, and total pressure (or volume) need be entered only as input data. The code automatically generates a list of all possible stoichiometric compounds found in the program data base as well as in the user's private input data. All possible compounds with a concentration larger than 10^{-5} mole are considered in the equilibrium calculation. The program then predicts the combination of reaction products which is most stable at the specified temperature and pressure. At 1173 K and 0.365 atm. pressures, FACT analysis showed that UF_6 was favored to react with Y_2O_3 at the given conditions to form YF_3, U_3O_8, UO_2 in solid phase and O_2 in gas phase. Similarly, UF_4 reacting with yttria forms YF_3,

UO_2, Y_2O_3 in solid phase, and F_2 reaction with yttria releases YF_3, Y_2O_3 in solid phase and O_2 in gas phase. Results are presented in Table 3.4.

Table 3.4 Thermodynamic Results of UF_6 Reaction with Y_2O_3 at 1173 K and 0.365 atm Pressure

REACTANTS MOLE	PRODUCTS	STATE	CONCENTRATION MOLE
UF_4 (1)	UO_2	Solid	1.
Y_2O_3 (1)	YF_3	Liquid	1.3333
	Y_2O_3	Solid	0.3333
F_2 (1)	YF_3	Liquid	0.66667
Y_2O_3 (1)	O_2	Gas	0.99986
	Y_2O_3	Solid	0.66667
UF_6 (1)	O_2	Gas	1.
Y_2O_3 (1)	YF_3	Solid	2.
	U_3O_8.	Solid	0.33333

According to the X-ray and thermodynamic results, the chemical reactions occuring are as follows:

at the inner-outer interface,

$$3UF_6(g) + 3Y_2O_3 \text{ ----> } 6YF_{3(s)} + U_3O_{8(s)} + 0.5\ O_2(g) \quad [3\text{-}2]$$

$$3UF_4(g) + 2Y_2O_3 \text{ ----> } 3UO_{2(s)} + 4YF_{3(s)}, \quad [3\text{-}3]$$

also, a possible reaction according to literature (32,41)

$$F_2 + O_2 + 4UO_{2(s)} \text{ ----> } UO_2F_{2(s)} + U_3O_{8(s)}, \quad [3\text{-}4]$$

and at the inner layer-substrate interface,

$$3F_{2(g)} + Y_2O_3 \text{ ----> } 2YF_{3(s)} + \frac{3}{2}\ O_2(g). \quad [3\text{-}5]$$

3.3 Characterization of the Reaction Layers After UF_4 Test

The Y_2O_3 sample (85%) which was exposed to the liquid UF_4 at 1220 K showed 0.167(g/cm^2) weight change in 1 minute. This value is much higher than the data obtained from the

exposure of gaseous UF_6. Also, a small piece of yttria crystal which was 100% close to theoretical density was tested in liquid UF_4 at 1480 K. It was observed that the sample reacted completely, after 5 min.

In the gas phase of UF_4, two set of experiments, one at 1650 K and the other at 1740 K at nearly 84.6 KPa (635 Torr, 0.835 atm), were performed from 5 to 40 min.

3.3.1 Weight Change Analysis

The results of these experiments are given in Figure 3.8. In both cases, the weight change by time showed an increase in 5, 10, and 15 minutes, while it decreased for longer times. Eventually, samples were lost completely. The samples used at operating temperatures 1650 and 1740 K were originally different in size. Hence, a small difference in weight gain was found between the two experiments. However, Figure 3.8 reveals the similar trend of the weight gain for both temperatures. The argon pressure during the experiments is given in Figure 3.9. It was observed that no significant rise in pressure was recorded due to the chemical reactions during the experiments. The pressure increased due to the expansion of the argon gas while the temperature was rising. The curves which had nearly equal initial pressures were almost overlapped as expected.

3.3.2. SEM Analysis

In general, the formation of three consecutive layers

has been observed with SEM[††] : a) outer layer b) center layer, and c) inner layer. Below, Figure 3.10 shows the polished cross section of the yttria sample at 50 times magnification exposed to gaseous UF_4 at 1740 K for 40 min .

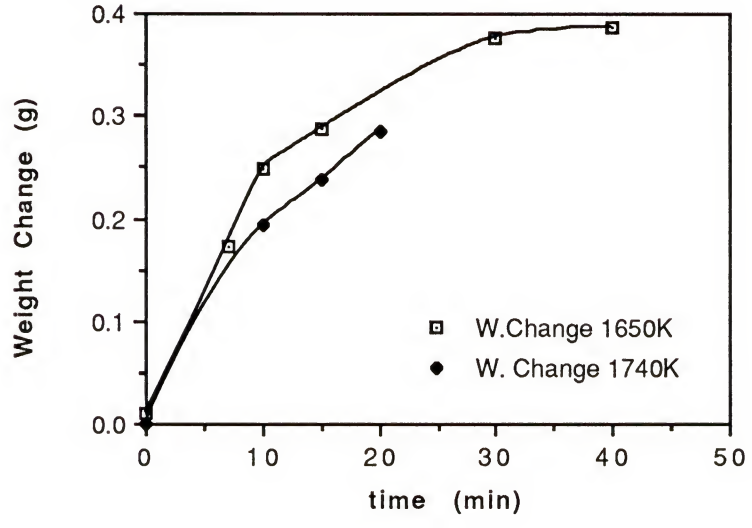

Figure 3.8 Weight Change of Yttria Exposed to UF_4

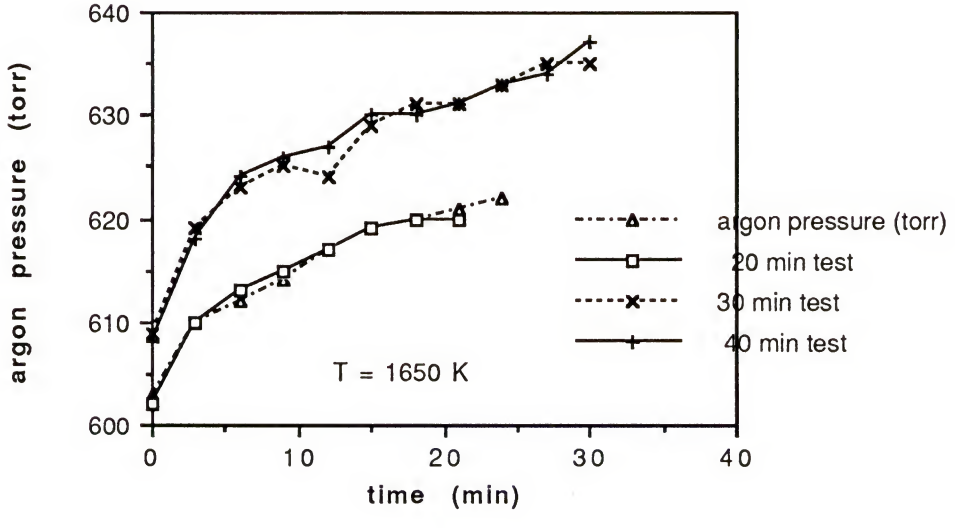

Figure 3.9 Pressure Change During the Test of Yttria in UF_4

[††] JSM-6400 Scanning Microscope, Tracor Northern Comp. Sys.

Figure 3.10 Cross Section of the Yttria Sample Tested in UF_4 in Gas Phase at 1740 K for 40 min

A primary dendritic phase formation, a secondary phase surrounding the primary phase, and a eutectic phase were observed in the outer layer. Figure 3.11 taken in backscattering mode shows that the center layer and the primary dendrites have the same degree of contrast, whereas the eutectic phase is barely distinguishable. A picture taken at 650 magnification on the broken cross section shows the granular structure of the center layer (Figure 3.12-a). The finely dispersed eutectic phase and secondary dendrites are clearly visible in Figure 3.12-b taken at 500 mag.

3.3.3 Optical Microscope Analysis

Observations made using a Zeiss optical microscope showed that the reaction layers grew thicker as the exposure time increased. Figure 3.13 shows a four consecutive sample exposed for 10, 15, 20, and 30 min at 1650 K. Figure 3.14 shows a scheme of the moving reaction boundaries. The distances were measured using a micrometer connected to the optical microscope. It was observed that for most of the samples the reaction boundaries moved outward and the sample increased in volume. From the scheme, the approximate interface velocities were found to be 0.6μ/min for UO_2-Liquid interface and 100μ/min for the Liquid-Vapor interface. The growth rate measurements are given in Figure 3.15a-b. The inner layer grows faster than the center layer at both temperatures.

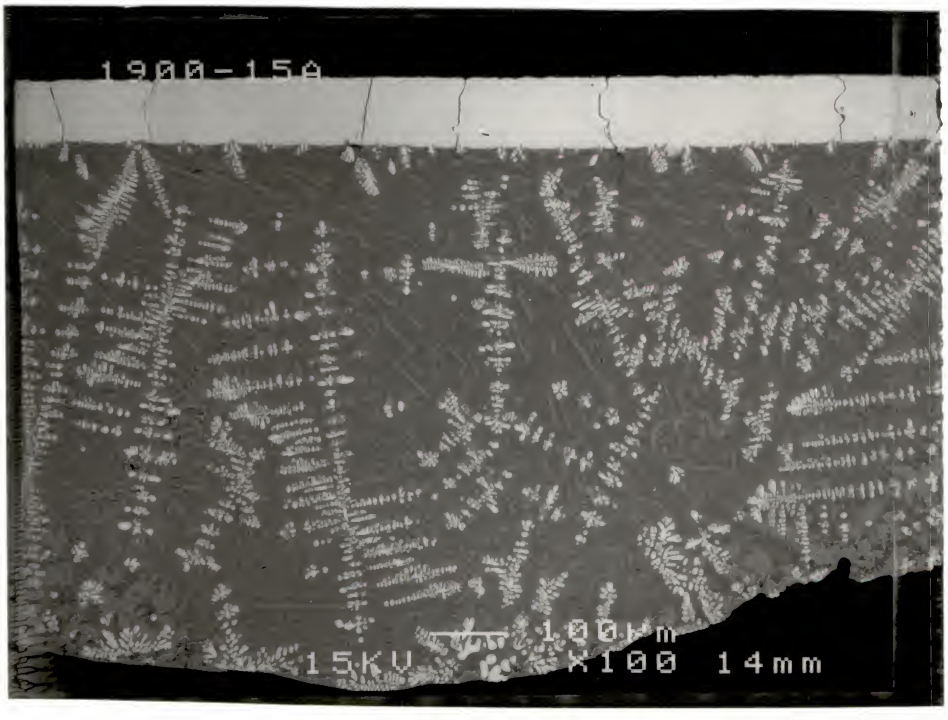

Figure 3.11 SEM Micrographs Taken in Backscattering Mode at 650 mag; Layers with Dendrites and Eutectic.

Figure 3.12 SEM Micrographs of a Yttria Sample Tested in UF_4 at 1650 K for 20 min
a. broken cross section of the center layer
b. secondary dentrites, peritectic and eutectic phases in the outer layer

Figure 3.13 Optical Micrographs Taken at 50 mag of the Yttria Samples Exposed to UF_4

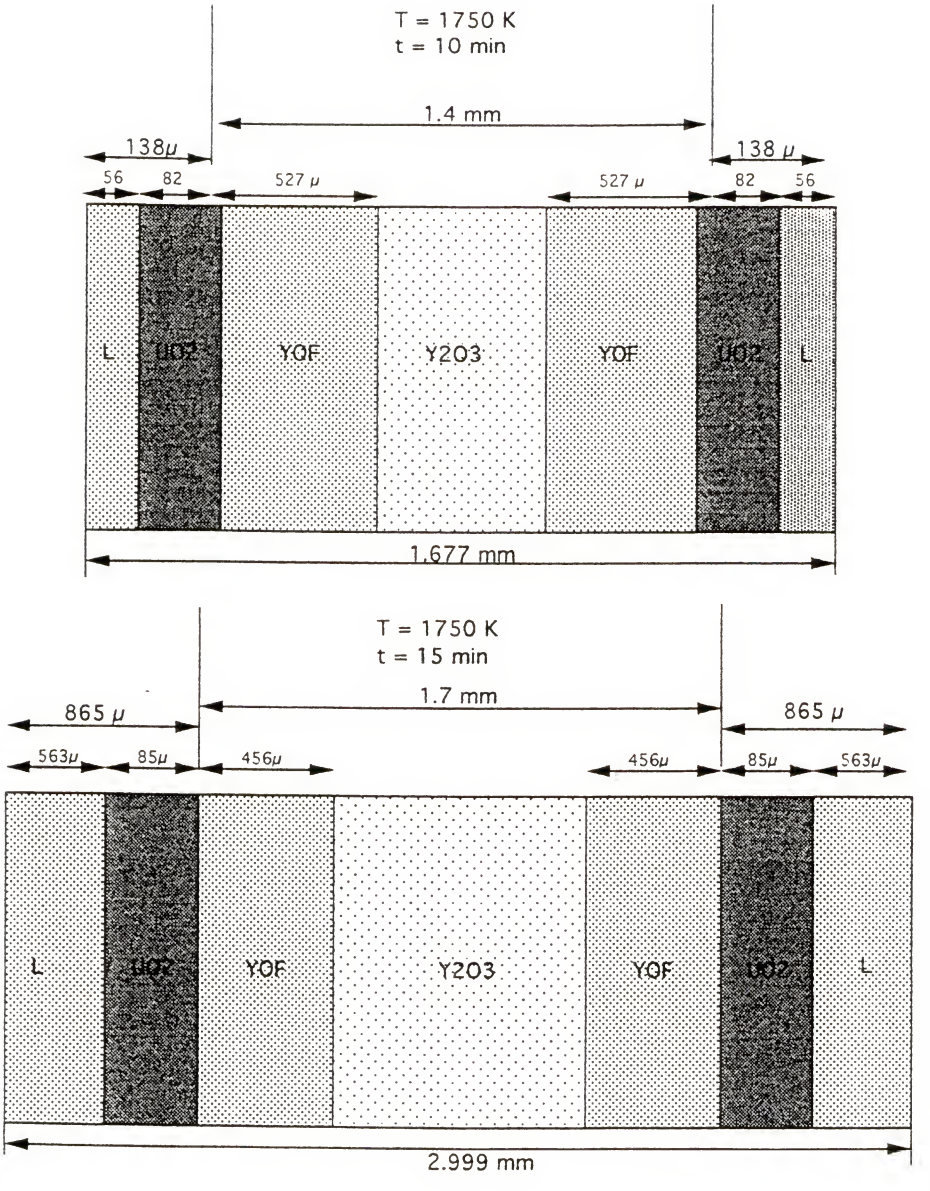

Figure 3.14 Reaction Layers and Original Sample Dimensions for 10 and 15 min Tests at 1750 K in UF_4

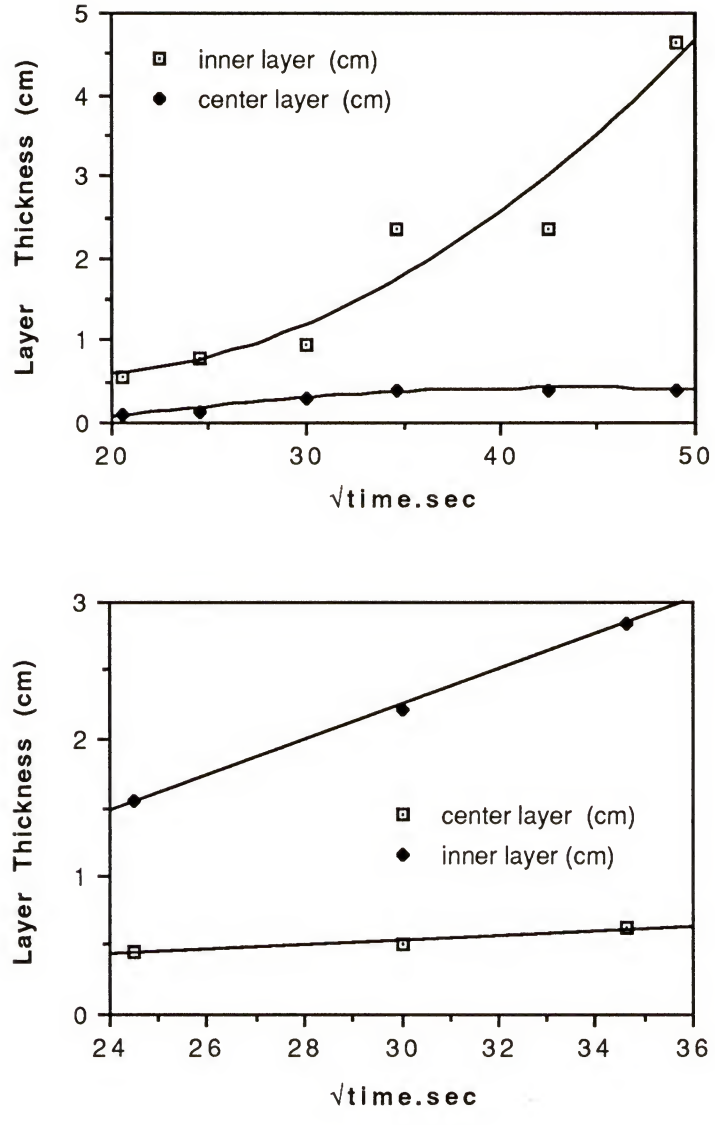

Figure 3.15 Growth Rate of the Layers at 1650 K and 1740 K
a. At 1650 K b. At 1740 K

At 1650 K (or 1800 K, which is measured tube temperature), the center layer growth is parabolic, which explains that the growth is diffusion controlled. The almost exponential growth of the inner layer is due to the easy exchange of oxygen and fluorine ions in the lattice during the diffusion; then the inner layer forms and grows with further diffusion and reaction of fluorine with the yttria matrix. The rate constant k of the inner layer is found to be about 10 times larger than the center layer at 1740 K.

$K_{inner} = 6.45 \times 10^{-4} \frac{cm}{sec}$ and $K_{center} = 8 \times 10^{-5} \frac{cm}{sec}$

3.3.4 EMP Analysis

EMP analysis† was performed on the reaction layers after samples were polished down to 1μ size. The result of a scan across the outer, center, and inner layers of a sample exposed to UF_4 at 1740 K for 20 min is presented in Figure 3.16. The spikes seen were due to the presence of mixed phases in the outer layer and also partly due to the porous nature of the sample. It was found that the eutectic phase was composed of a mixture of dark and gray plate-like layers. The composition of dark regions were $Y_{11}U_{7.8}F_{80}$ or nearly $YU_{1-x}F_8$, and gray regions were composed of $YU_{3.5}F_{12}$ or nearly YUF_7 (3,41). The peritectic region surrounding the secondary dendrites was formed by gray layer with identical composition (YUF_7). The dendrites and the center layer were

† Jeol Superprobe 733, Tracor Northern Computer System

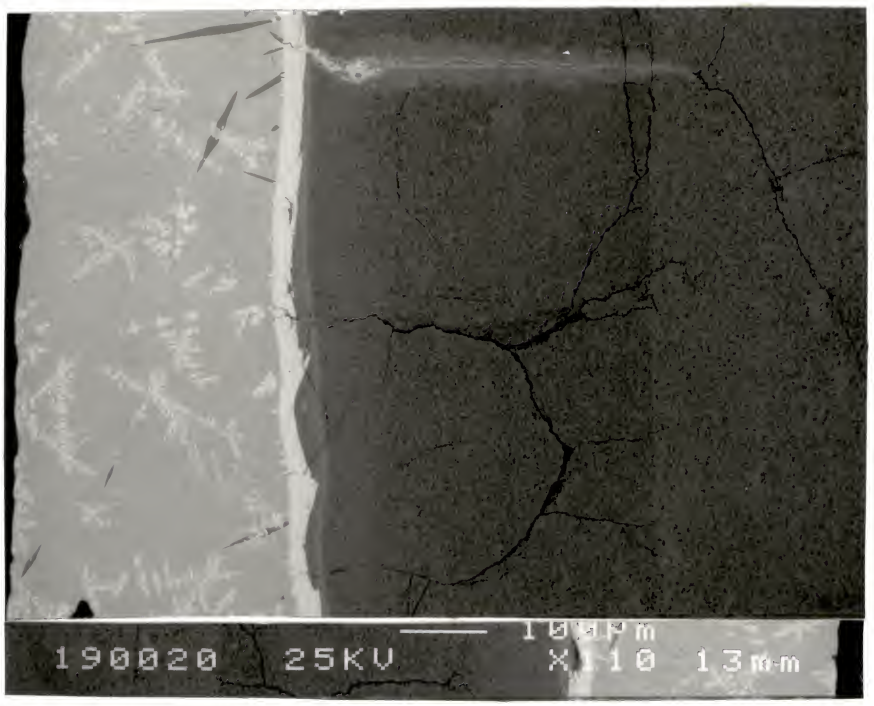

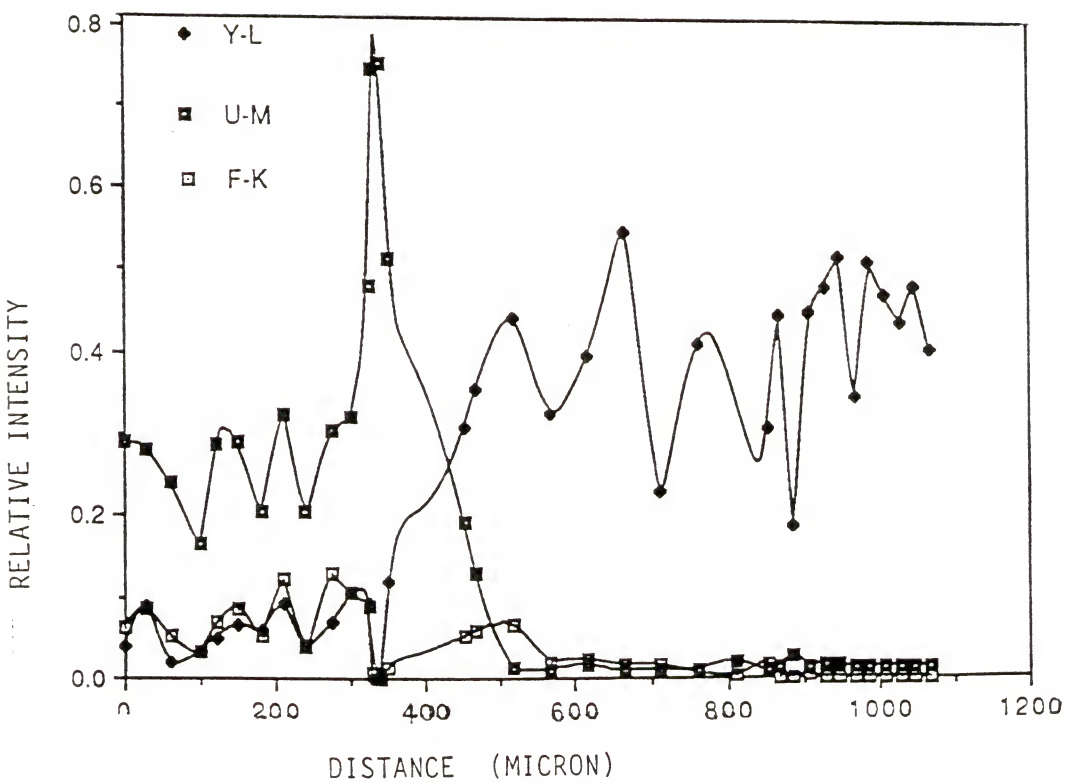

Figure 3.16 EMP Result of a Yttria Sample Tested in UF_4 at 1740 K for 20 min

hypostoichiometric UO_2 where O/U = 1.922. Finally the composition of the inner layer was found to be $Y_{.34}O_{.33}F_{.33}$ or YOF. Some uranium diffusion through a crack across the inner layer is seen close to the upper edge of Figure 3.16. This suggests that UF_4 gas was inserted through the existing crack in the beginning of the reaction.

3.3.5 XRD Analysis

Similarly, X-rays diffraction analysis[††] was performed to the yttria samples after the reaction with UF_4. For the sample tested in UF_4 at 1740 K for 15 min, XRD patterns showed the presence of YOF, Y_2O_3, UO_{s2}. For the sample tested at 1740 K for 40 min, the results were YOF, Y_2O_3, UO_2. The x-ray powder patterns are provided in Figure 3.17, Table 3.5.

3.3.6 Thermodynamic Analysis

FACT analysis showed the presence of YF_3 and UO_2 at 1740 K and 0.004 atm pressure. Since the presence of YF_3 (yttrium fluoride) does not match with x-ray results (YOF was detected in this case), data sources in this program are questionable. Thermodynamic results of the Y_2O_3 reaction with UF_4 gas are provided in Table 3.6.

[††] Philips APD 3720

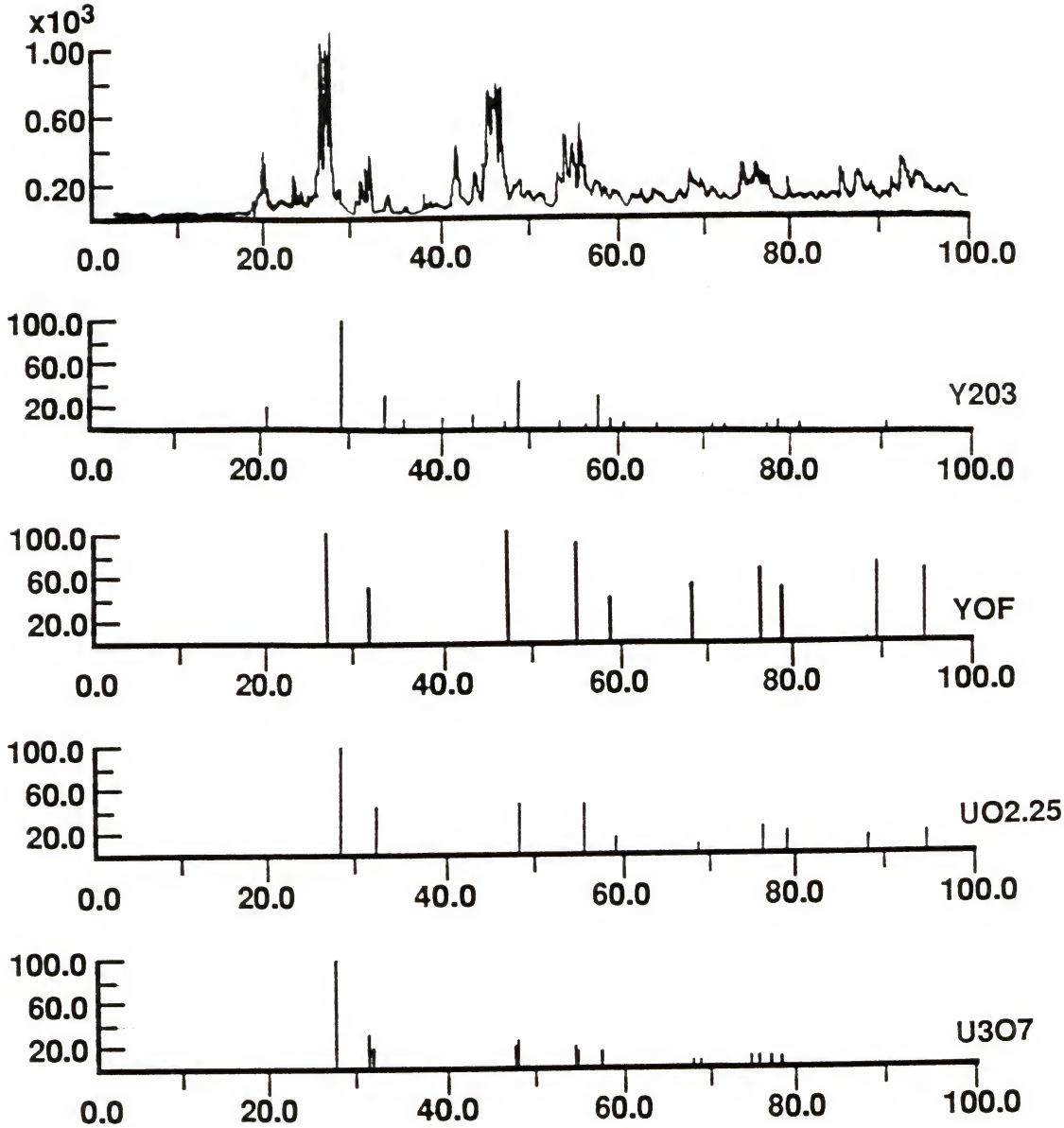

Figure 3.17 XRD Patterns of a Yttria Sample Exposed to UF_4

Table 3.5 X-Ray Diffraction Powder Pattern of the Yttria Sample after UF_4 Reaction

EXPER. 2Ø	I/I_0 %	YOF 2Ø	I/I_0	UO_2 2Ø	I/I_0	U_3O_7 2Ø	I/I_0
28.280	87.31	28.776	100	28.245	100	28.401	100
28.797	81.62	33.280	50	32.717	48	32.865	30
29.205	100.00	47.969	100	46.943	49	33.204	20
32.757	18.48	56.860	90	55.697	47	47.150	20
33.227	22.42	59.642	30	58.397	13	47.359	25
33.827	30.06	69.820	50	68.539	9	55.844	20
43.275	26.10	77.400	65	75.727	18	56.479	15
43.485	28.38	79.870	45	78.077	15	58.888	15
46.977	58.25	89.103	75	87.297	13	68.653	5
47.425	50.45	96.313	65	94.146	15	69.642	5
47.922	57.31	108.69	45	105.61	6	75.870	10
48.575	63.11	116.06	80	112.95	15	76.372	10
55.695	39.60	118.78	45	115.46	8	78.077	10
57.615	45.28	130.27	75	125.87	9	79.079	10
69.682	17.95	140.48	60	134.92	7		

Table 3.6 Thermodynamic Results of UF_4 Reaction with Y_2O_3 at 1740 K at 0.004 atm Pressure

REACTANTS MOLE	PRODUCTS	STATE	CONCENTRATION Mole
Y_2O_3 (1)	YF_3 Y_2O_3	Liquid Solid	1.3333 0.33333
UF_4 (1)	UO_2	Solid	1.

3.4 Analysis Results of Molybdenum Exposed to UF_4

According to FACT analysis (40), Mo showed good thermodynamical compatibility with both liquid and gaseous UF_4 at a temperature range of 1000-2300 K. A set of experiments with pure Mo exposed to gas and liquid UF_4 was performed for different time exposures in order to investigate whether any diffusion or dissolution occured after the reaction. The experiment settings were exactly the same as in the yttria case.

3.4.1 Weight Change Analysis

The weight change of these experiments was given in Table 3.7. In the gravimetric analysis of Mo samples at 1480 K in liquid UF_4, an insignificant amount of weight change was observed after the exposure testing. The experiment was repeated for 45 min exposure in order to check the reproducibility of the results. Then, the samples were annealed at 1500 K for 1 hour under argon atmosphere at 600 Torr pressure. The weights of the annealed samples were found to be the same as the original samples (Table 3.7).

Table 3.7 Weight Change Results of Mo Tested in Liquid UF_4

TIME Min	W_i g	W_a g	W_{an} g	Size cm^2	Vacuum Torr	Argon Torr	W_a-W_i/s g/cm^2
15	.22778	.23384	.22743	.924	$2x10^{-5}$	720	.00656
30	.24336	.26309	.24337	.979	$2x10^{-5}$	734	.02015
45	.22520	.22929		.905	$2x10^{-5}$	730	.00451
45	.21688	.22450	.21680	.897	$2x10^{-5}$	742	.00849
60	.21318	.21992	.21276	.88	$2x10^{-5}$	776	.00766
75	19955	.20830	.19953	.803	$1x10^{-5}$	767	.01089

This fact proved that, at 1480 K, for short exposure times such as 15 to 75 min, no reaction of U, F, or UF_4 occurred through the Mo sample. The weight analysis after testing at 1800 K, 2000 K, and 2200 K with gaseous UF_4 showed much less deposition on the samples with respect to the liquid phase tests; in the vapor phase the deposition rate seemed to decrease by time (Figure 3.18).

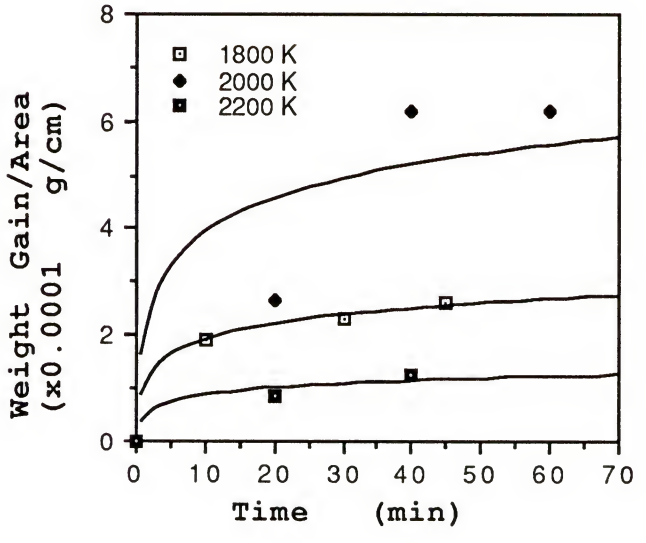

Figure 3.18 Weight Change of Mo Tested at 1800, 2000, 2200 K

3.4.2 SEM Analysis

During SEM analysis, it was observed that the grain size varyed throughout the crosssection and the grain growth occurred in samples exposed at 1480 K (Figure 3.19 a-b). The flow lines in the as-received sample disappeared after the test, and the grains recrystallized upon heating, having an average size of nearly 20 μm. At the end of the exposures at 2000 and 2200 K, it was found that there was some particle deposition on the surface of the samples (Figure 3.20 a-b). These particles were identified as being as U, F, O with Energy Dispersive Spectroscopy† (EDS).

3.4.3 EMP Analysis

After the exposure testings, samples were cut by a diamond saw and prepared for post-test analysis. After being mounted in epoxy resin, they were ground and polished as previously done for the yttria case. During sample preparation, distilled water was used and samples were polished separately in order to prevent any contamination effects. The EMP was done across the cross section from one edge to the other with equal scanning steps. The result was that the U and F concentrations were very low and discontinuous. Results in both line scanning and spot scanning cases were almost the same, and no significant diffusion of U or F was found on the cross sections (Figure 3.21).

---

† JSM-6400 Scanning Microscope, Tracor Northern Comp. Sys.

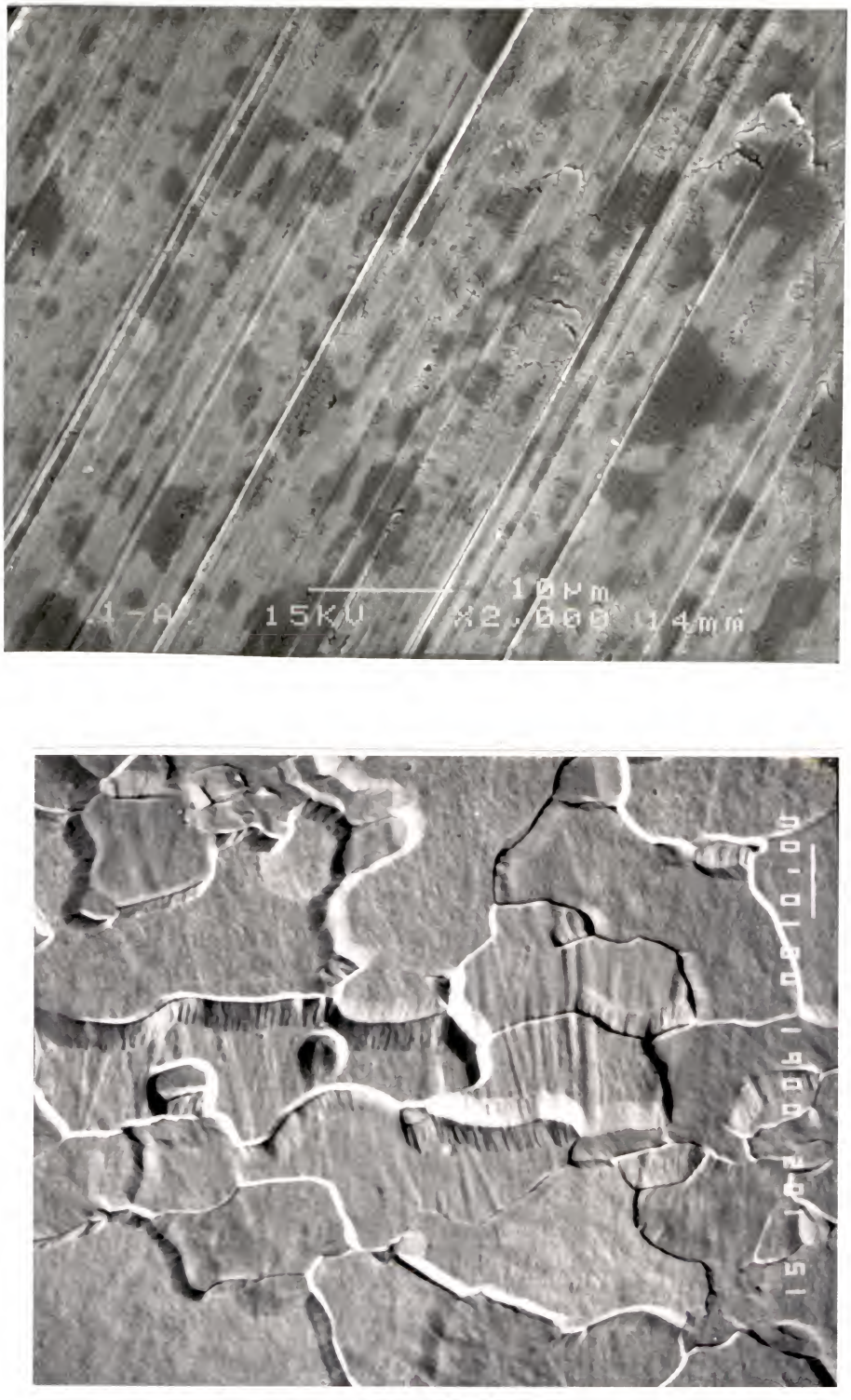

Figure 3.19 Micrographs of a Mo Sample Before and After UF_4 Test

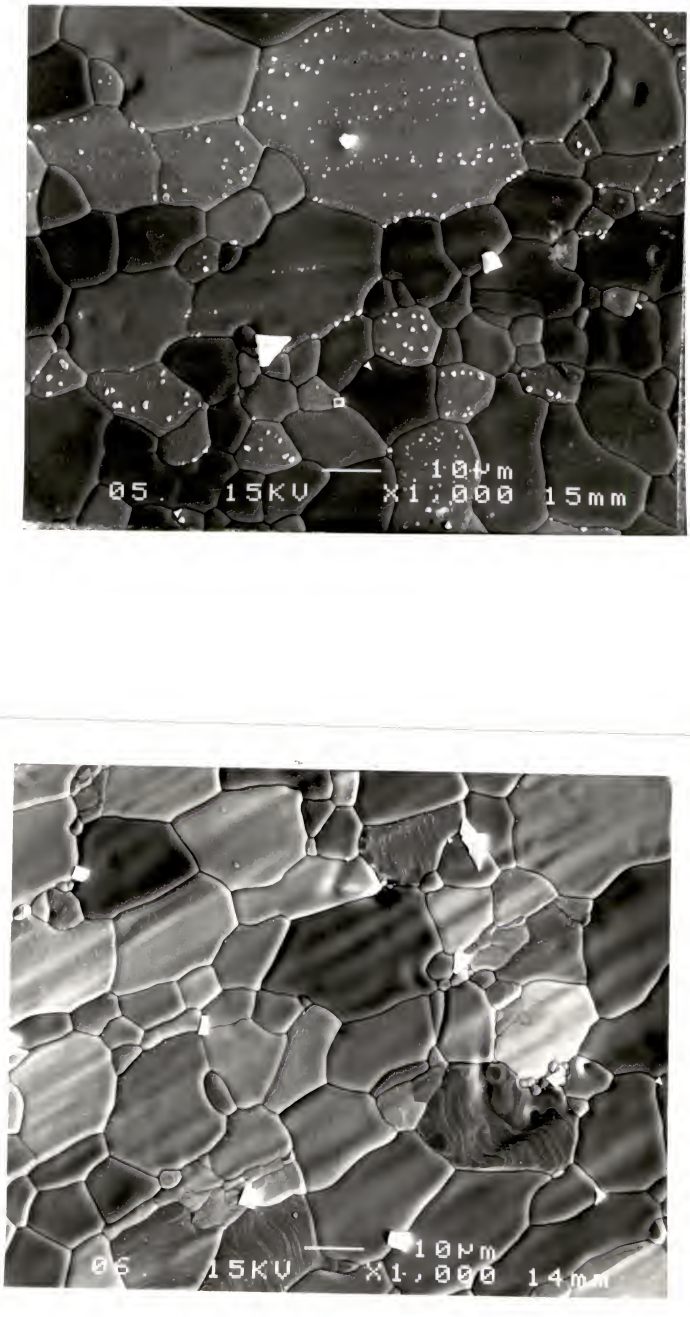

Figure 3.20 SEM Results of Mo Exposed to UF_4 at 2000 K and 2200 K

For each time interval at 1480 K, the uranium K ratio stayed within the limits of 0.0025/1 and fluorine K ratio was within 0.001/1. These limits were in the statistical fluctuation range of the instrument being used. In addition, in order to see the long term effect of the liquid and gaseous UF_4 to the Mo, two small pieces of the Mo crucible, one from the upper side, the other from the bottom side, were cut after many experiments were performed using the same crucible. The EMP analysis was performed along the cross-sections of these samples; no significant U and F atoms were detected for an average testing temperature of 1730 K and an average testing time of 9 hours. The results of the long exposure test were given in Table 3.8.

Table 3.8 Atomic Concentration of U and F in Mo Sample Exposed to UF_4 for 9 Hours at 1730 K

	UPPER CRUCIBLE			BOTTOM CRUCIBLE		
POINTS	MICRONS	U-M	F-K	MICRONS	U-M	F-K
1	0.0	0.00	0.00	0.0	0.00	0.00
2	94.4	0.00	0.00	83.6	0.00	1.58
3	188.9	0.03	0.61	167.1	0.00	0.00
4	283.3	0.02	1.98	250.6	0.04	0.00
5	377.8	0.00	0.87	334.2	0.00	0.36
6	472.2	0.00	0.51	417.7	0.00	0.77
7	566.6	0.04	0.00	501.3	0.02	0.00
8	661.1	0.00	0.10	584.9	0.02	0.47
9	755.5	0.00	0.00	668.4	0.02	0.05
10	850.0	0.00	0.00	752.0	0.14	0.00

CHAPTER 4
THE EVOLUTION OF THE REACTIONS AND SOLIDIFICATION

In this chapter, the mechanism of the chemical reactions at the interfaces, the solid state diffusion mechanism of the ions, and the formation of various phases following the solidification are explained using a phenomenological approach.

4.1 Reactions and Diffusion of the Components

When UF_4 first came in contact with the yttria wall, it reacted with yttria and exchange reaction occurred between oxygen and fluorine. At the early stages of the reaction (approximately the first 10 minutes), a solid wall of UO_2 (experimental ratio of O/U is 1.922) was formed on the surface of the sample while YF_3 was released in gas phase as a second reaction product at the operating temperature, which was 1380 and 1468 °C. The reactions [4-1] and [4-2] explain the formation of the center layer and are in good agreement with both theoretical and experimental results.

$$2Y_2O_{3\,(s)} + UF_{4\,(g)} \text{ -----> } 4YF_{3\,(g)} + 3UO_{2\,(s)} \qquad [4\text{-}1]$$

$$YF_{3(g)} + Y_2O_3 \text{ ------> } 3YOF_{\,(s)} \quad (Y_{1+x}OF_{2+y}) \qquad [4\text{-}2]$$

Then, the gaseous YF_3 advanced through interconnected porosity and reacted rapidly with yttria matrix according to the reactions given above; hence, the inner layer formed as a different phase following the reactions (Figure 4.7). Since we observed experimentally the presence of both yttrium and oxygen atoms in the outer layer after the formation of the UO_2 wall, it was concluded that these elements diffused through the center layer during the reaction at temperatures about 1460 °C. During the reactions, it is also assumed that no oxygen remained in the chamber after high vacuum was achieved. The diffusion of those elements was mainly due to the higher chemical potential of the substrate with respect to the layers. At the operating temperature ranges, UO_2 can behave intrinsically where the point defects, primarily vacancies, could appear by thermal effects. The defect reactions can be presented as follows:

$$\begin{aligned} UO_2 \text{ --> Null --> } & V_u'''' + 2\ V_o^{\wedge\wedge} \\ O_o \text{ --> } & O_i'' + V_o^{\wedge\wedge} \\ U_u \text{ --> } & U_i^{\wedge\wedge\wedge\wedge} + V_u'''' \end{aligned} \qquad [4\text{-}3]$$

in which O_o and U_u stand for one oxygen atom placed in oxygen site and uranium atom locating in uranium site, and O_i'' is the oxygen interstitial carrying two negative charges and $V_o^{\wedge\wedge}$ is the oxygen vacancy carrying two positive charges. Similarly, $U_i^{\wedge\wedge\wedge\wedge}$ stands for a uranium interstitial carrying four positive charges and V_u'''', a uranium vacancy with 4

negative charges. Experiments showed that the UO_2 wall was found to be almost stoichiometric (O/U = 1.922).

Knowledge of the atomic structure of the nonstoichiometric phases is important in interpreting the thermodynamic behavior of the material and the dependence of transport properties, such as electrical conductivity and diffusivity, upon the O/M ratio. According to the literature (41), among the 40 different oxides, more than one oxide phase might be in equilibrium at room temperatures such as UO_2 with alpha U_4O_9 between 2-2.23 range and gamma UO_3 in equilibrium with alpha U_3O_{8+x} over 2.6 of U/O ratio. In addition, each oxide phase might be present with various crystalline modifications. It is significant that the lattices of most phases may be derived with only minor modifications from a few basic structures. Thus, the fluoride lattice of the most stable oxide of tetravalent uranium, UO_2, offers the opportunity for the formation of many discrete oxides by the acceptance of various amounts and by different positioning of the oxygen atoms at interstitial sites and/or slight lattice distortions. Such properties are critically dependent upon the positions of the excess oxygen atoms in the crystal structure. Stoichiometric UO_2 crystallizes in the fluoride structure, which is shown in Figure 4.1. Deviations of uranium from exact stoichiometry are permissable since it has many valence states in which U^{4+}, U^{5+}, and U^{6+} states tend to be the most stable. The different phase regions with respect to O/U ratio and temperature are presented in Figure 4.2.

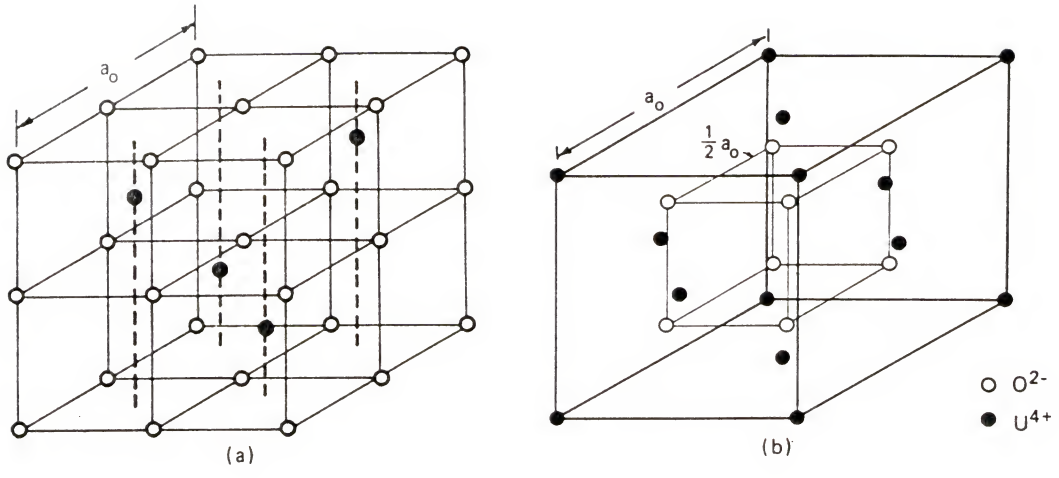

Figure 4.1 The Fluorite Structure of UO_2
a. The sc structure of the anion sublattice
b. The fcc structure of the cation sublattice
From Olander D.R., Fundamental Aspects of the Nuclear Reactor Fuel Elements

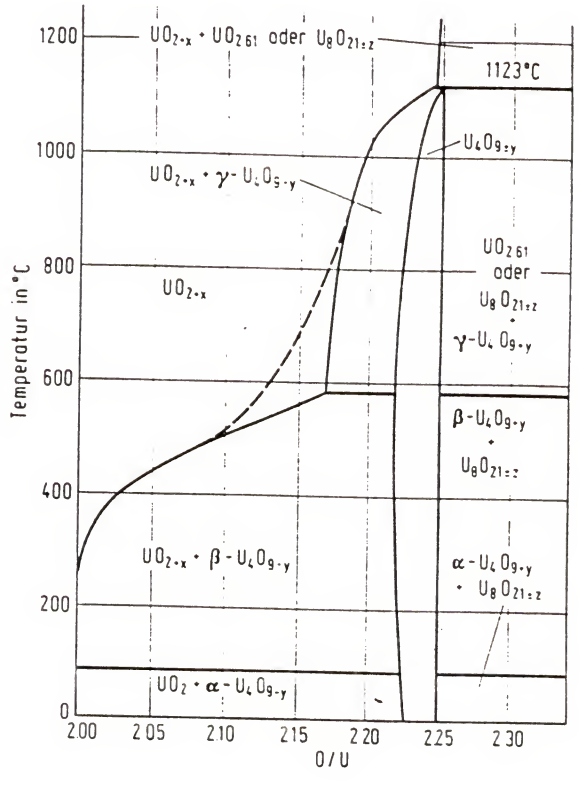

Figure 4.2 Oxygen-Uranium Phase Equilibrium System
From: Gmelin, Handbuch der Anorganishen Chemie, U Uran

When the oxygen atoms are removed (vacancies) or added (interstitials) to the lattice of the stoichiometric UO_2, in order to hold the electrical neutrality, U^{4+} ions are converted to U^{+5} or U^{+6} in hyperstoichiometric UO_{2+x} or they are converted to U^{2+} in hypostoichiometric UO_{2-x} crystal. The largest open spaces in this lattice are the centers of the cubes formed by the eight oxygen ions in the simple cubic sublattice. In UO_2, half of these these cubes are occupied by uranium ions, but the other half are empty. Figure 4.3 shows the empty cube formed by eight normal oxygen ions with the locations of the two types of interstitials sites for oxygen: type 1 and type 2. The type 1 sites lie along each of the six diagonals in [110] directions half way between the cube center and the midpoints of the cube edges. There are 12 type 1 sites in each empty oxygen cube. Since there are four such cubes in the fluoride unit cell, the unit cell contains 48 type 1 oxygen interstitial sites, or 12 for each uranium ion in the lattice. The Type 2 interstitials sites are located midway from the cube center to the cube corners in [111] directions. There are 16 type 2 sites in each UO_2 unit cell, or 4 per uranium ion. In total, 64 sites are available for excess oxygen to diffuse through the UO_2 unit cell. For small values of x, an occasional unit cell of the fluoride lattice is presented in Figure 4.4. The defect complex consists of two type 1 oxygen interstitials, two type 2 oxygen interstitials, two vacant oxygen sites, and four U^{5+} ions on nearby normal cation sites. To maintain charge

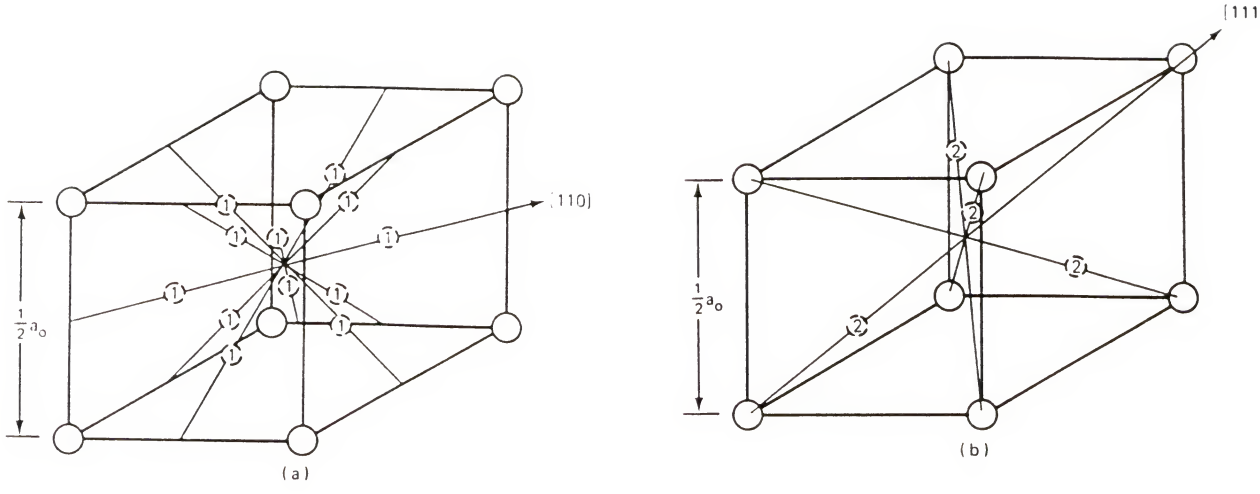

Figure 4.3 Sites for Interstitial Oxygen in UO_2
○,Normal oxygen ions ①,type 1 interstitial sites ②,type 2 interstitial sites

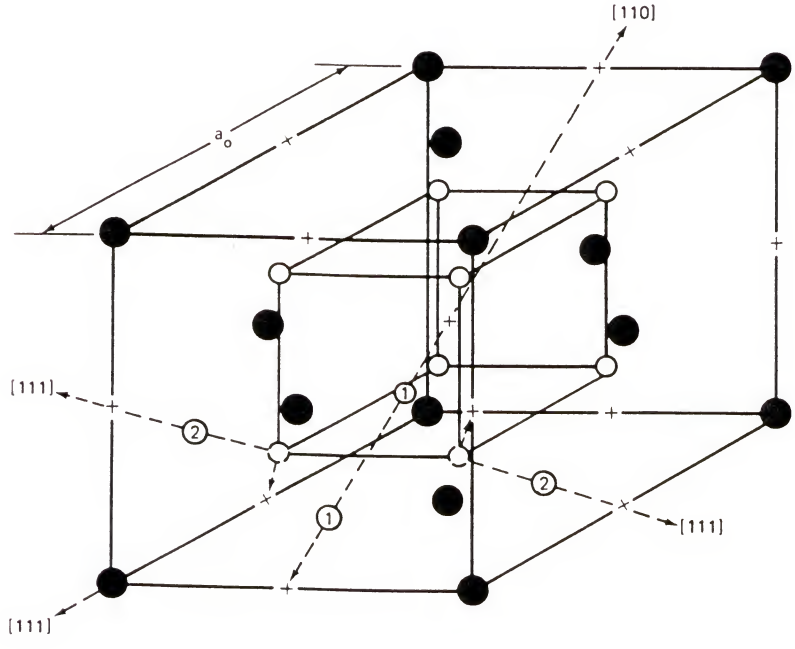

Figure 4.4 Defect complex in UO_2
From: Olander D.R., Fundamental Aspects of the Nuclear Reactor Fuel Elements.

neutrality, four U^{4+} ions nearest to the type 1 oxygen ions are converted to U^{5+} ions. Because of the coulombic repulsion the two oxygen ions nearest to the pair of the extra oxygen ions relax outward along the possible [111] direction, leaving their anion sites vacant (42). The mechanism of this substitution can be described as follows:

$$2UO_2 + O^{--} \longrightarrow 2U_u^{\wedge} + 4O_o + O_i'' \qquad [4-4]$$

This equation describes the two uranium ions in stoichiometric UO_2 which were converted from +4 to +5 valence state by forming a hole in its uranium site, thus preserving the charge neutrality. Also the mass balance on both sides of the equation was preserved. Equation [4-4] provides an explanation for oxygen ions to diffuse from the oxygen rich yttria site through the UO_2 center layer into the outer layer via migration of oxygen interstitials. As mentioned earlier, yttrium ionic diffusion must occur to some extent through the solid UO_2 wall. This can be explained by the following substitution reaction:

$$\{2Y^{+3}, 3O^{-2}\} + V_U^{+4} + 2V_O^{-2} \xrightarrow{\text{in } UO_2} Y_u' + 2O_o + O_i'' + Y_i^{\wedge\wedge\wedge} \qquad [4-5]$$

For a one UO_2 vacancy which could be produced by thermal effects, one yttrium ion of charge +3 can substitute a uranium site, thus creating a -1 extra charge while the other yttrium ion can be an interstitial by carrying +3 positive

charge. For the oxygen ions coming from yttria, two of them are located in the vacant oxygen site of the UO_2 empty cell, while the other ion occupies an interstitial site carrying -2 negative charge. In this way, both charge balance and atomic balance were held in the equation. Again, due to the chemical potential, the diffusion of oxygen and yttrium species might occur via migration of interstitials through vacancies at high temperatures from high concentration to the low concentration side.

When those species come in contact with UF_4 molecules, the probable reaction which forms the liquid can be expressed as follows:

$$\{Y_i^{\cdot\cdot\cdot}, O_i''\} + UF_{4(g)} \longrightarrow UO_{2(s)} + \{Y^{+3}, U^{+4}, F^-, O^{--}\}_{(L)} + \{F^-\}_{(Diff)} \quad [4\text{-}6]$$

According to the reaction [4-1], UO_2 must form in the outer interface of the center layer, thus contributing to the increase in thickness of the center layer. The curvature of the outer interface is probably due to the divergence of the diffusing fluxes of yttrium and oxygen ions (Figure 4.5). Fluorine and some uranium diffusion must also occur simultaneously through the center layer, since the inner layer grows with time. Its mecanism can be explained similarly by the following reaction:

$$2V_u^{+4} + 4V_O^{-2} + \{U^{+4},\ 4F^-\} \xrightarrow{\text{in } UO_2} U_u + V_u'''' + 4F_o^{\cdot} \quad [4\text{-}7]$$

In this case, the diffusion of fluorine and uranium ions proceeds via a vacancy mechanism at high temperatures. The rate of the diffusion also depends on the thickness of the UO_2 wall. This can be seen easily in Figure 4.5, in which the inner (dark) layer is thicker at places, where the wall is thinner. As mentioned earlier, cation diffusion (U^{+4}) is slower than anion diffusion. Uranium diffusion via a vacancy mechanism was investigated by Lidiard (43). He assumed that the uranium diffused by means of uranium vacancies in UO_{2+x} and interstitial cations U^{4+}. Figure 4.6 shows the experimental diffusivities of uranium and oxygen (44). This prediction was confirmed by the results of Matzke (44-46). In his experiments, Matzke tested UO_2 with impurities Nb_2O_5, La_2O_3, and Y_2O_3. The uranium diffusion coefficient increased in the material containing Nb_2O_5 and decreased in the presence of La_2O_3 or Y_2O_3. Since additions of Nb_2O_3 lead to an excess oxygen content in UO_2, and La_2O_3 or Y_2O_3 reduce the oxygen content ($U_{1-x}Nb_xO_{2+x/2}$ and $U_{1-x}La_xO_{2-x/2}$), this indicates that the diffusion of uranium is accelerated in material containing an excess of oxygen. The best estimate which is in agreement with most of the experimental data is found to be for 1500°C:

$$\log D = -10.85 + 1.5 \log x.$$

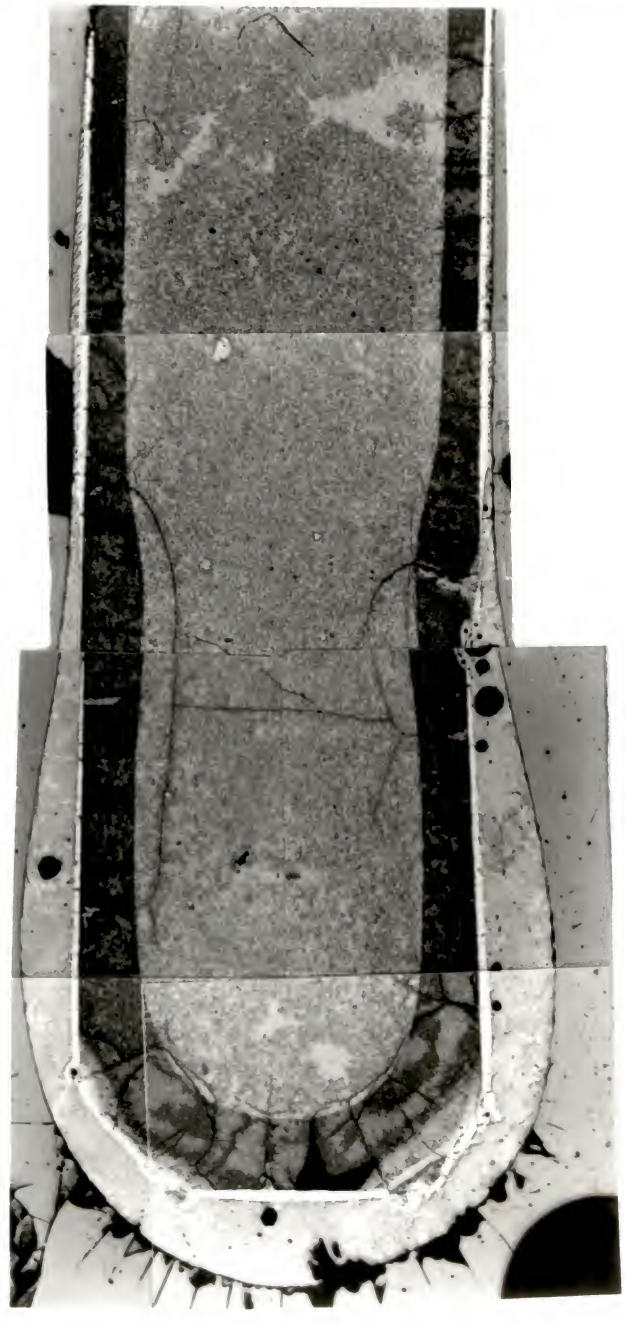

Figure 4.5 Cross Section of a Yttria Sample Exposed to UF_4 at 1650 K for 15 min

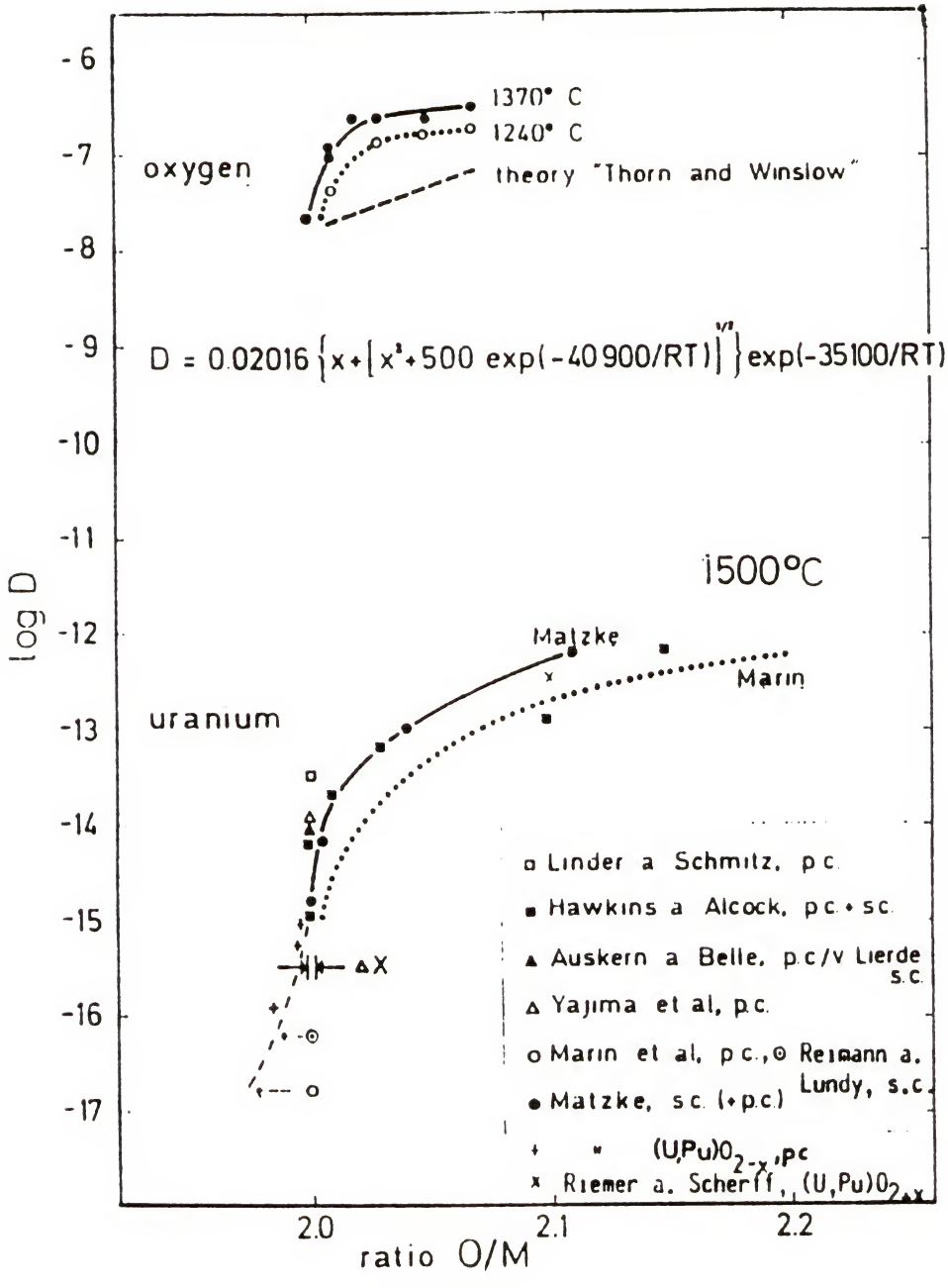

Figure 4.6 Diffusion Coefficient of Uranium with Respect to O/M Ratio
From Matzke, H.J., On Uranium Self-Diffusion in UO_2 and UO_{2^+}

The most reliable data relating to the activation energy of volume diffusion of uranium is found to be 70 kcal/mol for UO_2 to 105 kcal/mol for $UO_{2.1}$ (48). Substitutional effects between YOF and Y_2O_3 molecules are also possible due to the high temperature and volumetric changes in small amounts which can cause vacancy formation.

$$2V_u^{+4} + 4V_o^{-2} + YOF \xrightarrow{\text{in } Y_2O_3} Y_y + O_o + F_o^{\wedge} + V_o^{\wedge\wedge} + V_y''' \quad \text{Substitution} \qquad [4\text{-}8]$$

The yttrium and oxygen vacancies become the sinks for a backward ionic oxygen and yttrium migration in the system. Figure 4.7 shows a scheme of the ionic diffusion through UO_2 wall. As mentioned before, at the later stage of the reaction, a liquid phase starts to appear on the outer face of the uranium oxide layer. This liquid phase is basically a eutectic mixture of U, F, O, Y which constitutes a 4-component phase system in which oxygen and yttrium ions cross the UO_2 wall during the reaction. During the second stage of the reaction, F ions diffuse through liquid phase continuing to react with yttria matrix, and the incoming oxygen ions react with uranium in liquid phase, contributing to the further increase of the center layer thickness.

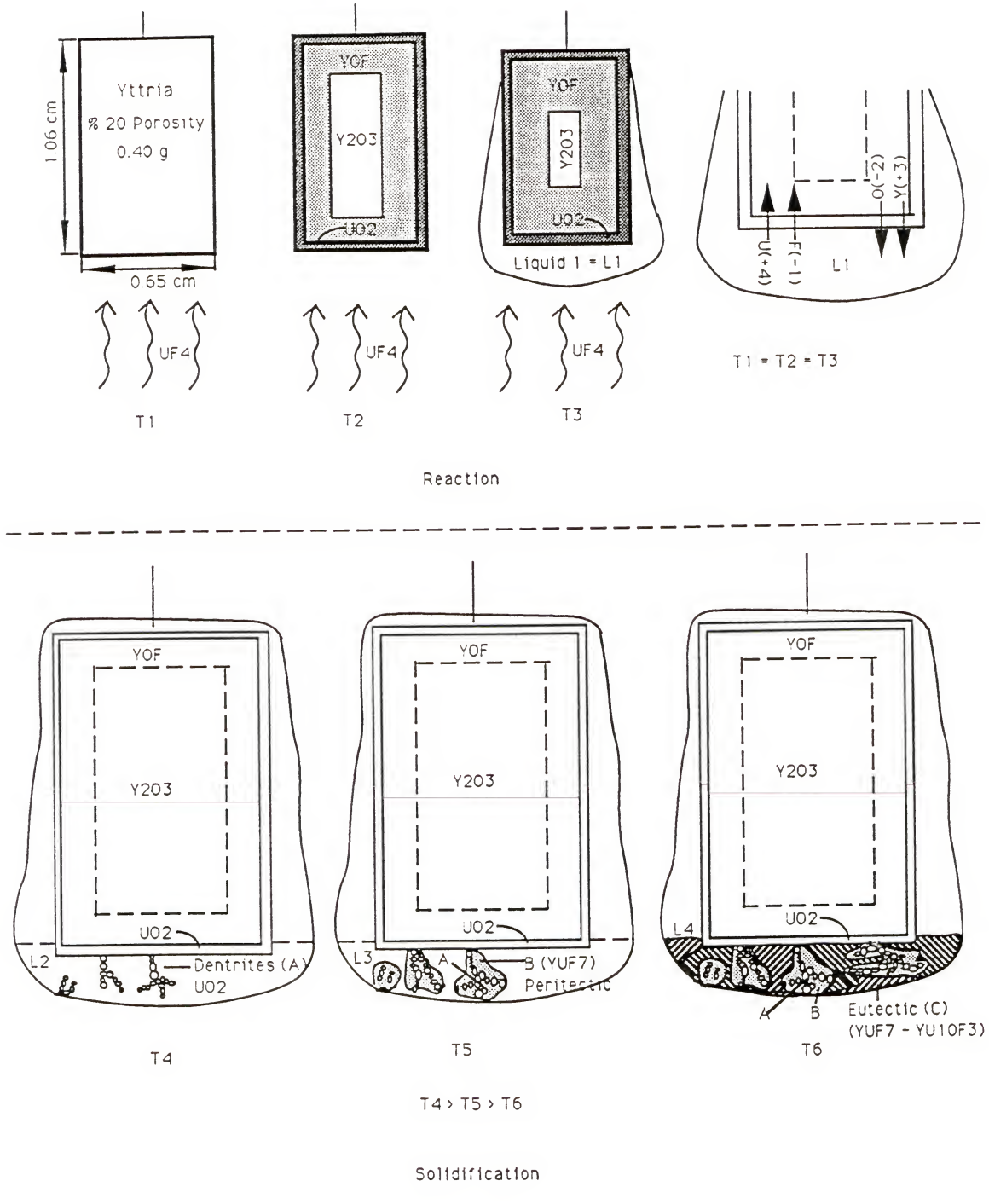

Figure 4.7 Reaction and Solidification Scheme

4.2 Solidification

During cooling, at temperature T_2, primary dentrites within the eutectic composition start to appear in liquid phase L_1, hence changing L_1 to L_2 as described below:

$$A_{(s)} + L_1 \text{ ------> } A_{(s)} + A'_{(s)} + L_2 \qquad [4\text{-}9]$$

where $A_{(s)} = UO_2$ in solid phase

$A'_{(s)}$ = Primary dentrites (UO_2) in solid phase.

At T_3, a peritectic reaction (47) occurs in which A' phase reacts with L_2 to give $B_{(s)}$ which is YUF_7. The fluorine-rich, yttrium uranium fluorite phase (YUF_7) encircles A' and prevents further reaction of the liquid with the dentrites (A'). Consequently, L_2 changes to L_3.

$$A_{(s)} + A'_{(s)} + L_2 \text{ -----> } A_{(s)} + A'_{(s)} + B_{(s)} + L_3 \qquad [4\text{-}10]$$

where $B = YUF_7$.

Finally at T_4, L_3 crystallizes to give lamellar type eutectic

$$A_{(s)} + A'_{(s)} + B + L_3 \text{ ------>} A_{(s)} + A'_{(s)} + B_{(s)} + (B+C)_{(s)} \qquad [4\text{-}11]$$

where B= YUF_7 and C = $YU_{10}F_{3-x}$ forms the eutectic phase.

The directions of the primary dendrites indicate the direction of the heat flow. The lamellar formation suggests that the rate of cooling was moderate (49). As seen from the micrograph (Figure 3.13), wall thickness increases toward the

bottom end; this is due to the fact that the reaction rate is faster because of the higher influx of UF_4 which first strikes the bottom portion of the sample. The droplet shape at the bottom end of the sample is due to the surface tension of the liquid coupled with gravitational force.

Basically, three layers were formed during the reaction. The concentration of the components through the layers was almost constant and time independent.

CHAPTER 5
THEORETICAL APPROACH TO THE PHYSICAL SITUATION

In this chapter, a summary review of the diffusion models which are thought to be applicable to the present physical conditions of this work is presented. Due to the complex nature of the multiphase, multicomponent system, some assumptions are made to simplify the problem which can be stated as follows: one dimensional diffusion, steady boundary conditions, uniform temperature distribution occur throughout the samples and, at the later stage of the experiment, the growth of the modeled phases is to be diffusion controlled and obeys the parabolic rate law since the process is assumed to be slower than the rate of the chemical reactions.

The first part of this chapter analyzes the presence of chemical reactions at phase boundaries under nonequilibrium conditions. It is assumed that this state represents the initial stage of the experiments (0 to 7 min), in which a single, UO_2 phase is growing primarily. The second part of the chapter deals with multiphases under local equilibrium conditions at the phase boundaries. This represents the later period of the experiments (7 to 45 min) in which five phases (Vapor, Liquid, UO_2, $Y_xO_yF_z$, Y_2O_3) are present. The solution of Ficks Equation for a binary and quaternary multiphase system is given as a basis for future work.

A theoretical treatment of the problem using flux-phase velocity relations is also presented in the second half of the chapter. For the stoichiometric phases, the fluxes at the facing boundaries of each phase are assumed to be equal, and the boundary velocities are the ratio of the flux difference and concentration difference of the two adjacent phases. If the chemical reactions occuring at the interface are assumed to be occuring rapidly, then the layer growth is primarily controlled by the mass transport carried by the fluxes in the adjacent phases. This is a relatively slower process with respect to the chemical reactions. The practical importance of this analysis is

a. one can find the growth rate of a multiphase system given a particular flux and the interface concentrations,
b. by estimating a single flux in a particular phase and measuring the growth rate of this phase, it is possible to calculate the fluxes in the adjacent phase.

5.1 Nonequilibrium Conditions at the Phase Boundary

5.1.1 Time Independent Case (Steady State)

For a first order chemical reaction occuring at the interface x_1, and neglecting the reaction sink term, Fick's second law becomes

$$D_{AB} \frac{\partial^2 C}{\partial x^2} = 0 \qquad [5\text{-}1]$$

with the boundary conditions

$$C(0) = C_0 \qquad \text{BC1}$$

$$C(x) = C_1 \qquad \text{BC2}$$

$$\text{at } x = x_1 \qquad -D_{AB}\frac{dC}{dx} = k_1 C_1^{\,n} \qquad \text{BC3}$$

Solving [5-1], and applying BC1 and BC2, we can find

$$C(x) = \frac{C_1 - C_0}{x_1} X + C_0 \qquad [5\text{-}2]$$

Applying BC3, the reaction rate constant k_1, can be estimated

$$k_1 = \frac{-D_{AB}}{x_1} \left(\frac{C_1 - C_0}{C_1^{\,n}}\right) \qquad [5\text{-}3]$$

where D_{AB} must be determined experimentally.

According to the experimental data, the diffusion coefficient of oxygen atoms in UO_2 is about 10^{-7} $\frac{cm^2}{sec}$ (46) at a temperature of 1773 K for stoichiometric UO_2. From Figure 3.13, in the ellypsoidal regions of the sample, the center layer growth rate was found to be 1.8×10^{-5} $\frac{cm}{sec}$ and from Figure 3.14, the growth of the center and outer layer occured mostly outward causing the swelling of the sample with respect to its initial thickness. Two basic assumptions are made in this treatment: k_1 is assumed to be analogous to the growth rate, and the effect of fluorine and yttrium diffusion through the UO_2 layer is neglected since the atomic concentrations of fluorine and yttrium are small compared to concentration of uranium and oxygen. Applying equation [5-3] to a binary

single phase system, it is possible to find n, with the following experimental data:

$$D_O = 10^{-7}\ \frac{cm^2}{sec}\ ,\quad k_1 = 1.8x10^{-5}\ \frac{cm}{sec}\ ,$$

$$x_1 = 0.0085\ cm,\quad C_1 = 64\ ,\ C_0 = 68.$$

The power term n is calculated to be n = -1.39.

Keeping the power term as unity, it is found that

$D_O = 24.5x10^{-7}\ \frac{cm^2}{sec}$,which is close to the experimental data.

The difference between experiment and theory is due to the deviation in the measurement of k_1 and to the possible fluctuation of the extrapolated value of the diffusion coefficient in Figure 4.6 at temperatures around 1750 K.

5.1.2 Time Dependent Case (Nonsteady State)

For this case, equation [5-1] gains one additional derivative term representing the time change.

$$\frac{\partial Cu}{\partial t} = D_{AB}\frac{\partial^2 Cu}{\partial x^2} \qquad [5\text{-}4]$$

with the boundary and initial conditions:

$t \geq 0$	x=0	$C_O = C1$	BC1
$t > 0$	x=x1	$D_O\frac{\partial C_O}{\partial x} = -k1Cu$	BC2
t=0	0<x<L	$C_O = 0$	IC

The solution of [5-4] with the above boundary and initial conditions is given below:

$$C_U(x,t)=-Lx + C_1 + 2\sum_{n=0}^{\infty} \frac{L}{K_n}\left\{\left[\cos\left(K_n x_1\right)\right]- \frac{\sin\left(K_n x_1\right)}{K_n x_1} - \frac{c_1}{x_1}\left(1-\cos K_n x_1\right)\right\}\sin\left(K_n x\right)e^{-K_n^2 Dt}$$

$$K_n=\sqrt{\frac{\lambda_n}{D}} \quad L=\frac{k_1 C_1}{1+k_1 x_1} \qquad [5-5]$$

where C_O is the concentration of oxygen ions and D_O is the diffusion coefficient of oxygen ions through the reaction layer. Using the initial condition at t=0, K_n can be found from the transcendental equation given below.

$$K_n = -k_1 \tan(K_n x_1) \qquad [5-6]$$

In Figure 5.1, the graphical solution of [5-6] is given.

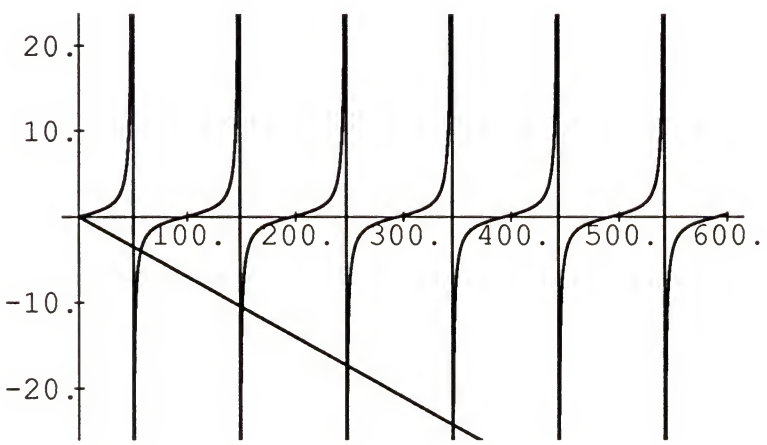

Figure 5.1 Graphical Solution of the Transcendental Function

The six solutions of this transcendental equation are

K_0 = 49.24, K_1 = 147.72, K_3 = 344.69, K_4 = 443.17, K_5 = 541.65

with $k_1 = 8\times10^{-5} \frac{cm}{sec}$, $C_1 = 68\%$, $x_1 = 0.0319$ cm,

$D_O \approx 10^{-7} \frac{cm^2}{sec}$, $L = 5.30\times10^{-3}$.

Figure 5.2 shows the calculated oxygen concentration profile with respect to x. The solution of [5-5] reaches a steady, exponential concentration profile after 15 minutes. The theoretically calculated concentration drop is found to be 1.3%, which was lower than the experimental value of 10.8% (Figure 5.3). The reasons for this difference are as follows:

a. In Figure 5.3, the situation represents a multiphase, multicomponent diffusion system. The theoretical calculation in Figure 5.2 assumes oxygen diffusion only in single phase without the coupling effects of uranium and fluorine.

b. Another reason could be that [5-5] does not contain the moving boundary conditions in which x also changes with respect to time. Equation [5-5] is found by 1) dividing, C(x,t) by its steady state and transient state components as being $C(x,t) = C_\infty(x,t) + C_{tr}(x,t)$; 2) solving the first component, assuming the concentration behaves linearly at steady state; 3) reformulating the boundary conditions for the non-steady component; 4) applying the separation of variables method in order to solve the partial differential equation with two variables.

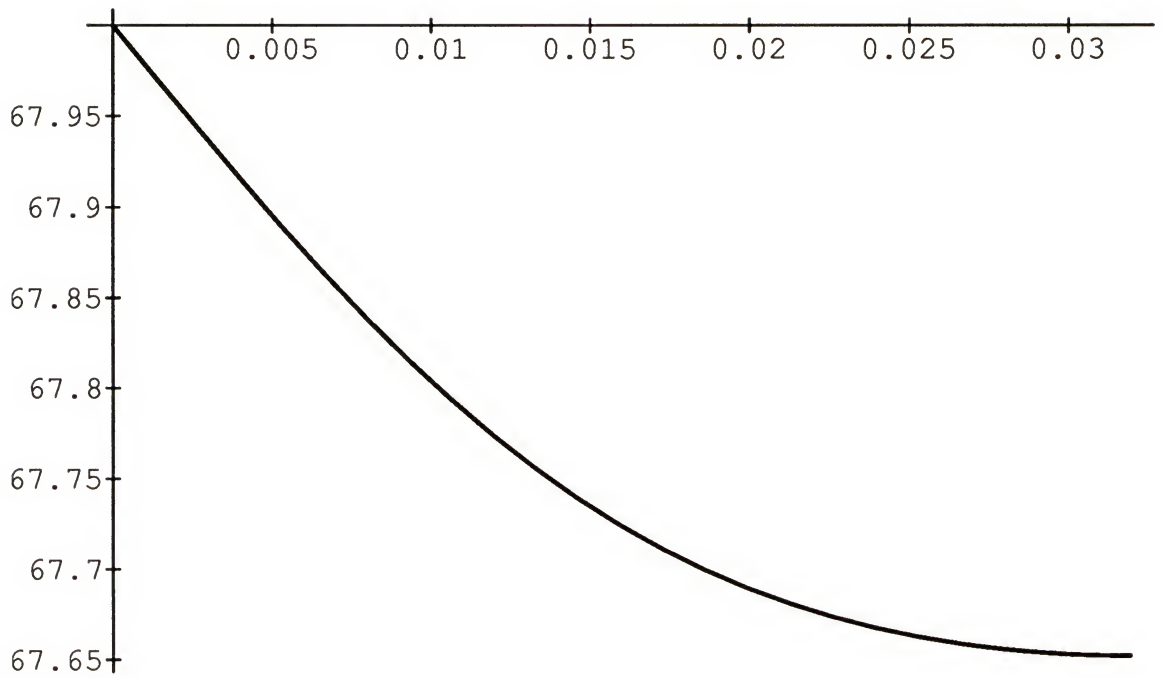

Figure 5.2 Calculated Oxygen Concentration Profile.
(y-axis is atomic percent, x-axis is in microns)

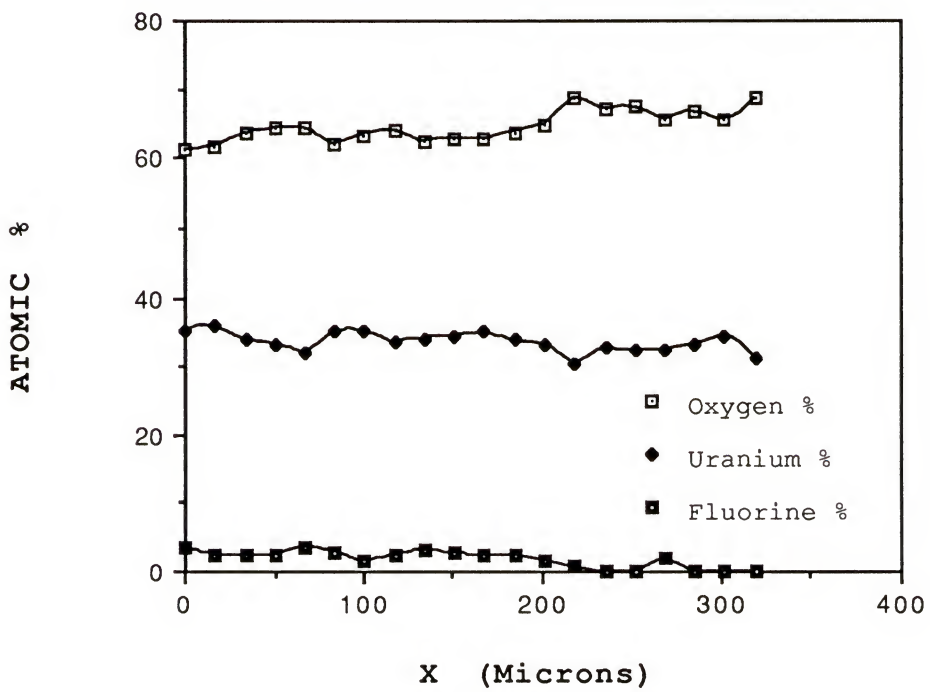

Figure 5.3 Experimental Oxygen, Uranium and Fluorine Concentration.

5.2 Equilibrium Conditions at the Phase Boundaries

During the experiment, UF_4 vapors reacted with the surface of the sample and formed the reaction layers as mentioned previously. The reaction layers (right half) and the measured concentration profiles for U, F, O, Y are presented in Figure 5.3.

5.2.1 Binary, Three-Phase System

Basically, the system has four diffusing components: uranium, fluorine, oxygen, and yttrium, with five phases present. Three of them are in the solid state, one is in the gas phase, and the other in the liquid phase. Fick's second law (Eqn. [5-4]) is valid for solid phases. In liquid and gas phases, at the experimental conditions (1480°C) where there is continuous motion, it is reasonable to assume that the components are homogeneously mixed and the concentration is constant. However, close to the boundaries, the fluid motion approaches stagnancy, and it can be assumed that concentration gradients in both liquid and gas phases exist near the phase boundaries.

According to the literature, the Fick's second law is studied for binary systems (two-component systems) with three phases, ternary systems with a single phase, and for single-component systems with N phases present (50). Some of these solutions are briefly discussed in this section. For a two-component three-phase system,

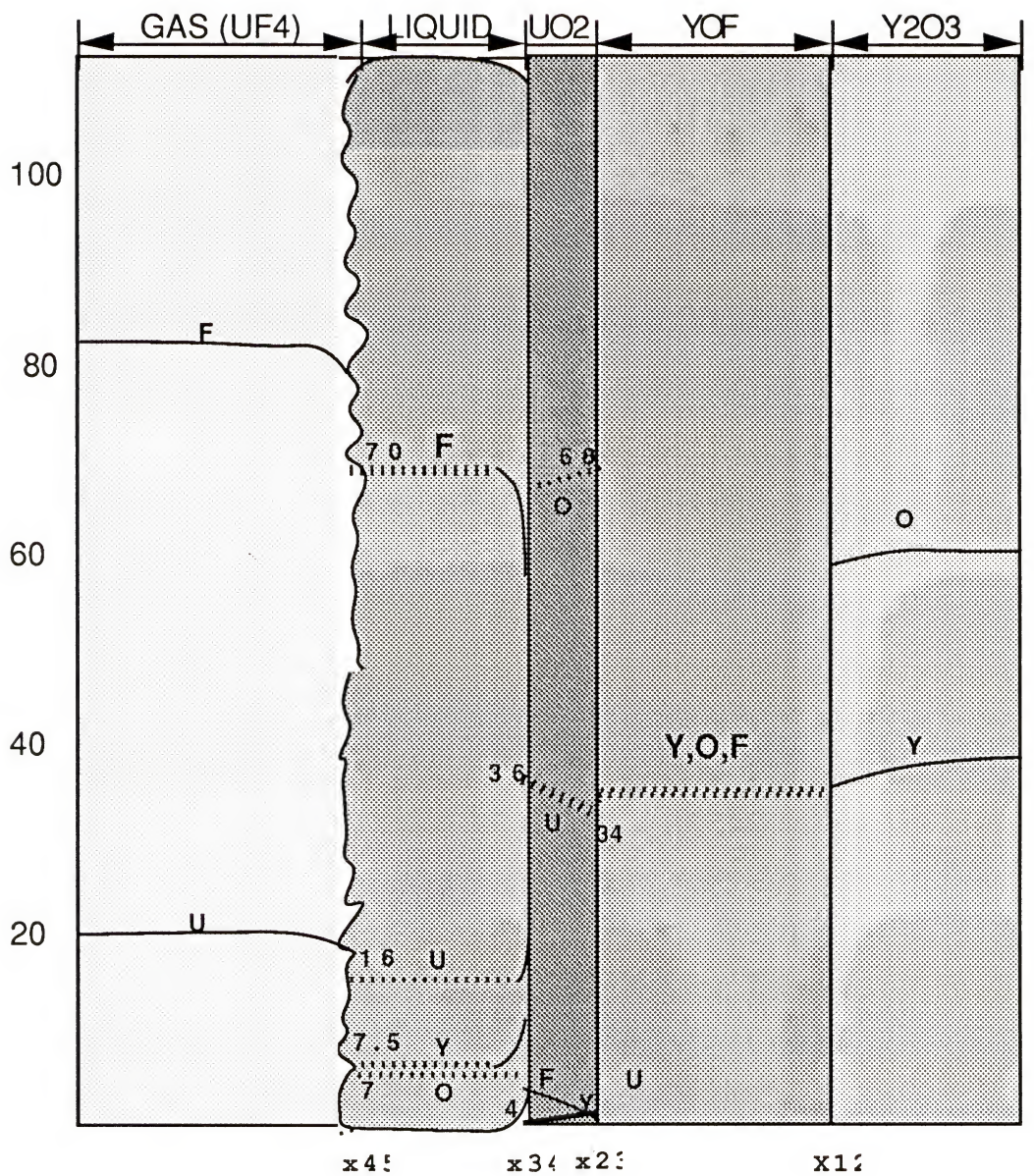

Figure 5.4 Experimental Concentration Profiles After the Reaction of Yttria with UF_4

Note: Dashed lines are inferred to data

with semi-infinite boundary conditions, after solving [5-4] for three phases, the concentrations are found to be the sum of the error functions:

$$C^{\alpha}(x,t) = C_{-}^{\alpha} + (C^{\alpha\beta} - C_{-}^{\alpha}) \frac{\operatorname{cerf} \frac{x}{2\sqrt{D^{\alpha}t}}}{\operatorname{cerf}\eta_1}$$

$$C^{\beta}(x,t) = C^{\beta\gamma} - (C^{\beta\gamma} - C^{\beta\alpha}) \frac{\operatorname{cerf}\eta_2 - \operatorname{cerf} \frac{x}{2\sqrt{D^{\beta}t}}}{\operatorname{cerf}\eta_2 - \operatorname{cerf} R_1\eta_1}$$

$$C^{\gamma}(x,t) = C_{+}^{\gamma} - (C_{+}^{\gamma} - C^{\gamma\beta}) \frac{1 - \operatorname{cerf} \frac{x}{2\sqrt{D^{\gamma}t}}}{1 - \operatorname{cerf} R_2\eta_2} \qquad [5\text{-}7]$$

where the interfaces are $\xi^{\alpha\beta} = 2\eta_1\sqrt{D^{\alpha}t}$, $\xi^{\beta\gamma} = 2\eta_2\sqrt{D^{\beta}t}$ and R_1, R_2 are defined as $R_1 = \sqrt{\frac{D^{\alpha}}{D^{\beta}}}$, $R_2 = \sqrt{\frac{D^{\beta}}{D^{\gamma}}}$. In equation [7], the unknowns are η_1, η_2 and R_1, R_2. In order to complete the solutions, two expressions for the interface velocity are derived and set equal to each other. The interface velocities are defined as follows:

$$v_1 = \frac{dx_1}{dt} = \eta_1\sqrt{\frac{D^{\alpha}}{t}} = \frac{J^{\alpha\beta} - J^{\beta\alpha}}{C^{\alpha} - C^{\beta\alpha}} \quad , \quad v_2 = \frac{dx_2}{dt} = \eta_2\sqrt{\frac{D^{\beta}}{t}} = \frac{J^{\beta\gamma} - J^{\gamma\beta}}{C^{\beta\gamma} - C^{\gamma\beta}} \qquad [5\text{-}8]$$

Using $J^m = -D^m\frac{\partial C}{\partial x}$, the fluxes can be calculated from [5-7], and substituting the fluxes into [5-8], two expressions with two unknowns are obtained provided the values of R_1 and R_2.

$$1 = \frac{1}{\eta_1}\left[\frac{C^{\alpha} - C^{\alpha\beta}}{C^{\alpha\beta} - C^{\beta\alpha}}\right]\frac{e^{-\eta_1^2}}{4\sqrt{\Pi}\,\mathrm{cerf}\eta_1} + \frac{1}{\eta_1}\left[\frac{C^{\beta\gamma} - C^{\beta\alpha}}{C^{\alpha\beta} - C^{\beta\alpha}}\right]\frac{e^{-(\eta_1 R_1)^2}}{4\sqrt{\Pi}R_1(\mathrm{cerf}\eta_2 - \mathrm{cerf}(R_1\eta_1))}$$

$$1 = \frac{1}{\eta_2}\left[\frac{C^{\beta\alpha} - C^{\beta\gamma}}{C^{\beta\gamma} - C^{\gamma\beta}}\right]\frac{e^{-\eta_2^2}}{4\sqrt{\Pi}\,(\mathrm{cerf}\eta_2 - \mathrm{cerf}(R_1\eta_1))} + \frac{1}{\eta_2}\left[\frac{C^{\gamma} - C^{\gamma\beta}}{C^{\beta\gamma} - C^{\gamma\beta}}\right]\frac{e^{-(\eta_2 R_2)^2}}{4\sqrt{\Pi}R_2(1 - \mathrm{cerf}(R_2\eta_2))} \qquad [5\text{-}9]$$

By solving Equation [5-9] simultaneously, η_1 and η_2 can be found for an initial estimate of the diffusion coefficients. Equation [5-9] is an example showing the complexity of the binary sytems with three phases. The experimental results revealed in this research present a more complex system with four components and three solid phases. Therefore, a set of differential equations given in the following section describes the phenomenon completely.

5.2.2 Quaternary, Multiphase Systems

Fick's first law can be generalized as follows:

$$J_i = -\sum_{k=1}^{n-1} D_{ik}\nabla C_k \qquad [5\text{-}10]$$

Combining [5-10] with the continuity equation, one obtains the set of (n-1) partial differential equations, which basically is Fick's second law (50).

$$\frac{\partial C_i}{\partial t} + \nabla . J_i = 0$$

$$\text{and} \quad \frac{\partial C_i}{\partial t} = \nabla . \sum_{k=1}^{n-1} D_{ik}\nabla C_k \qquad [5\text{-}11]$$

For a quaternary system with three phases in which the relative changes in concentrations are small, the diffusion coefficients may be approximated by constants, and [5-11] reduces to

$$\frac{\partial C_1}{\partial t} = D_{11}\nabla^2 C_1 + D_{12}\nabla^2 C_2 + D_{13}\nabla^2 C_3$$
$$\frac{\partial C_2}{\partial t} = D_{21}\nabla^2 C_1 + D_{22}\nabla^2 C_2 + D_{23}\nabla^2 C_3 \qquad [5\text{-}12]$$
$$\frac{\partial C_3}{\partial t} = D_{31}\nabla^2 C_1 + D_{32}\nabla^2 C_2 + D_{33}\nabla^2 C_3$$

with the following boundary conditions:

$C_i(z < 0,0) = C_i(-\infty,t) = C_{iN}$, z is the value of x.

$C_i(z > 0,0) = C_i(+\infty, t) = C_{i1}$

$C_i(\rho^{mn}_-, t>0) = C_i^{mn}$, ρ_- is the phase boundary at the m side and mn signifies the multiphases. $C_i(\rho^{mn}_+, t>0) = C_i^{nm}$, ρ_+ is the phase boundary at the n side. Being analogous to the ternary, multiphase system (50), and using the superposition principle, the solution of the diffusion equation for a quaternary system with the above boundary conditions can also be expressed as a sum of the complete error functions:

$$C_i^m = a_{i0}^m + \frac{a_{i1}^m}{I_1^m}\left[\operatorname{cerf}\left(\frac{z}{2(u_1^m t)^{1/2}}\right) - \operatorname{cerf}\left(\frac{\xi^{mn}}{2(u_1^m t)^{1/2}}\right)\right] +$$
$$\frac{a_{i2}^m}{I_2^m}\left[\operatorname{cerf}\left(\frac{z}{2(u_2^m t)^{1/2}}\right) - \operatorname{cerf}\left(\frac{\xi^{mn}}{2(u_2^m t)^{1/2}}\right)\right] +$$
$$\frac{a_{i3}^m}{I_3^m}\left[\operatorname{cerf}\left(\frac{z}{2(u_3^m t)^{1/2}}\right) - \operatorname{cerf}\left(\frac{\xi^{mn}}{2(u_3^m t)^{1/2}}\right)\right] \qquad [5\text{-}13]$$

in which $\operatorname{cerf}(x) = \frac{1}{2}[1 + \operatorname{erf}(x)]$ and,

the normalization integrals are

$$I_k^m = \mathrm{erfc}\left(\frac{\xi^{m+1,n+1}}{2\sqrt{u_k^m t}}\right) - \mathrm{erfc}\left(\frac{\xi^{mn}}{2\sqrt{u_k^m t}}\right)$$

The indices m,n can be m,n = vapor, liquid, α, β, γ where $\alpha =$ UO_2, β = YOF, $\gamma = Y_2O_3$. The coefficients a_{ij}, u_{ij} with i=1..3, j=1..3 can then be expressed explicitly using the matrix algebra and flux-interface velocity relationships. They are the complex combinations of the diffusion coefficients and the boundary conditions.

5.3 Description of the Fluxes and Their Relations with the Interface Velocities

An investigator of multicomponent diffusion phenomena once declared that the formalism of the phenomenological coefficients requires an experimentally difficult and tedious procedure for the evaluation of a set of descriptors of diffusion that have little practical value and almost no physical significance. The diffusion equation for multicomponent, multiphase systems becomes very complicated due to the dependency of the diffusion coefficients to each other. As an example, the coefficients entering in [5-11] are linked in the particular case of a three-component system by the following (6):

$$D_{11}^{*} = (1 - C_1)D_{11} - C_1(D_{21} + D_{31});$$

$$D_{12}^{*} = (1 - C_1)D_{12} - C_1(D_{22} + D_{32});$$

$$D_{21}^{*} = (1 - C_2)D_{21} - C_2(D_{11} + D_{31});$$

$$D_{22}^{*} = (1 - C_2)D_{22} - C_2(D_{12} + D_{32}).$$

From these relations it follows that for a complete description of the process of interdiffusion in a three-component system (actual system has four components), it is necessary to experimentally determine six partial coefficients: D_{11}, D_{12}, D_{21}, D_{22}, D_{31}, and D_{32} which is practically not possible with the present experimental facilities. Therefore, the following approach is introduced as a first order treatment of the present multiphase, multicomponent diffusion problem.

Given n phases in a system, the fluxes of each species at each interface can be expressed in terms of one single flux under local equilibrium conditions at the boundaries.

a. the concentrations are in equilibrium:

$$C_i^{mn} <-> C_i^{nm}, \quad m=\alpha,\beta.., \; n = \alpha,\beta.., \; m \neq n,$$

b. the chemical potentials are equal: $\mu_i^m = \mu_i^n$, i = A,B..Z and,

c. the pressures and temperatures are equal: $T^m = T^n$, $P^m = P^n$.

For stoichiometric phases, mass transport occurs from one interface to the other without causing an accumulation of matter in the phase; therefore, from the conservation of mass law, it is reasonable to assume the incoming and outgoing fluxes of each component are equal in each layer. To simplify the problem, it is assumed that the chemical reactions at the interface are sufficiently rapid that local equilibrium conditions apply. Figure 5.5 describes an n phase system with initial and final fluxes. The first index

indicates the phase in which the flux exists, the second index shows the neighboring phase.

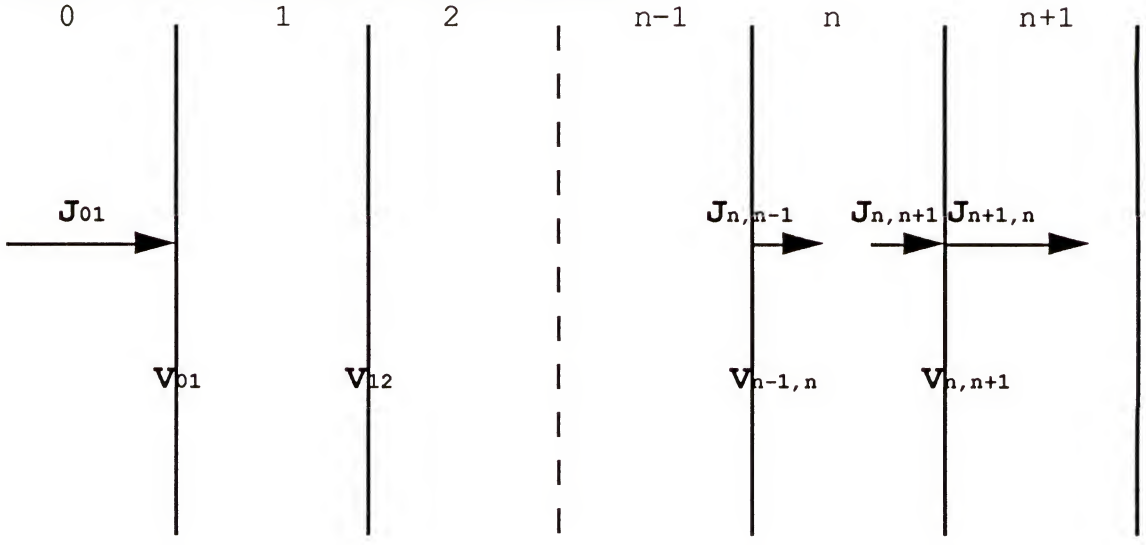

Figure 5.5 Theoretical N Phase System with Initial and Final Fluxes

The mathematical representations of flux for a given component is $J_i = -D_i\frac{\partial C_i}{\partial x}$ $[\frac{1}{cm^2 sec}]$ where D_i is the diffusion coefficient of the component in the phase and $\frac{\partial C_i}{\partial x}$ is the concentration gradient. It is assumed that D_i is space and time independent. Two basic relationships concerning the fluxes, interface velocities and concentrations are derived for this matter:

a. For a given component, in a given phase, the fluxes are assumed to be equal at the facing boundaries. Equation [5-14] represents the fluxes in the m phase which is adjacent to the (m-1) and (m+1) phases.

$$J_i^{m(m-1)} = J_i^{m(m+1)} \qquad [5\text{-}14]$$

When the interface having a surface A, moves a distance of ds in a time interval dt, the number of added atoms dn, can be expressed in terms of concentrations and fluxes:

$$dn = (C_i^{m(m+1)} - C_i^{(m+1)m})Ads = (J_i^{m(m+1)} - J_i^{(m+1)m})Adt \ .$$

Therefore, as mentioned earlier, the velocity $\frac{ds}{dt}$ can be expressed as follows:

$$\frac{ds}{dt} = V_{m(m+1)} = \frac{J_i^{m(m+1)} - J_i^{(m+1)m}}{C_i^{m(m+1)} - C_i^{(m+1)m}} \qquad [5\text{-}15]$$

in which $m = 0,1,2...n$ and $i = A,B.....Z$ (m is the name of the phase and i the name of the component).
In a similar way, for the (m-1) phase, it is possible to write [5-15] by adjusting the indices:

$$V_{(m-1)m} = \frac{J_i^{(m-1)m} - J_i^{m(m-1)}}{C_i^{(m-1)m} - C_i^{m(m-1)}} \qquad [5\text{-}16]$$

Then from [5-15] and [5-16], the flux differences can be expressed by the product of the velocity and concentrations of the m and m+1 phases:

$$J_i^{m(m+1)} - J_i^{(m+1)m} = V_{m(m+1)}\Delta C_i^{m(m+1)} \qquad [5\text{-}17]$$

$$J_i^{(m-1)m} - J_i^{m(m-1)} = V_{m(m-1)} \Delta C_i^{m(m-1)} . \qquad [5-18]$$

From [5-14], it is seen that the first term of [5-17] and the second term of [5-18] are equal; therefore, by eliminating these terms, the flux entering the phase (input flux) can be written in terms of the flux leaving the phase (output flux) with the velocities of the two interfaces of the phase [5-19].

$$J_i^{(m-1)m} = J_i^{(m+1)m} + V_{m(m-1)} \Delta C_i^{m(m-1)} + V_{m(m+1)} \Delta C_i^{m(m+1)} \qquad [5-19]$$

Using [5-14], it is possible to write, $J_i^{(m+1)m} = J_i^{(m+1)(m+2)}$. Then, from [5-19], $J_i^{(m+1)(m+2)}$ can be expressed in terms of velocities by substituting $J_i^{(m-1)m}$. Since the first index (m+1) and second index (m+2) are twice larger than (m-1) and m, respectively, the indices at the right side of Equation [5-19] are increased twice. The flux expression at phase (m+1),(m+2) is as follows:

$$J_i^{(m+1)(m+2)} = J_i^{(m+3)(m+2)} + V_{(m+1)(m+2)} \Delta C_i^{(m+2)(m+1)} + V_{(m+2)(m+3)} \Delta C_i^{(m+2)(m+3)} \qquad [5-20]$$

Next, [5-20] can replace $J_i^{(m+1)m}$ in [5-19] since they are equal; therefore, an expression containing four velocities is

obtained and $J_i^{(m-1)m}$ is found in terms of $J_i^{(m+3)(m+2)}$ which is located in the fourth phase. By recurrence, a general formula can be written as follows:

$$J_j^{m(m+1)} = J_j^{n(n-1)} + \sum_{j=A}^{Z} \sum_{i=m}^{n-1} V_{i(i+1)} \delta_j^{i(i+1)} \qquad [5\text{-}21]$$

This formula allows one to determine every flux of a particular specie, in terms of a reference flux, in an n phase system. Application of [5-21] to the present work is given in the following pages. A system with five phases (V, L, α, ß, μ), four interfaces ($X^{12}, X^{23}, X^{34}, X^{45}$), and four components, each of them having two fluxes at the interface, can have 32 fluxes. Assuming there is no solubility of uranium in YOF, Y_2O_3 matrices, and fluorine in the Y_2O_3 matrix, the present experimental system has 11 equations which satisfies [5-14] and 15 equations satisfying [5-15] and 6 null equations. Then, for a total of 32 fluxes and 32 equations, each flux can be determined quantitatively. Description of the fluxes and the relationships are given in Figure 5.6, Table 5.1 and Table 5.2 which represent Equations [5-14] and [5-15] for different components.

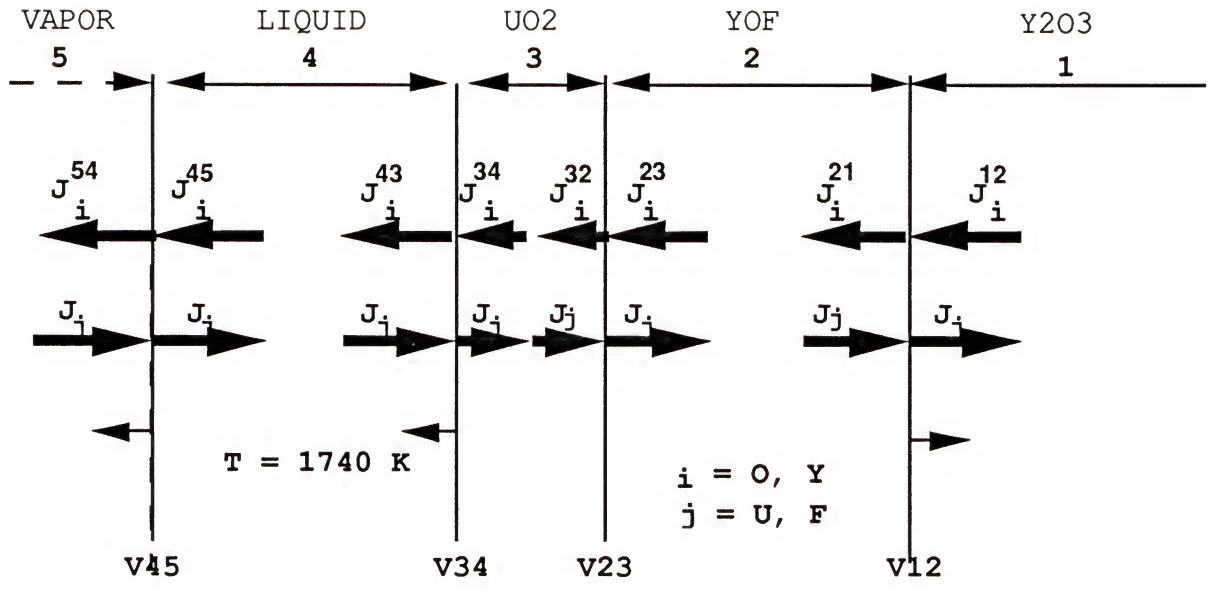

Figure 5.6 Theoretical Prediction of the Fluxes at the Interfaces

For the {O.F,U,Y} system, the null fluxes and equivalent interface fluxes with respect to [5-14] are given in Table 5.1. In Figure 5.6, the oxygen diffusion direction is considered positive with respect to the fluxes and velocities.

Table 5.1 Null and Equivalent Fluxes in {O.F,U,Y} System

VAPOR	LIQUID	UO_2	YOF	Y_2O_3
$J_o^{54} = 0$	$J_o^{45} = J_o^{43}$	$J_o^{34} = J_o^{32}$	$J_o^{23} = J_o^{21}$	J_o^{12}
$J_y^{45} = 0$	$J_y^{45} = J_y^{43}$	$J_y^{34} = J_y^{32}$	$J_y^{23} = J_y^{21}$	J_o^{12}
J_u^{54}	$-J_u^{45} = -J_u^{43}$	$-J_u^{34} = -J_u^{32}$	$-J_u^{23} = -J_u^{21} = 0$	$-J_u^{12} = 0$
J_u^{45}	$-J_f^{45} = -J_f^{43}$	$-J_f^{34} = -J_f^{32}$	$-J_f^{23} = -J_f^{21}$	$-J_f^{12} = 0$

Table 5.2 Theoretical Predicted Velocity, Flux, Concentration Relationships

$\frac{J_o^{12} - J_o^{21}}{\Delta c_o^{12}} = \frac{J_y^{12} - J_y^{21}}{\Delta c_y^{12}} = \frac{J_f^{21}}{\Delta c_f^{12}} = V_{12}$
$\frac{J_o^{23} - J_o^{32}}{\Delta c_o^{23}} = \frac{J_y^{23} - J_y^{32}}{\Delta c_y^{23}} = \frac{J_u^{32}}{\Delta c_u^{23}} = -\frac{J_f^{23} - J_f^{32}}{\Delta c_f^{23}} = V_{23}$
$\frac{J_o^{34} - J_o^{43}}{\Delta c_o^{34}} = \frac{J_y^{34} - J_y^{43}}{\Delta c_y^{34}} = -\frac{J_u^{34} - J_u^{43}}{\Delta c_u^{34}} = -\frac{J_f^{34} - J_f^{43}}{\Delta c_f^{34}} = V_{34}$
$\frac{J_o^{45}}{\Delta c_o^{45}} = \frac{J_y^{45}}{\Delta c_y^{45}} = -\frac{J_u^{45} - J_u^{54}}{\Delta c_u^{45}} = -\frac{J_f^{45} - J_f^{54}}{\Delta c_f^{45}} = V_{45}$

According to [5-15] and the equations presented in Table 5.2, J_o^{45} can be calculated directly using the velocity and concentration difference of interface 45. Then, it is reasonable to express fluxes in terms of J_o^{45} or J_o^{43}. In Figure 5.7, the slopes obtained from the linear regression of the experimental data represent the approximate gradient of the components at the UO_2-Liquid and UO_2-YOF interfaces.

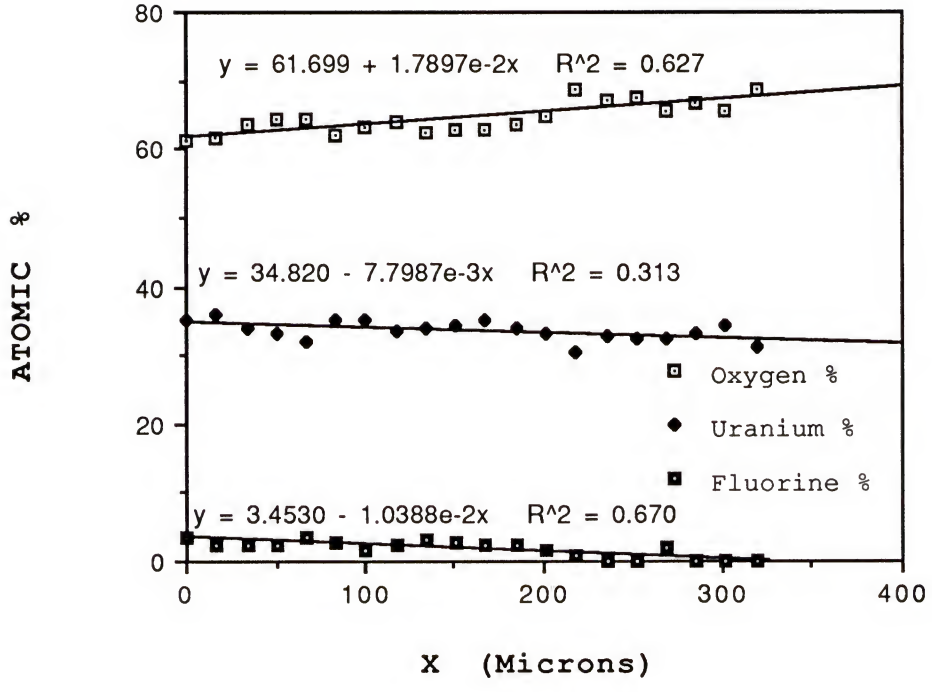

Figure 5.7 Linear Regression of the Experimental Concentration Data in UO_2 Layer

From [21], the oxygen fluxes in terms of J_o^{45} or J_o^{43} are

$$J_o^{43} = J_o^{45} = \Delta C_o^{45} V_{45}$$

$$J_o^{12} = J_o^{43} + \Delta C_o^{12} V_{12} + \Delta C_o^{23} V_{23} + \Delta C_o^{34} V_{34}$$

$$J_o^{21} = J_o^{23} = J_o^{43} + \Delta C_o^{23} V_{23} + \Delta C_o^{34} V_{34}$$

$$J_o^{34} = J_o^{32} = J_o^{43} + \Delta C_o^{34} V_{34} \qquad [5\text{-}22]$$

From the measurements on Figure 3.13, 3.14, and 3.15, it was concluded that the growth of the center and inner layer was diffusion controlled at 1740 K and obeyed the parabolic rate law which is defined as $x = k\sqrt{t}$ where k is the slope.

Then, the first derivative gives the instantaneous velocity of the layers.

$$V = \frac{dx}{dt} = \frac{k}{2\sqrt{t}} \qquad [5\text{-}23]$$

For a 15 min (900 sec) exposure, the measured rate constants for center, inner, and outer layers are

$$k_c = 8\times10^{-5}\ \frac{cm}{\sqrt{sec}} \qquad k_i = 6.5\times10^{-4}\ \frac{cm}{\sqrt{sec}} \qquad k_o = 2.6\times10^{-3}\ \frac{cm}{\sqrt{sec}}\ .$$

From Figure 3.14, for a sample exposed to UF_4 for 15 min, the center (UO_2), and outer (liquid) layers grew mainly outward, and interface X_{23} is assumed to stay almost immobile; the inner (YOF) layer advanced inward. For an average testing time of 15 min, the instantaneous velocities can then be calculated by substituting the rate constants in [5-23]. Table 5.3 shows the interface velocities. The measured average atomic ratio percentage, the atomic concentration, and concentration differences of the components in adjacent phases are given in Table 5.4.

Table 5.3 Calculated Interface Velocities

Calculated Velocity	(cm/sec)
V_{12}	-1.083×10^{-5}
V_{23}	-10^{-14}
V_{34}	1.330×10^{-6}
V_{45}	4.380×10^{-5}

Table 5.4 Experimental Interface Concentrations

	Oxygen	Yttrium	Uranium	Fluorine
Outer Layer	7	7.5	16	70
MV=58.1 cm^3				
C^4	0.120	0.129	0.275	1.2
$C^4-C^5= \Delta C^{45}$	0.12	0.129	0.275	1.2
UO_2 Layer	64.5	0.07	33.57	1.79
MV=24.6 cm^3				
C^3	2.62	0.0028	1.36	0.073
$C^3-C^4= \Delta C^{34}$	2.5	-0.126	1.085	-1.127
YOF Layer	33.66	31.93	0	34.39
MV=24.1 cm^3				
C^2	1.39	1.32	0	1.43
$C^2-C^3= \Delta C^{23}$	-1.23	1.317	-1.36	1.357
Y_2O_3 Layer	62.75	37.25	0	0
MV=45 cm^3				
C^1	1.39	0.827	0	0
$C^1-C^2= \Delta C^{12}$	-0.002	-0.493	0	-1.43

In order to find the average atomic concentration of oxygen, yttrium, uranium, and fluorine atoms in the liquid outer layer, the approximate volume ratios of different phases (dendrites, eutectic, peritectic) are determined from the micrographs taken by SEM after solidification; then, concentration data of these components for the phases are multiplied by their volume percentages. For the other layers, arithmetic averaging was performed to the data obtained from EMP. The atomic concentrations are expressed in terms of mole/cm^3 after being divided by the approximate molar volumes of each phase (3,39). The molar volume of the YOF and YUF_7 phases are found by dividing their molar mass by the density. The liquid outer layer is assumed to contain

only YUF_7 component as a single phase. Substituting the concentrations and velocities for oxygen ions in [5-22], the theoretical values for the fluxes are obtained. They are stated in Table 5.5 in which

$$J_O^{12} > J_O^{21}, J_O^{23} > J_O^{34}, J_O^{32} >> J_O^{45}, J_O^{43} .$$

The inequality among oxygen fluxes in phases 34, 12 and 45 is the driving force for the growth of the UO_2 and YOF layers. By knowing the oxygen flux at the interfaces of UO_2 phase, it is possible to calculate the diffusion coefficient of the oxygen ions and compare it with its experimental value. From Ficks 1st law, J_O^{32} can be expressed as a product of the diffusion coefficient and the gradient $J_O^{32} = D_O^{32}\frac{\partial C_O}{\partial x}$. In Figure 4.6, the experimental value for D_O^{32} can be estimated being $D_O^{32} \approx 10^{-7}\ \frac{cm^2}{sec}$ for a ratio of O/U = 2 at 1750 K. For 0.0319 cm thickness of UO_2, linear regression analysis in Figure 5.7 gives the approximate gradient of the oxygen atoms, which is $\frac{\partial C_O}{\partial x} = 7.27\ [\frac{mole}{cm^4}]$. The theoretical value for J_O^{34}, J_O^{32} is $8.58 \times 10^{-6}\ \frac{Mole}{cm^2 sec}$; therefore, it is calculated that $D_O^{32} = 11.8 \times 10^{-7}\ \frac{cm^2}{sec}$ which is 10 order of magnitude larger than experimental data. The discrepancy can be accounted for the extrapolated value of the diffusion coefficient in Figure 4.6. For other components, a similar

treatment is valid. According to [5-21], the fluxes for uranium atoms can be given as follows:

$$J_u^{54} = J_u^{32} + V_{45}\Delta C_u^{45} + V_{34}\Delta C_u^{34}$$

$$J_u^{34} = J_u^{32}$$

$$J_u^{45} = J_u^{43} = J_u^{32} + V_{34}\Delta C_u^{34} \qquad [5\text{-}24]$$

and in Table 5.2, it is seen $J_u^{32} = V_{23}\Delta C_u^{23}$ and from the measured velocity and concentration, it is found that, $J_u^{32} = 1.36\text{x}10^{-14}\ [\frac{\text{mole}}{\text{cm}^2\text{sec}}]$. Applying J_u^{32} into [5-24], the remaining fluxes of uranium are calculated. The fluxes are stated in Table 5.5

where $J_u^{54} > J_u^{45} = J_u^{43} >> J_u^{34} = J_u^{32}$.

For uranium compounds, the source is generated from vapor phase. It is therefore reasonable to obtain higher flux values in the vapor phase than in the liquid and solid UO_2 phase. Also, the oxygen flux in UO_2 phase is seven orders of magnitude higher than the uranium flux. This fact explains that the growth of this layer is mainly due to the oxygen diffusion from Y_2O_3 phase to the liquid phase, and boundary 34 moves left as the diffusion proceeds.

The experimental value (45) for the uranium diffusion coefficient is

$$D_u^{32} \approx 10^{-14}\ \frac{\text{cm}^2}{\text{sec}} \quad \text{in } UO_2 \text{ at } 1773 \text{ K} \quad (45)$$

and it is found that $J_u^{32} = 1.36\times10^{-13}$ $[\frac{\text{mole}}{\text{cm}^2\text{sec}}]$. From Figure 5.7, the approximate interface gradient is $\frac{\partial C_u}{\partial x} = -3.17$ $[\frac{\text{mole}}{\text{cm}^4}]$, then D_u^{32} is found to be -4.29×10^{-14} which is close to the experimental value in magnitude. The negative sign shows that the concentration is decreasing with increasing x. From the results given above, we can conclude that it is a good approximation to assume the velocity V_{23} being very close to zero as shown in Table 5.3.

For the yttrium and fluorine fluxes, from Table 5.5 it is observed that J_y^{45} and J_f^{21} have a finite value; therefore, the remaining fluxes can be expressed in terms of these fluxes. Using Equation [5-21], one obtains for yttrium flux:

$$J_y^{43} = J_y^{45} = V_{45}\Delta C_y^{45}$$

$$J_y^{32} = J_y^{34} = J_y^{45} + V_{34}\Delta C_y^{34}$$

$$J_y^{21} = J_y^{23} = J_y^{45} + V_{34}\Delta C_y^{34} + V_{23}\Delta C_y^{23}$$

$$J_y^{12} = J_y^{45} + V_{12}\Delta C_y^{12} + V_{23}\Delta C_y^{23} + V_{34}\Delta C_y^{34} \qquad [5\text{-}25]$$

and for the fluorine flux:

$$-J_f^{23} = -J_f^{21} = V_{12}\Delta C_f^{12}$$

$$J_f^{34} = J_f^{32} = J_f^{21} + V_{23}\Delta C_f^{23}$$

$$J_f^{45} = J_f^{43} = J_f^{21} + V_{23}\Delta C_f^{23} + V_{34}\Delta C_f^{34}$$

$$J_f^{54} = J_f^{21} + V_{23}\Delta C_f^{23} + V_{34}\Delta C_f^{34} + V_{45}\Delta C_f^{45}\ , \qquad [5\text{-}26]$$

and, the theoretical quantitative values for [5-25] and

[5-26] are presented in Table 5.5.

Table 5.5 Calculated Fluxes of the Components at the Interfaces

FLUXES $\frac{cm^2}{sec}$	OXYGEN	URANIUM	YTTRIUM	FLUORINE
J_i^{12}	8.61×10^{-6}	0	3.484×10^{-5}	
$J_i^{23} = J_i^{21}$	8.59×10^{-6}	0	5.480×10^{-6}	1.549×10^{-5}
$J_i^{34} = J_i^{32}$	8.58×10^{-6}	1.36×10^{-4}	5.480×10^{-6}	1.549×10^{-5}
$J_i^{45} = J_i^{43}$	5.26×10^{-6}	1.46×10^{-6}	5.650×10^{-6}	1.399×10^{-5}
J_i^{54}	0	1.35×10^{-5}	0	6.655×10^{-5}

From Table 5.5, it is observed that,

$$J_y^{12} > J_y^{23} = J_y^{21},\ J_y^{34} = J_y^{32},\ J_y^{45} = J_y^{43}$$

which is expected since higher concentrations of yttrium atoms exist in region 1. For the fluorine compound, region 5 has the highest potential since it generates fluorine during the reaction.

$$J_f^{54} > J_f^{45} = J_f^{43},\ J_f^{34} = J_f^{32},\ -J_f^{23} = -J_f^{21}.$$

However, in the yttrium case, $J_i^{45} = J_i^{43}$ is higher and for fluorine is lower than the preceding fluxes. This inconsistency is probably due to the large deviation in the estimation of the molar volume of the region 4, which is the liquid outer layer.

By knowing $J_f^{34} = J_f^{32} = 1.549\text{x}10^{-5}$ $[\frac{\text{Mole}}{\text{cm}^2\text{sec}}]$ and from Figure 5.7, it is found $\frac{\partial C_f}{\partial x} = -4.22$ in the UO_2 layer; therefore, D_f^{32} can be estimated to be $3.67\text{x}10^{-6}$ $[\frac{\text{cm}^2}{\text{sec}}]$. Table 5.6 summarizes the theoretical and experimental diffusion coefficients of the oxygen, uranium and fluorine atoms in nearly stoichiometric UO_2 at temperatures 1740 K.

Table 5.6 Theoretical and Experimental Data of the Diffusion Coefficients for UO_2 Layer

DIFFUSION C.	OXYGEN	URANIUM	FLUORINE
D^{32} $[\frac{\text{cm}^2}{\text{sec}}]$ (Theoretical)	$11.8\text{x}10^{-7}$	$4.29\text{x}10^{-14}$	$3.67\text{x}10^{-6}$
D^{32} $[\frac{\text{cm}^2}{\text{sec}}]$ (Experimental)	$\approx 1\text{x}10^{-7}$	$\approx 1\text{x}10^{-14}$	Not known

Finally, it is important to once more summarize the assumptions made for the modeling of the problem discussed in this chapter. They are stated as follows:

a) no chemical reactions occur in the product layer during the diffusion,

b) the diffusion coefficient D_{AB} is independent of the concentration and time,

c) a thin, stagnant boundary layer was assumed to exist between the liquid and gas phases, and also between the liquid and solid UO_2 phase in which the diffusion effect becomes significant, and

d) one-dimensional diffusion in rectangular slab geometry was assumed.

In concluding Chapter 5, an attempt in determining the diffusion coefficients of uranium, oxygen, and fluorine ions is made using the interface velocities and concentration gradients of the components. Also, with the assumption of a single-phase, binary system, the diffusion coefficient of the oxygen ions was found from the solution of the Ficks law for steady state case. The theoretical values are compared with the experimental data for the oxygen and uranium components.

CHAPTER 6
SUMMARY AND CONCLUSION

A detailed analysis of yttria reacting with UF_6 and UF_4 was performed in this research. The compatibility of Mo with UF_4 in liquid and gas phases was also tested.

Samples of yttria were prepared using sintering and hot-pressing techniques. Disk shaped samples first was prepared by compressing the yttrium oxide powder, then sintering was performed at 1973 K in an electrical furnace and about 85% of the theoretical density was reached after this process. For hot-pressing, a high strenght graphite die was used in which the precompressed sample was placed between two tungsten disks. Three samples were pressed at 1873 K under pressures ranging from 30 to 45 MPa pressure in argon atmosphere. Densities reaching above 99% of the theoretical density of yttria were obtained after hot-pressing. Due to color changes of the samples, partial transparency was observed; however, following an annealing period of 3 hours at 1473 K this contamination problem was removed and fully white samples were obtained. Uranium hexafluoride gas at 1173 K was used first to test the yttria samples in a flowing loop system. This provided a more realistic approach to gas core conditions and decreased UF_6 losses due to oxygen reactions and dissociation to lower fluorine compounds.

Extensive corrosion of yttria was observed after the experiments for short periods of time (5 to 20 min). For longer exposure times, samples fully reacted and dispersed in the reaction chamber. Products from UF_6, mainly free fluorine and UF_4, caused the breakdown of the high temperature ceramic material. The multilayer formation following the chemical reactions was observed with SEM technique. The observed reaction layers were named as outer, center, and inner layers. Following the XRD and EMP analyses, it was found that the outer layer was a mixture of UO_2, U_3O_8 and YF_3 while the inner layer was only composed of yttrium and fluorine without the presence of uranium atoms. It was concluded that UF_6 gas reacted with yttria following a complex chemical reaction scheme and at least two simultaneous chemical reactions formed two moving reaction boundaries in the samples.

In the second phase of the experiments, samples of yttria and molybdenum were tested with UF_4 in a stainless steel reaction chamber. This time, oxygen contamination of the chamber due to the external factors such as the silica or alumina container tube was totally removed by placing the yttria and molybdenum samples into a molybdenum tube. The insertion of argon gas into the chamber, which was under high vacuum of approximately 10^{-5} Torr, further helped to minimize contamination. The oxydation of molybdenum and loss of UF_4 at temperatures above 1273 K was prevented in this manner. Yttria samples reacted extensively, in a maner similar to the

UF_6 case, while molybdenum showed good compatibility at temperatures up to 2273 K. The reaction products with yttria at 1750 K were analyzed extensively with optical microscope, scanning electron microscopy (SEM), electron microprobe (EMP) and x-ray diffraction analysis. In this case, three reaction boundaries were formed. The UF_6 caused only two reaction boundaries in the yttria sample. The existing components in the three reaction boundaries were found to be UO_2, YOF, YF_3, and U_3O_{7-8}. Uranium oxide (UO_2) formed a solid wall between the liquid outer layer and solid inner layer at the time of the experiment. This layer did not form during the UF_6 exposures, because the lower operating temperature (1200 K) significantly decreased the diffusion of the O and Y ions, thus preventing the formation of a liquid eutectic mixture and the accumulation of the center UO_2 layer. The higher activity of the UF_6 gas, due to its higher fluorine concentration increased the intensity of the reactions, accelerating the corrosion of the material. The higher reactivity of fluorine compared to uranium ions showed itself in both UF_6, UF_4 cases by advancing and reacting further in the yttria matrix, thus forming the inner layer. The outer layer showed extensive sponge-like porosity after UF_6 reaction. However, in the UF_4 case, the presence of the liquid phase and its solidification during the cooling period produced an outer layer without porosity. It was also found that the outer layer was composed of a significant amount of dendrites surrounded with a gray peritectic phase. This

phase itself was followed by lamellar, finely dispersed eutectic. The dendrites were found to be composed of hypostoichiometric UO_2 while the peritectic and the eutectic layer were a mixture of uranium, yttrium and fluorine.

In the case of molybdenum, due to the presence of oxygen, formation of MoO_3 and $MoOF_4$ on the surface at temperatures over 1273 K was observed. However this problem was eliminated after modifications were done to the system. Contrary to the previous work performed with melted uranium (25,26,27,28), molybdenum resisted the UF_4 at any temperatures below 2300 K. No significant diffusion nor reaction was detected in the samples after EMP, SEM, and EDS analyses. However, samples became more brittle after each experiment. This is due to the rapid cooling rate from temperatures over 1273 K after turning off the power. In order to model the reactions, a diffusion analysis was performed applying Ficks second law to the multiphase multicomponent system and also deriving flux-interface relationships on the layer boundaries of the yttria sample.

The major conclusions derived from this research are:

a. The complex multilayer structure of the yttrium oxide ceramic containing different phases, after being exposed to UF_4 and UF_6 gases at temperatures between 1173 and 1750 K, was analyzed and a semi-quantitative model describing the process was developed. The experimental and predicted diffusion coefficients of uranium and fluorine atoms in UO_2 is compared according to the model developed.

b. High purity molybdenum was found to be resistant to liquid and gas phase UF_4 at ranges 1273-2273 K. Molybdenum was found to be a promising material for the corrosive environments of the proposed gas core reactors. Further testing of its chemical and mechanical properties has to be done at temperatures above 2273 K.

LIST OF REFERENCES

1. Dugan E.T., Welch G.E., Kahook S., in: Proc.of the 24th Energy Conversion Engineering Conference, Ed. W.D. Jackson, IECEC-89, Washington, DC (Aug. 6-11,1989).

2. Cochran R.G., Tsoulfanidis N., The Nuclear Fuel Cycle: Analysis and Management, American Nuclear Society (ANS), La Grange Park, IL (1990).

3. Bacher W., Karlsruhe K., Jakob E., 'Uran' in: Gmelin Handbuch der Anorganischen Chemie, Ed. Keller C., Kerntechnik S.F., Karlsruhe K., C8, Springer-Verlag, Berlin (1980).

4. Hagenmuller P., Inorganic Solid Fluorides, Chemistry and Physics, Academic Press, Orlando, FL (1985).

5. El-Wakil M.M., Nuclear Energy Conversion, ANS, La Grange Park IL (1978).

6. Fedorov G.B., Smirnov E.A., Diffusion in Reactor Materials, Trans Tech Publications, Aedeermannsdorf Switzerland (1984).

7. Assuncao F.C.R., Diffusion Study in the Fe-Co-Ni-Au System using the Penetration Tendency Approach, Doctoral Dissertation, University of Florida, Gainesville (1978).

8. Crank J., The Mathematics of Diffusion, Oxford University Press, Bristol, England (1975).

9. Jost, W., Diffusion in Solids, Liquids, Gases, Academic Press, New York (1960).

10. Crank J., Free and Moving Boundary Problems, Clarendon Press, Oxford (1984).

11. Hill J.M., One-Dimensional Stefan Problems, An Introduction, John Wiley & Sons, New York (1987).

12. Barrer R.M., Diffusion In and Through Solids, Cambridge University Press, London (1941).

13. Geiger G.H., Poirier D.R., Transport Phenomena in Metallurgy, Addison-Wesley, Reading, MA (1973).

14. Murch G.E., Nowick A.S., Diffusion in Crystalline Solids, Academic Press, Orlando (1984).

15. Romig A.D., Dayananda M.A., Diffusion Analysis and Applications, The Minerals, Metals & Materials Society, Chicago (1989).

16. Ozisik M.N., Mikhailov M.D., Unified Analysis and Solutions of Heat and Mass Diffusion, John Wiley & Sons, New York (1984).

17. Szekely J., Evans J.W., Sohn H.Y., Gas-Solid Reactions, Academic Press, New York (1976).

18. Wong K.Y., Mathematical Models for Gas-Solid Reactions, Master's Thesis, University of Florida, Gainesville (1976).

19. Incropera F.P., De Witt D.P., Fundamentals of Heat and Mass Transfer, John Wiley & Sons, New York (1990).

20. Borg R.J., Dienes G.J., An Introduction to Solid State Diffusion, Academic Press Inc., San Diego (1988).

21. Wise H., Oudar J., Material Concepts in Surface Reactivity and Catalysis, Academic Press, San Diego (1990).

22. Laidler, J.K., Chemical Kinetics, Harper & Row, New York (1987).

23. Kondratiev V.N., Nikitin E.E., Gas-Phase Reactions: Kinetics and Mechanisms, Springer-Verlag, Berlin (1981).

24. Ovchinnikov A.A., Timashev S.F., Belyy A.A., Kinetics of Diffusion Controlled Chemical Processes, Nova Science Publishers, New York (1986).

25. Kuznietz M., Livne Z., Cotler C., Erez G., J. Nucl. Mater., 152, 235-245 (1988).

26. Kuznietz M., Livne Z., Cotler C., Erez G., J. Nucl. Mater., 160, 69-74 (1988).

27. Kuznietz M., Livne Z., Cotler C., Erez G., J. Nucl. Mater., 160, 196-200 (1988).

28. Lundberg L.B., J. Nucl. Mater., 167, 64-75 (1989).

29. Hale C.F., Barber E.J., Berhardt H.A., High Temperature Corrosion of Some Metals and Ceramics in Fluorinating Atmospheres, Report K-1459, Union Carbide Nuclear Co., Oak Ridge National Lab., Oak Ridge, TN (1960).

30. Florin A.E., Some Corrosion Tests of Materials in UF_6, LA-7327-MS, Los Alamos National Lab., Los Alamos, NM (1978).

31. Whitney E.D., Kim D.J., Tucker D.S., Nucl.Technol., 69, 154 (1985).

32. Collins C., Reaction Between ZrO_2 and UF_6 at Elevated Temperatures, Master's Thesis, University of Florida, Gainesville (1988).

33. Wang S.C.P., Anghaie S., Whitney D., Collins C., High Temperature Testing of Alumina and Zirconia in Uranium Hexafluoride Environment, Nucl. Technol., 93[3], 399 (1991).

34. LeRoy, Furlong R., Domingues L.P., Sintering of Yttrium Oxide, Ceramic Bulletin, 45[12], 1051 (1966).

35. Sordelet J.D., Akinc M., Sintering of Monosized, Spherical Yttria Powders, J. Am. Ceram. Soc., 71[12], 1148 (1988).

36. Alper M.A., High Temperature Oxides, Academic Press, New York (1971).

37. Aitcin P.C., Density and Porosity Measurement of Solids, J. Mater., JMLSA, 6[2], 282 (1971).

38. ASTM Standards, C20-80a, American Society for Testing and Materials, Philadelphia, PA.

39. Chemical Rubber Company (CRC), Handbook of Chemistry and Physics, 68^{th} edition, CRC Press, Boca Raton, FL (1987-88).

40. Thompson W.T., Pelton A.D., Bale C.W., Facility for the Analysis of Chemical Thermodynamics, Ecole Polytechnique de Montreal, Montreal, Quebec (1985).

41. Bacher, W., Gmelin Handbuch der Anorganischen Chemie, U Uran, C1, Springer Verlag, Berlin, New York (1980).

42. Olander D.R., Fundamental Aspects of Nuclear Reactor Fuel Elements, Technical Information Center, U.S. Department of Energy, Washington, DC (1976).

43. Lidiard A.B., J.of Nucl. Mater., 19, 106-108 (1966).

44. Matzke H.J., Diffusion in Doped UO_2, Trans. Amer. Nucl. Soc., 8[5], 26-27, (1970).

45. Matzke H.J., Lattice Disorder and Metal Self-Diffusion in Non-Stoichiometric UO_2 and (U, Pu)O_2, Journal de Physique, 34[11-12], 317 (1973).

46. Matzke H.J., On Uranium Self-Diffusion in UO_2 and UO_2^+, J of Nuclear Mater., 30[1-2], 26-35 (1969).

47. Guy A.G., Essentials of Materials Science, McGraw-Hill, New York (1976).

48. Kingery W.D., Bowen H.K., Uhlmann D.R., Introduction to Ceramic, John Wiley & Sons, New York (1976).

49. Rostoker W., Dvorak J.R., Interpretation of Metallographic Structures, Academic Press, San Diego (1990).

50. Denton E.C., Interface Stability During Isothermal Ternary Phase Transformations, Doctoral Dissertation, McMaster University, Hamilton, ON, Canada (1970).

BIOGRAPHICAL SKETCH

Ziya Engin Erkmen was born in Eskisehir, Turkey, in 1960. In 1971, he attended Saint Joseph French High School for eight years intensive education. Then, between 1979 and 1983, he studied Metallurgical Engineering in the Istanbul Technical University and received his BSE degree being ranked 1st in his class. In August 1983, he won the scholarship offered by the Ministry of Education to pursue a Ph.D degree in USA, in Nuclear Materials. Then, he started his graduate studies in the Department of Nuclear Engineering of the University of Michigan in Ann Arbor. After completing the requirements of the new department, he received his MSE degree in May 1987. In 1988, he attended the University of Florida to continue his Ph.D degree in the same field. He was sponsored then, by the Innovative Nuclear Space Power Institute (INSPI) in the Department of Nuclear Engineering Sciences and has been working under the supervision of Dr. S. Anghaie in INSPI Laboratories. His research was concentrated on the analysis of ultra-high temperature materials behavior with nuclear gases which is presented here.

I certify that I have read this study and that in my opinion it conforms to acceptable standards of scholarly presentation and is fully adequate, in scope and quality, as a dissertation for the degree of Doctor of Philosophy.

S. Anghaie, Chairman
Professor of Nuclear
Engineering Sciences

I certify that I have read this study and that in my opinion it conforms to acceptable standards of scholarly presentation and is fully adequate, in scope and quality, as a dissertation for the degree of Doctor of Philosophy.

N. Diaz
Professor of Nuclear
Engineering Sciences

I certify that I have read this study and that in my opinion it conforms to acceptable standards of scholarly presentation and is fully adequate, in scope and quality, as a dissertation for the degree of Doctor of Philosophy.

D. Hintenglang
Assistant Professor of
Nuclear Engineering Sciences

I certify that I have read this study and that in my opinion it conforms to acceptable standards of scholarly presentation and is fully adequate, in scope and quality, as a dissertation for the degree of Doctor of Philosophy.

R. DeHoff
Professor of Materials
Science and Engineering

I certify that I have read this study and that in my opinion it conforms to acceptable standards of scholarly presentation and is fully adequate, in scope and quality, as a dissertation for the degree of Doctor of Philosophy.

R.J. Hanrahan
Professor of Chemistry

This dissertation was submitted to the Graduate Faculty of the College of Engineering, and to the Graduate School and was accepted as partial fulfillment of the requirements for the degree of Doctor of Philosophy.

August, 1992

for Winfred M. Phillips,
Dean, College of Engineering

Madelyn M. Lockhart
Dean, Graduate School